

PB 207 369

Study of Membrane-Solution Interfaces by Electrochemical Methods

United States Department of the Interior



Reproduced by
**NATIONAL TECHNICAL
INFORMATION SERVICE**
Springfield, Va. 22151

Office of Saline Water • Research and Development Progress Report No. 353

(21)

**SELECTED WATER
RESOURCES ABSTRACTS
INPUT TRANSACTION FORM**

1. Report No. 2.

3. Accession No.

W

4. Title

Study of Membrane-Solution Interfaces by Electrochemical Methods

7. Author(s)

Spiegler, K. S.

9. Organization

University of California, Berkeley, California

5. Report Date

6.

8. Performing Organization Report No.

10. Project No. OSW R&D
Progress Report 353

11. Contract/Grant No.

14-01-0001-652

13. Type of Report and Period Covered

12. Sponsoring Organization

15. Supplementary Notes

112 pages, 36 tables, 0 tables

16. Abstract This is the first stage of a fundamental experimental study of mass-transfer at membrane-solution interfaces; the practical purpose of this investigation is the characterization of efficient spacers and turbulence promoters.

In the study of polarization at anion-exchange membranes in a laboratory cell by a 4-electrode method, limiting current plateaus were not observed. Addition of polystyrene sulfonate brought the current-voltage curves much closer to the shape of the polarographic plateaus predicted by solution of the Nernst-Planck equations.

The current-voltage curves suggested that membrane heterogeneity may play an important part in polarization. Heterogeneities should show up as dispersions of dielectric constant and frequency in the radio-frequency range. Dispersions were indeed observed and are reported for future network analysis.

These electrochemical studies were supplemented by laser interferometry and a method for the interferometric observation of the membrane-solution interfaces at low Reynolds numbers was developed. The results of the electrochemical studies

17a. Descriptors

Electrodialysis*, Membranes*, Electrochemistry*, Desalination*, Interfaces*, Reverse Osmosis, Pressure, Electrodes

17b. Identifiers

Membrane-Solution Interfaces*, Current-Voltage Curves*, Polarization*, Limiting Current Plateaus, Laser Interferometry, Microelectrodes

17c. COWRR Field & Group

20. Security Class.
(Page)

22. Price

WATER RESOURCES SCIENTIFIC INFORMATION CENTER
U.S. DEPARTMENT OF THE INTERIOR
WASHINGTON, D. C. 20240

Abstractor Lee M. Kindley

Institution Office of Saline Water

formed the basis for the design of a pilot-size unit for detailed mapping of polarization on a single plant-size (1.5 X 1.5 foot) membrane.

Electrochemical studies of modified cellulose acetate membranes for reverse osmosis were initiated by studying potential differences across a tubular reverse osmosis membrane as a function of pressure and circulation rate. The electrode at the low-pressure side of the membrane was always found to be positive with respect to the high-pressure electrode; after correction for the concentration difference the streaming potentials were found to be 8-10 millivolt per 100 psi when dilute sodium chloride solutions were used as feed. The potential differences increase with increasing circulation rate. Flow rate is proportional to pressure.

Microelectrodes for membrane surface mapping were prepared and tested, viz. hybrid platinized platinum-silver/silver chloride electrodes and micro pH electrodes made of antimony.

Theoretical work on reverse osmosis (jointly with O. Kedem) resulted in prediction of salt rejection as a function of production rate by extension of the Staverman-Katchalsky-Kedem equations, and in a mechanistic interpretation of the "reflection factor" which expresses the degree of semipermeability of a membrane for reverse osmosis.

Study of Membrane-Solution Interfaces by Electrochemical Methods

By K. S. Spiegler, Sea Water Conversion Laboratory, University of California, Berkeley, California, for Office of Saline Water, J. A. Hunter, Director; W. Sherman Giliam, Assistant Director, Research; Harold E. Podali, Chief, Polymer and Biophysics Division

Grant No. 14-01-0001-652

Created in 1849, the Department of the Interior—America's Department of Natural Resources—is concerned with the management, conservation, and development of the Nation's water, wildlife, mineral, forest, and park recreational resources. It also has major responsibilities for Indian and Territorial affairs.

As the Nation's principal conservation agency, the Department of the Interior works to assure that nonrenewable resources are developed and used wisely, that park and recreational resources are conserved for the future, and that renewable resources make their full contribution to the progress, prosperity, and security of the United States—now and in the future.

FOREWORD

This is one of a continuing series of reports designed to present accounts of progress in saline water conversion and the economics of its application. Such data are expected to contribute to the long-range development of economical processes applicable to low-cost demineralization of sea and other saline water.

Except for minor editing, the data herein are as contained in a report submitted by the contractor. The data and conclusions given in the report are essentially those of the contractor and are not necessarily endorsed by the Department of the Interior.

TABLE OF CONTENTS

	Page No.
Roster of Personnel	ii
LIST OF FIGURES	iv
ACKNOWLEDGMENTS	vi
I. ABSTRACT	1
II. SUMMARY	3
III. ELECTRODIALYSIS	9
III.A. Current-Voltage Curves	9
III.A.1 Introduction	9
III.A.2 Experimental	11
III.A.3 Theory	17
III.A.4 Results and Discussion	37
III.B. Laser Interferometry of Membrane-Solution Interfaces	56
III.B.1 Principle	56
III.B.2 Interferometer Cell	60
III.B.3 Procedure and Results	63
III.C. Microelectrode Development	66
III.D. Membrane Roughness Measurements	69
III.E. Pilot-Size Cell	71
III.F. Radio-Frequency Measurements	72
III.F.1 Introduction	72
III.F.2 Principle	73
III.F.3 Apparatus	76
III.F.4 Evaluation and Results	76
IV. REVERSE OSMOSIS	86
IV.1 Introduction	86
IV.2 Layout of Apparatus	87
IV.3 Membranes	95
IV.4 Electrodes	96
IV.5 Results and Discussion	98
REFERENCES	106
LIST OF PUBLICATIONS RESULTING FROM THIS RESEARCH	110
LIST OF SYMBOLS	111

LIST OF FIGURES

Figure No.	Caption	Page No.
1	SCHEMATIC OF POLARIZATION MEASUREMENT APPARATUS	12
2	SOLUTION COMPARTMENT OF LABORATORY CELL FOR CURRENT-VOLTAGE CURVES	14
3	SCHEMATIC OF FIELD AND ION FLOW AT ANION-EXCHANGE MEMBRANE	18
4	CALCULATED CURRENT-VOLTAGE CURVE IN ABSENCE OF "SUPPORTING" ELECTROLYTE; EQUATION (39)	30
5	CALCULATED CURRENT-VOLTAGE CURVE IN PRESENCE OF "SUPPORTING" ELECTROLYTE; EQUATION (62)	34
6	CURRENT-VOLTAGE CURVES OF 0.01N KCL SOLUTION (111 BZL 183)	38
7	CURRENT-VOLTAGE CURVES OF 0.026 AND 0.06N KCL SOLUTIONS IN 5% PSS (111 BZL 183)	39
8	CURRENT-VOLTAGE CURVES FOR MEMBRANE CA-1	40
9	CURRENT-VOLTAGE CURVES FOR MEMBRANE A-101-B	41
10	CURRENT-VOLTAGE CURVES FOR MEMBRANE MA 3236	43
11	CURRENT-VOLTAGE CURVES FOR MEMBRANE MA 3475 XL	44
12	EXTRAPOLATED "LIMITING" CURRENT VS. FLOW RATE	46
13	"NORMALIZED" CURRENT-VOLTAGE CURVES FOR DIFFERENT MEMBRANES	49
14	COMPARISON OF EXPERIMENTAL CURRENT-VOLTAGE CURVE WITH CALCULATED CURVE	51
15	CURRENT-VOLTAGE CURVES IN PSS SOLUTIONS CONTAINING ONLY 0.0001N KCL	53
16	CHANGE OF CURRENT-VOLTAGE CURVES WITH TIME	54
17	SCHEMATIC OF LIGHT PATH IN WEDGE INTERFEROMETER	57
18	ASSEMBLY VIEW OF O'BRIEN INTERFEROMETER	61
19	MEMBRANE HOLDER FOR CELL	62
20	LASER INTERFEROGRAMS OF MICROELECTRODIALYSIS CELL	64
21	SURFACE ROUGHNESS MEASUREMENTS OF THREE ION-EXCHANGE MEMBRANES	70
22	CELL FOR RADIO-FREQUENCY MEASUREMENTS AT DIFFERENT ELECTRODE DISTANCES	77
23	SCHEMATIC REPRESENTATION OF CELL AND TRANSMISSION LINE AT TWO DIFFERENT ELECTRODE DISTANCES	78
24	EQUIVALENT CIRCUITS FOR CELL AND TRANSMISSION LINE	79

Figure No.	Caption	Page No.
25	RADIO-FREQUENCY RESPONSE CHARACTERISTICS OF ION-EXCHANGE MEMBRANES (AMERICAN MACHINE & FOUNDRY CO.)	82
26	RADIO-FREQUENCY RESPONSE CHARACTERISTICS OF ION-EXCHANGE MEMBRANES (IONICS, INC.)	83
27	RADIO-FREQUENCY RESPONSE CHARACTERISTICS OF ION-EXCHANGE MEMBRANES (ASAHI CHEMICAL CO.)	84
28	TEST SECTION FOR MEASURING ELECTRIC POTENTIALS DURING REVERSE OSMOSIS	88
29	PROFILE OF REVERSE OSMOSIS TEST SECTION	89
30	REVERSE OSMOSIS FLOW SHEET; TEST SECTION	91
31	VOLTAGE ACROSS MEMBRANE VS. PRESSURE (70°F)	99
32	STREAMING POTENTIAL VS. PRESSURE (70°F)	100
33	STREAMING POTENTIAL VS. CIRCULATION RATE (70°F)	101
34	HYPERFILTRATE CONCENTRATION VS. PRESSURE (70°F)	102
35	HYPERFILTRATE CONCENTRATION VS. CIRCULATION RATE	103
36	HYPERFILTRATION FLUX VS. PRESSURE (70°F)	104

ACKNOWLEDGMENTS

The author expresses his thanks to Professor Charles W. Tobias for his help and his many valuable suggestions during the whole course of this work; to Professor Kenneth S. Cole, Berkeley; to Dr. Hamish Small of the Dow Chemical Company, Midland, Michigan; Dr. R. H. Muller of the Lawrence Radiation Laboratory, Berkeley; Dr. C. Calmon, Vice-President, Ionac Chemical Company, Birmingham, New Jersey; and Dr. S. Loeb, University of California, Los Angeles, for their valuable advice; and to the companies who contributed membranes and other materials for this work. The cellulose acetate membranes were kindly supplied by Dr. Loeb and his group.

This research was carried out in the Sea Water Conversion Laboratory, University of California, Berkeley, which is under the overall direction of Professor E. D. Howe.

During the period of this grant the following faculty, staff, and students have participated in this work (on a part-time basis).

Faculty:	K. Arulanandan R. N. O'Brien (Visiting Professor Lawrence Radiation Laboratory)
Staff:	E. Ewoldsen J. Leibovitz S. A. Weiner
Students:	K. Beach A. C. Eisenberger D. Q. Fletcher R. Hubata C. Minning H. Schwember

I. ABSTRACT

This work is the first stage of a fundamental experimental study of mass-transfer at membrane-solution interfaces; the practical purpose of this investigation is the characterization of efficient spacers and turbulence promoters.

In the study of polarization at anion-exchange membranes in a laboratory cell by a \bar{L} -electrode method, limiting current plateaus were not observed. Addition of polystyrene sulfonate (molecular weight 30,000, Dow Chemical Company, Midland, Michigan) brought the current-voltage curves much closer to the shape of the polarographic plateaus predicted by solution of the Nernst-Planck equations. The values of the "plateau" currents are strongly dependent on the hydraulic conditions; it is therefore likely that they will prove useful as experimental criteria for spacer efficiencies in electrodialysis units.

The current-voltage curves suggested that membrane heterogeneity may play an important part in polarization. Therefore a systematic study of small membrane-solution stacks in the radio-frequency range was begun. Heterogeneities should show up as dispersions of dielectric constant and frequency in this range ("Maxwell-Wagner effect"). Dispersions were indeed observed and are reported for future network analysis.

These electrochemical studies were supplemented by laser interferometry. A method for the interferometric observation of the membrane-solution interfaces at low Reynolds numbers was developed; an example is shown in this report. The results of the electrochemical studies formed the basis for the design of a pilot-size unit for detailed mapping of polarization on a single plant-size (1.5 x 1.5 foot) membrane.

Electrochemical studies of modified cellulose acetate membranes for reverse osmosis were initiated by studying potential differences across a tubular reverse-osmosis membrane as a function of pressure and circulation rate. The electrode at the low-pressure side of the membrane was always found to be positive with respect to the high-pressure electrode; after correction for the concentration difference the streaming potentials were found to be 8-10 millivolt per 100 psi when dilute sodium chloride solutions were used as feed. The potential differences increase with

increasing circulation rate. Flow rate is proportional to pressure. These results suggest the use of electrical signals from reverse osmosis plants as criteria for flow conditions and/or concentration polarization. They served as the basis for the design of a test unit with well-defined hydraulic flow conditions and segmented electrodes.

Microelectrodes for membrane surface mapping were prepared and tested, viz. hybrid platinized platinum-silver/silver chloride electrodes and micro pH electrodes made of antimony. While these electrodes were primarily designed for electro dialysis studies, their future use in reverse osmosis research may prove possible.

Theoretical work on reverse osmosis (jointly with O. Kedem) resulted in prediction of salt rejection as a function of production rate by extension of the Staverman-Katchalsky-Kedem equations, and in a mechanistic interpretation of the "reflection factor" which expresses the degree of semipermeability of a membrane for reverse osmosis.

II. SUMMARY

The present investigation deals with mass transfer at the interfaces of membranes and aqueous solutions under the influence of electrical forces and/or pressure. Thus it has direct bearing on electro dialysis and reverse osmosis. An appreciable portion of this research dealt with the development of methods and designs for the study of these mass transfer processes. Specifically, a method for obtaining true limiting currents at anion-exchange membranes under polarization conditions was investigated; an interferometric method for the observation of the interface developed; progress was made in the development of micro-electrodes for the local probing of membrane surface areas; the study of membrane heterogeneity by radio-frequency measurements was begun; the existence of streaming potentials across modified cellulose acetate membranes (Loeb-Sourirajan type) was demonstrated for dilute feed solutions, and design of pilot plant size cells for the utilization of these findings under a new grant (14-01-0001-1295) was begun. A theory of reverse osmosis based on non-equilibrium thermodynamics was developed jointly with O. Kedem.

Polarization Studies

The voltage between two micro-probe electrodes on opposite sides of anion-exchange membranes was measured as a function of the current passed through the membrane cell, as well as the composition and the flow rate of the solutions flowing on the two sides of the membrane. A small laboratory cell was used (Figures 1,2). Current densities ranged well into the polarization range. These current-voltage curves are important data in the study of the mechanism of polarization.

For membrane III BZL 183 (Ionics, Inc., Cambridge, Massachusetts) in KCl solutions, characteristic current-voltage curves are \surd shaped; no well-defined plateau was observed (Figure 6). On the other hand, addition of 5 percent (by weight) of soluble sodium polystyrene sulfonate (PSS), molecular weight 30,000 (Dow Chemical Company, Midland, Michigan), causes a characteristic simplification of the curves: with increasing voltage the current rises at first very steeply, and then a long region of much lower and constant slope is observed (Figure 7). The addition of polystyrene sulfonate is believed to reduce the ohmic drop in the depleted

boundary layer and quench the high electric fields otherwise prevailing there, thus permitting us to study the influence of hydrodynamic factors on polarization without the disturbing influences of high ohmic drop and "water-splitting" in the boundary layer.

The slope of the "inclined plateau" regions of the current-voltage curves was found independent of the solution flow rate, but the curves shift to higher current values with increasing flow rate. This suggests that the current in the polarization region is composed of two additive parts, viz:

- (a) a limiting current controlled by mass transfer in the boundary layer (this portion increases with increasing flow rate); and
- (b) a superimposed ohmic leak current due to a parallel conductance element which is almost independent of the flow rate, and is, therefore, probably located within the membrane, rather than in the boundary layer.

When the current of type (b) is eliminated by graphical extrapolation, the (hypothetical) true limiting current is found to increase with a power greater than 0.5 of the flow rate (at linear flow rates above 150 cm min^{-1}) (Figure 12).

It was verified that the slope of the "inclined plateau" regions is not primarily due to variations of boundary layer thickness along the membrane.

Results obtained with membrane CA-1 (Asahi Chemical Company, Figure 8) were similar to those with III BZL 183. Membrane A-101 (American Machine & Foundry Company) also behaved in similar fashion (Figure 9); this membrane exhibited a rapid "poisoning" effect, which seems to be only superficial, because (a) light sanding will restore the original curve, and (b) the current still increases rapidly with increasing flow rate. (With the Ionics membrane, this effect was much slower.) On the other hand, membranes MA-3236 and MA-3475 XL (Ionac Chemical Company) gave current-voltage curves which are little affected by flow rate and indicate high d.c. resistance (Figures 10, 11). It is clear that current-voltage curves thus show significant differences in the polarization behavior of membranes which are similar in permselectivity.

[These conclusions should under no circumstances be viewed as recommendations or condemnations of any of these membrane brands.]

To compare these results to those expected from the simple Nernst-Planck model (Figure 3), equations were derived for the current-voltage curves in the absence and presence of polystyrene sulfonate (Equations 39 and 62 respectively; a list of symbols and units to be used in these equations is found on page 111) and numerical examples calculated for each of these cases. The results are presented in Figures 4 and 5 respectively. The predicted current-voltage curves rise at first linearly and then approach an asymptotic value (plateau) rapidly. This is true whether the membrane is ideally permselective or not. The initial slope does not represent the ohmic resistance alone but also contains contributions from the membrane and junction potential.

From the experimental results, it is clear that for membrane-KCl solution systems the situation is usually much more complicated than predicted by the simple theory. On the other hand, the shape of the current-voltage curves in the presence of "supporting" electrolyte (polystyrene sulfonate, "PSS") comes much closer to the theoretically predicted curves (Figure 14). In this case theory predicts a concentration gradient of K^+ across the boundary about half in magnitude of the gradient of Cl^- , and an inverse gradient of the same magnitude as the K^+ gradient for PSS^- .

Hybrid microelectrodes containing silver-silver chloride and platinum proved useful as potential probes in chloride solutions. Development work on micro pH-electrodes dealt primarily with antimony electrodes. Three-electrode assemblies consisting of two micro-antimony electrodes and a Luggin capillary showed promise for local pH-measurement, but further testing is still necessary. One of the antimony electrodes serves to measure the pH, while the other periodically stimulates the measuring electrode by cyclic polarization.

A large cell was designed for the measurement of current-voltage curves at different locations of electro dialysis membranes, and in the presence of different spacers. Current can be measured in eight sections separately; provision is also made for the insertion of microelectrodes. Redox solutions can be used in the electrode compartments in order to reduce the voltage drop in them; laboratory experiments in a small cell

indicated that a sufficiently high voltage drop reduction is indeed possible.

Surface roughness of three commercial ion-exchange membranes was measured and considerable differences found (Figure 21). The roughness is at least of the same order of magnitude as the calculated boundary layer thickness, and might therefore play a significant part in the flow dynamics past the membrane.

The electrochemical studies were supplemented by laser interferometry of the interface. A wedge interferometer (Figures 18 and 19) was designed and built, which enabled us to observe polarization under conditions of natural convection and at low flow rates (laminar flow). The nature of the concentration polarization occurring near the interface is illustrated in Figure 20 which shows the concentration distribution in the micro-electrodialysis cell, built into an O'Brien laser wedge interferometer, before and during the passage of electric current. The interference fringes are roughly equal to concentration-distribution curves. The existence of depleted boundary layers in the central (diluate) compartment and of concentration enrichment in the adjacent compartments could be studied by preparing motion pictures of the phenomenon.

Radio-frequency measurements of different anion-exchange membranes were performed in a cell (Figure 22) containing consecutive layers of membrane and demineralized water. The influence of the transmission line was eliminated from the results by measuring membrane-solution stacks of different thickness (Figures 23, 24). After subtraction of the complex impedance of water, a dispersion of dielectric constant and conductivity of the membrane between 1 and 20 megacycle sec^{-1} was found (Figures 25-27). It is probable that this is a Maxwell-Wagner type dispersion and thus indicative of membrane heterogeneity. The dielectric constant of the membrane tends asymptotically to about 40 at the higher frequencies. Although the water layers separating the membranes were only 1/64-inch thick, their complex impedance in the frequency range 1-20 megacycle sec^{-1} is high; this reduces the accuracy of the results shown in Figures 25-27. The conclusions from these measurements should therefore be considered preliminary.

Electrical potential differences across modified cellulose acetate membranes (Loeb-Sourirajan type) were measured (Figures 28-30).

Streaming potentials had been observed previously in reverse osmosis experiments with ion-exchange membranes where the mechanism can be readily explained by the fixed-charge nature of these materials. It was found, however, that potential differences develop even across seemingly neutral modified cellulose acetate membranes, and that these potential differences depend on the applied pressure and the brine circulation rate. Sodium chloride solutions were circulated under pressure through a 6-inch long tubular reverse osmosis membrane (modified cellulose acetate type) cured at 94°C which contained a central Ag/AgCl electrode. The inside of the cylindrical support tube for the membrane was coated with silver and silver chloride, and thus acted as a second electrode which was completely insulated from the electrode inside the tube. Measurements of the potential difference between the electrodes as a function of pressure and circulation rate were performed. Hyperfiltration rates and product concentration were determined at the same time.

The results (Figures 31-36) show that the potential differences increase with the pressure at a rate of 8-10 millivolt/100 psi. The potential differences also increase with the circulation rate, this variation being most pronounced at the lowest flow rates. In all of these experiments, the low-pressure side was always positive.

After correction for the difference of the electrode potentials, the potential differences represent the algebraic sum of the junction potential between the bulk brine and the polarization layer, and the membrane streaming potential proper. By systematic variation of pressure, circulation rate and concentration, it might prove possible to separate these effects and obtain quantitative experimental data on the concentration in the polarization layer. A test apparatus permitting circulation of raw water under high pressure with suitable make-up pumps and prepurification devices was designed and built for future studies along these lines.

A theory of hyperfiltration, based on non-equilibrium thermodynamics, was developed jointly with Q. Kedem. The theory pinpoints criteria for salt-rejecting membranes; it does not deal with concentration polarization. The equations for water and salt flux across a differential membrane layer were derived from first principles, and integrated across

the membrane, assuming constancy of three coefficients, viz. the specific hydraulic permeability, \mathcal{D}_1 , the local solute permeability, \bar{P} , and the reflection factor, σ , which is known to be a quantitative index of salt rejection, varying from zero to unity (for non-rejecting to perfect membranes respectively). This procedure was justified by considerations based on the friction model of membrane transport processes. It was shown that $1 - \sigma$ is the product of an equilibrium term and a kinetic term. The first characterizes the static salt exclusion and hydrophilic properties of the membrane. The second is a quantitative expression for the kinetic characteristics of the membrane. This theory was published⁽⁶⁰⁾ and is not repeated in this report.

III. ELECTRODIALYSIS

III.A. Current-Voltage Curves

III.A.1 Introduction

When the voltage across an electro dialysis stack is raised, the current increases at first roughly in proportion to the voltage; the apparent resistance of the stack increases, however, and eventually a point is reached at which large voltage increments cause only small current increases. At this point, or near it, pH changes appear in brine and product streams. These phenomena, usually lumped into the single term "polarization," are caused by mass transfer limitations assumed to occur at the membrane-solution interfaces, and to the undesirable participation of hydrogen and hydroxyl ions in the electric conduction process; this effect is often called "water splitting." Polarization in electro dialysis sets an upper limit to the practical current density because of high power consumption and/or scale formation and, therefore, also limits the production rates. In many cases polarization thus prevents the optimal utilization of the capital investment in the electro dialysis plant.

Analysis of the limiting current phenomenon at membrane-solution interfaces ⁽¹⁻⁹⁾ revealed some analogy to polarographic situations at metal-solution interfaces ⁽¹⁰⁻¹²⁾. On both interfaces non-ohmic behavior in the vicinity of the electrode is due to a change of conduction mechanism. At the metal-solution interface this change is a radical one: not only does the transport number of the negative (and positive) current carriers change, but the nature of the current carriers themselves in the two phases, viz. ions and electrons, is different. At the membrane-solution interface, on the other hand, there is only a change of transport number, not of the basic character of the current carriers. Yet a change of transport number at any phase boundary is sufficient to cause non-ohmic behavior at that interface, and, ultimately some form of limiting current phenomenon.

While polarographic theory, based on the Nernst-Planck equations of ion migration, describes the current-voltage relationship for many metal-solution interfaces well, several important questions remain to be answered for membrane-solution interfaces. The equations for the current-voltage curves developed in detail under "Theory" (Section III.A.3), and the

shorter treatments in the literature^(4,6) all lead to the conclusion that a limiting current should be reached, in close analogy with polarography.* Moreover, cation-selective and anion-selective membranes should obey analogous equations, provided the basic assumption of all these treatments is correct viz. that the polarization phenomenon occurs in the dilute solution layer which is in contact with the membrane. In actual fact, however, different membranes exhibit considerable differences of polarization behavior. In particular, no well-defined limiting current plateaus are observed with anion-exchange membranes; and "water splitting" sets in at much lower voltages at these membranes than at cation-exchange membranes. Because anion-exchange membranes thus present more problems than cation-exchange membranes, we have concentrated our efforts on the study of the former.

Polarographic theory shows that without a large excess of "neutral" electrolyte which quenches the electrical field in the diffusion layer, well-defined limiting current plateaus over long voltage regions can not be expected. "Neutral" electrolytes are composed of ions which are not discharged in the potential range investigated. In order to study limiting currents at membrane-solution interfaces without undue interference of water splitting, one wishes to achieve a similar neutral electrolyte effect at the membrane-solution interface. This is particularly important if the influence of hydrodynamic factors on polarization is to be studied quantitatively. Since this is our purpose, we have tried to simulate the neutral electrolyte effect in polarography by adding to the solutions large, soluble polyelectrolyte ions which increase the solution conductivity but can not pass through the membrane. (Of course, the polyelectrolyte must also be non-poisonous to the membrane.) In a number of the experiments described in the following, the polyelectrolyte was sodium polystyrene sulfonate of nominal molecular weight 30,000^{**}. The addition of polyelectrolyte was indeed found to have an appreciable effect in the predicted direction on the current-voltage curves.

* If the electrode has a large surface, certain deviations from a constant plateau are to be expected because of hydrodynamic factors,^(2-3,8-10) but the observed deviations are frequently much larger (see Section III.A.4).

** Thanks are due to the Dow Chemical Company, Midland, Michigan, for the supply of this material and information on its properties.

III.A.2 Experimental

Figure 1 is a schematic of the apparatus used for the polarization studies. The cell [outside dimensions 13.5 horizontal (i.e., in direction of current) x 10 x 10 cm] is subdivided into four compartments which were continuously flushed with solutions moved by peristaltic circulation pumps (Model T-6S, Sigamotor Company, Middleport, New York) or, in the later experiments by corrosion-proof centrifugal pumps (Catalogue No. 7004-3, Cole Parmer Company, Chicago, Illinois). The circulation circuits also contained liquid reservoirs and small "accumulators" to buffer flow rate fluctuations. Flow rates were measured volumetrically first, but rotameters were installed at an early stage for continuous reading. In some experiments, microstirrers, provided with small rotating seals were inserted into the two center compartments, to provide additional fluid agitation.

In the center of the cell, a strip of ion-exchange membrane, M, 5 x 1 cm is exposed. The membrane compartments are separated from the electrode compartments by cellulose membranes, C (dialyzer tubing, Fisher Scientific Company, Pittsburgh, Pennsylvania). Electric current is fed into the cell through platinized platinum electrodes, Pt. The voltage-regulated power source was converted to near-galvanostatic operation by introducing a large variable resistor in series. Currents were read by means of a precise multi-range milliammeter, A, and the voltage between the platinum electrodes periodically checked by a high-impedance voltmeter, V, (microvolt-ammeter, Model 203A, Cohu Electronics, San Diego, California, or, later, with a Keithley Electrometer 610B).

The polarization voltage was measured by means of the probe micro-electrodes, P, which were Ag/AgCl electrodes prepared first by the thermal-electrolytic method⁽¹³⁾, and later hybrid platinized platinum-Ag/AgCl electrodes⁽¹⁴⁾ which yield very stable and reproducible potentials (see Section III.C). Their wires were sealed in glass capillaries and only the tips, of characteristic dimension 1 mm, were exposed. In Figure 1 these electrodes are shown in vertical position, for clarity, but in the actual cell they are inserted at 90° to the position shown (i.e., the wires are normal to the plane of the drawing). The probe electrode voltage was recorded by a "Serviter II" (Texas Instruments, Houston, Texas) of full scale sensitivity 1 mv and speed 0.25 sec full scale, after amplification or attenuation in a high-impedance amplifier-attenuator (the same

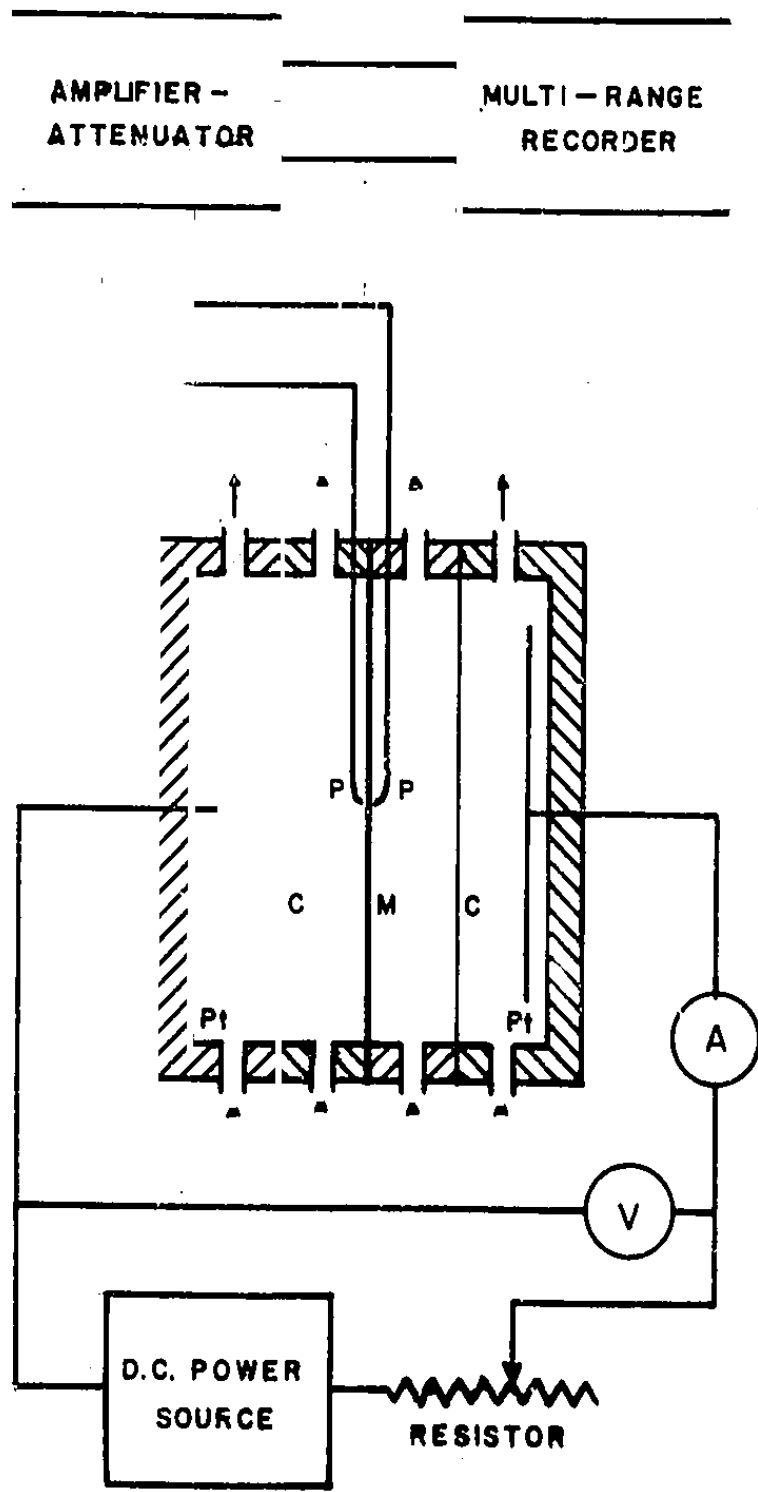


FIGURE 1. SCHEMATIC OF POLARIZATION MEASUREMENT APPARATUS

instrument, V , as used for voltage measurement was used, with the recorder connected to the microvolt-ammeter recorder output; the switching arrangement, as well as various minor attenuating potentiometer circuits are not shown in the schematic of Figure 1). The inclusion of the vacuum tube amplifier-attenuator was deemed necessary because it draws much less current than the recorder. The dimensions of the solution compartment are shown in Figure 2.

Current-voltage curves are determined by increasing the current stepwise and observing the change of voltage, V_p , between the microprobe electrodes. Upon application of a higher current, the voltage increases rapidly and after a period varying between a few seconds to two minutes (depending on flow rate, concentration, current, etc.) settles to a constant value. In many experiments, a slow increase of voltage rather than a constant value was observed, in which cases the voltage was extrapolated to zero time, i.e., to the moment at which the current was increased. Satisfactory constancy with respect to time was generally observed at low and high currents, while voltages in the intermediate region were less stable. There was also more voltage oscillation in this range. A number of experiments were performed with motorized linear current scan by driving the resistor in Figure 1 by a geared motor, and covering the full range in about 20 minutes. Most experiments reported here were obtained by the point-by-point procedure, however.

Solutions

Amount and composition of the circulating solutions were chosen such that mass transport through the dialyzer membranes during the experiment caused only very small concentration changes in the various streams. This was verified by analysis of the streams at the end of each experiment.

KCl solutions were prepared from analytical grade material and de-ionized water, and a trace of silver nitrate added to ensure saturation with respect to AgCl and thus prevent dissolution of AgCl from the microelectrodes.

Originally the solutions from the two electrode compartments were pumped from and into a common reservoir, and a similar procedure was followed for the solutions pumped past the membrane faces. In order to eliminate altogether external shorts, the solutions were later pumped in

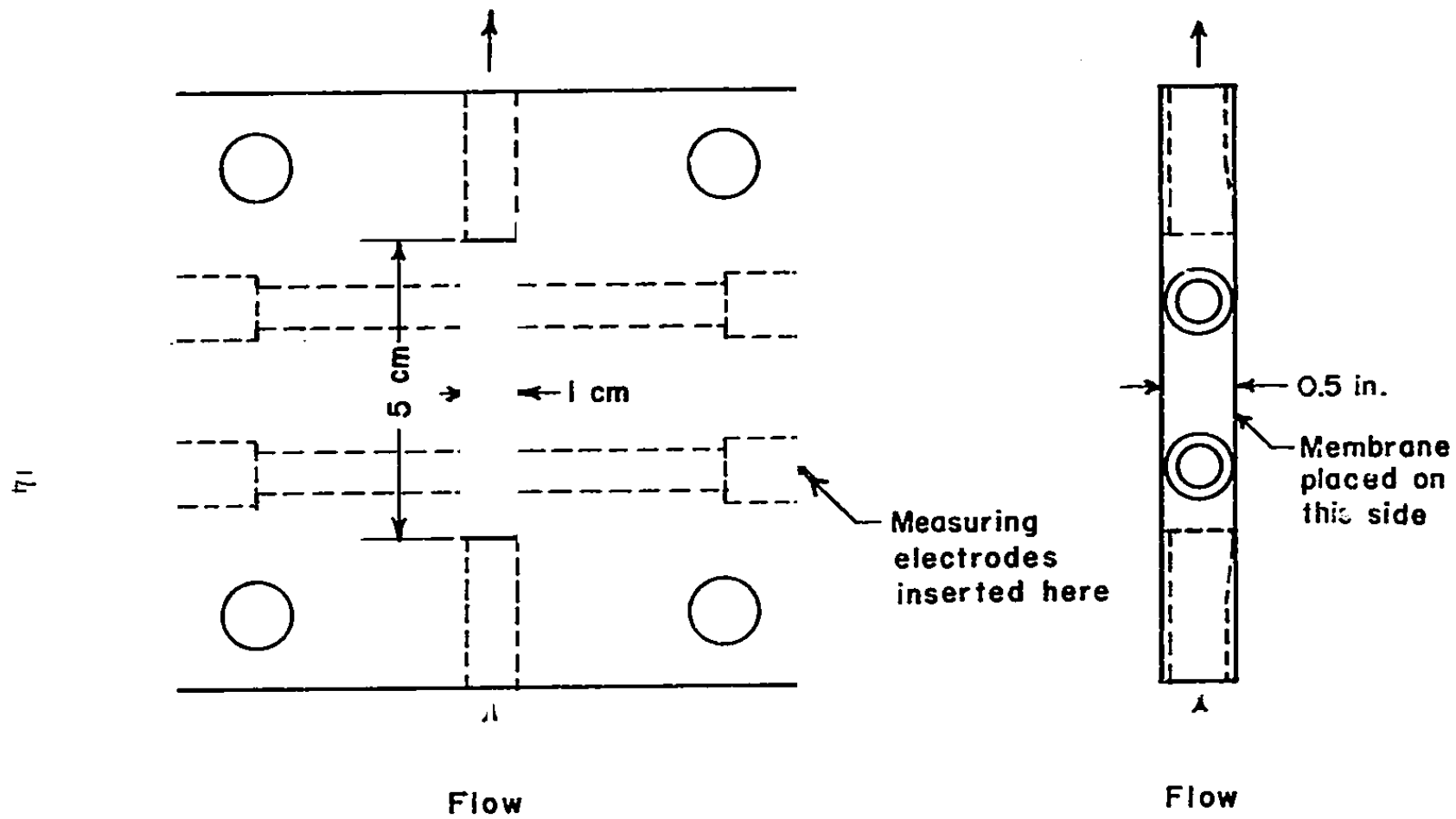


FIGURE 2. SOLUTION COMPARTMENT OF LABORATORY CELL FOR CURRENT-VOLTAGE CURVES

individual streams. It was found that any external shorts in the early experiments were so small, as not to warrant major efforts of correcting the reported results. The total solution inventory associated with each stream was about one liter.

The sodium polystyrene sulfonate (PSS) solutions supplied by the Dow Chemical Company contained about 5 percent (by weight) polymer of approximate molecular weight 30,000. They also contained much sodium bromide, which we removed by dialysis through Fisher dialyzer tubing until free of reaction with AgNO_3 . To remove the water which enters the polyelectrolyte solution during dialysis, the dilute solution was restored to its original volume by vacuum distillation. The resistivity of the purified solution at ambient temperature is 160 ohm cm (60 cycle a.c.).

The kinematic viscosity of the PSS solutions was determined with both a Seybolt and a Cannon-Fenske Viscometer. The results were 6.5 and 5.2 centistoke respectively. The measurements were performed at different times, and since it is known that some changes occur in the PSS solution, the discrepancy was not considered serious. In the following, we shall use a value of $\nu = 6.0$ centistoke, assigning somewhat higher weight to the more accurate Cannon-Fenske method. (Non-Newtonian behavior may also contribute to the discrepancy.)

Using this value, we can calculate the Reynolds number at the different flow rates used. The channel cross section was 1 cm wide \times 1.25 cm deep (length 5 cm), hence ratio, $r \equiv$ cross section/perimeter $= 0.278$ cm. Hence the Reynolds number, Re , for a linear flow rate, v , of 2.5 cm sec^{-1} is $Re \equiv 4vr/\nu = 4 \times 2.5 \text{ cm sec}^{-1} \times 0.278 \text{ cm} / 6.0 \times 10^{-2} \text{ cm}^2 \text{ sec}^{-1} = 46$. For velocities of 1.25 and 3.75 cm sec^{-1} we have $Re = 23$ and 70 respectively.

The magnitude of these Reynolds numbers indicates laminar flow conditions, but it should be noted that the small cell did not permit well-defined hydraulic conditions.

Membranes

The anion-exchange membranes used in this work were the following:

- A 101 B American Machine and Foundry Company, Springdale, Connecticut*
- CA - 1 Asahi Chemical Company, Tokyo, Japan*
- MA 3236 } Ionac Chemical Company, Birmingham, New Jersey*
- MA 3475 XL }
- 111 BZL 183 Ionics, Inc., Watertown, Massachusetts**

*Thanks are due to the manufacturers for supplying samples of these materials.

**Samples cut from replacement membranes for the Ionics Mark II stack in the electro dialysis pilot plant of the Sea Water Conversion Laboratory.

In the past, polarization at membrane-solution interfaces has been treated quantitatively from the standpoint of the classical theory of transport in electrolyte solutions, (Nernst-Planck equations), and assuming membrane selectivity, i.e., a radical change of ionic transport number at the interface^(1-3,6,9,15). It was either assumed or tacitly implied that the membrane is more or less homogeneous in the sense of not having a layered structure. Since our results, reported in the previous and the present quarterly report, and some recent observations by others^(8,17) indicate that matters are by no means so simple, it was deemed desirable to determine in detail what to expect from the consistent application of this simplified picture, so as to better understand the causes of the deviations therefrom. In particular it was considered important to derive expressions for the current-voltage curves both in the presence and absence of "supporting" (neutral) electrolyte; these curves can then be compared to the experimental ones. This treatment is presented in the following. It leads to equations for the current-voltage curves [Equation (39) and (62) for these two cases respectively]. The treatment contains many elements of the subject matter in references 1-3,6,9,15, and 16, which are used at various stages so as to lead to useful expressions for the polarization curves in terms of measurable parameters.

Ion Flux in Absence of Supporting Electrolyte

Consider steady-state ion transport in the solution in the boundary layer at the membrane-solution interface. The solution flushing rate is fast enough so that the bulk electrolyte concentration is not appreciably depleted along the membrane. It is also assumed that the hydraulic flow conditions are chosen such that variation along the membrane can be neglected. In this case, the solution concentration profile in the boundary is time-invariant and also does not vary along the membrane. This highly simplified picture is schematically shown in Figure 3 which depicts the membrane-solution boundaries at an anion-exchange membrane. The configuration corresponds to that in our laboratory cell [but the inert membranes separating the electrode compartments from the test compartments (Figure 1) and the probe electrodes are not shown in Figure 3]. Note that

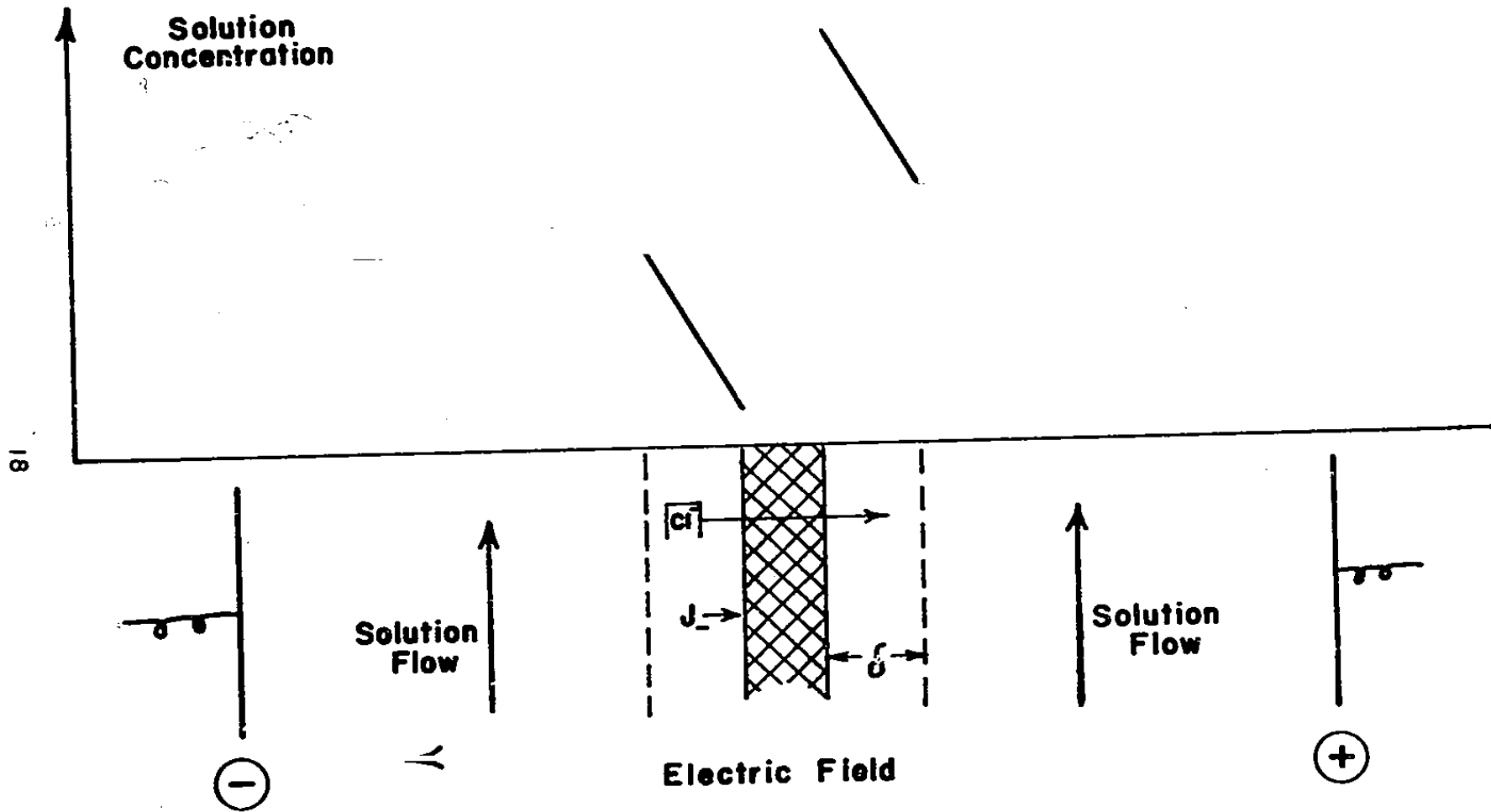


FIGURE 3. SCHEMATIC OF FIELD AND ION FLOW AT ANION-EXCHANGE MEMBRANE

when positive current flows from left to right, the current density i is taken positive. But in Figure 3 most of the current is carried by negative ions flowing from left to right; therefore, i is a negative quantity. Electric potential gradients are taken as potential on the right minus potential on the left divided by the distance. Therefore, in Figure 1, the electric potential gradient is positive.

Neglecting non-electrostatic interaction between the ions, and also neglecting electroosmosis, we can describe the ion fluxes, J , as products of respective mobilities,* m , concentrations, c , and forces (sums of potential gradients):**

$$J_+ = - \underbrace{(D_+/RT)}_{m_+} c_+ \left[z_+ \mathfrak{F}(dE/dz) + (d\mu_+/dz) \right] \quad (1)$$

$$J_- = - \underbrace{(D_-/RT)}_{m_-} c_- \left[z_- \mathfrak{F}(dE/dz) + (d\mu_-/dz) \right] \quad (2)$$

Because of electroneutrality in the solution phase

$$c_+ = c_- = c \quad (3)$$

For ideal solutions

$$\mu = \mu^\circ + RT \ln c \quad (4)$$

and therefore, for a dilute solution of a 1-1 electrolyte:

$$J_+ = - D_+ \left[(\mathfrak{F}/RT) c (dE/dz) + (dc/dz) \right] \quad (5)$$

$$J_- = - D_- \left[(-\mathfrak{F}/RT) c (dE/dz) + (dc/dz) \right] \quad (6)$$

In the membrane, the numerical value of the flux ratio, J_+/J_- , is equal to the transport number ratio \bar{t}_+/\bar{t}_- . Since, by definition of the

*The mobilities m_+ , m_- are equal to (D_+/RT) , (D_-/RT) respectively by the Nernst-Einstein law. D_+ , D_- are the respective ionic diffusion coefficients.

**For meaning of symbols and suggested set of consistent units, see list of symbols on page III.

steady state, the fluxes are independent of position z , the same flux ratio prevails also in the solution:

$$J_+/J_- = -\bar{t}_+/\bar{t}_- = -\bar{t}_+/(1 - \bar{t}_+) \quad (7)$$

(The negative sign is introduced because the J 's are vectors. In the membrane J_+ and J_- have opposite signs, while \bar{t}_+ and \bar{t}_- are always taken positive.)

From (5), (6) and (7):

$$-\frac{\bar{t}_- J_+}{\bar{t}_+ D_-} = \frac{\mathcal{F}c}{RT} \frac{dE}{dz} - \frac{dc}{dz} \quad (8)$$

From equation (8) substitute for $(\mathcal{F}c/RT) (dE/dz)$ in equation (5), and solve for J_+ :

$$J_+ = \frac{-2D_+}{1 - (D_+ \bar{t}_- / D_- \bar{t}_+)} \frac{dc}{dz} \quad (9)$$

and from (9) and (7)

$$J_- = \frac{2D_-}{1 - (D_- \bar{t}_+ / D_+ \bar{t}_-)} \frac{dc}{dz} \quad (10)$$

Since fluxes, ionic diffusion coefficients and membrane transport numbers are constant, it follows that dc/dz is constant also. In other words, the application of the Nernst-Planck equations [equations (5) and (6)] leads to a linear concentration gradient in the boundary.

It is often more convenient to express the fluxes in terms of the diffusion coefficient of the electrolyte, D , rather than the ionic diffusion coefficients, D_+ and D_- . Noting that in free solution

$$D_+/D_- = t_+/t_- = t_+/(1 - t_+) \quad (11)$$

and using the Nernst expression* for the diffusion coefficient of 1-1 electrolyte in dilute solution

*Equation (12) follows readily from the flux equations (5) and (6) because for electrolyte diffusion $J_+ = J_-$.

$$D = \frac{2D_+ D_-}{D_+ + D_-} = 2 \left(\frac{1}{D_+} + \frac{1}{D_-} \right)^{-1} = 2D_+ (1 - t_+) \quad (12)$$

we can rewrite equations (9) and (10) respectively:

$$J_+ = - \frac{2D_+}{1 - (t_+ \bar{t}_- / t_- \bar{t}_+)} \frac{dc}{dz} = - \frac{2D_+ (1 - t_+) \bar{t}_+}{\bar{t}_+ - t_+} \frac{dc}{dz} = - \frac{D \bar{t}_+}{\bar{t}_+ - t_+} \frac{dc}{dz} \quad (13)$$

$$J_- = - \frac{D \bar{t}_-}{\bar{t}_- - t_-} \frac{dc}{dz} = \frac{D \bar{t}_-}{\bar{t}_+ - t_+} \frac{dc}{dz} \quad (14)$$

For ideally selective cation-exchange membranes $\bar{t}_+ = 1$. Hence from equations (13) and (14):

$$J_+ = \frac{D}{t_-} \frac{dc}{dz}; \quad J_- = 0 \quad \text{Ideal c.e. membrane} \quad (15)$$

and for ideally selective anion-exchange membranes ($\bar{t}_- = 1$)

$$J_+ = 0; \quad J_- = - \frac{D}{t_+} \frac{dc}{dz} \quad \text{Ideal a.e. membrane} \quad (16)$$

It is of interest to digress here and compare equation (15) to the basic polarographic equation for a univalent cation, Cat^+ ,

$$J_+ = - D_+^{\text{Cat}} \frac{dc^{\text{Cat}}}{dz} \quad (17)$$

Here D_+^{Cat} and c^{Cat} are the ionic diffusion coefficient and molar concentration of Cat^+ respectively. This polarographic equation is readily obtained from equation (5) because, in a formal sense, we can consider the mercury-solution interface as ideally selective for cations Cat^+ , since no other ions can pass through it. Moreover, we set $(dE/dz) = 0$, because in polarographic experiments, a large excess of neutral electrolyte is usually added to the solution. This neutral electrolyte can not cross the metal-solution interface, but "quenches" the electric field in the solution.

Note that both equations (15) and (17) are of the type of Fick's law, but in the absence of neutral electrolyte the ratio D/t_- replaces the ionic diffusion coefficient D_+^{Cat} . Thus comparing the flux of common cations, e.g. K^+ or Na^+ in the absence and presence of neutral electrolyte it is found that the flux is higher in the absence of the neutral electrolyte, because the electric field provides additional driving force. This simple conclusion has indeed been amply confirmed in the polarographic literature.

Returning to the ion fluxes in the absence of neutral electrolyte [equations (13) and (14)], we can calculate the electric current density, i , from Faraday's law:

$$i = z(J_+ - J_-) \quad (18)$$

Substituting the fluxes from equations (13) and (14) we obtain

$$i = - \frac{z D}{(\bar{t}_+ - t_+)} \frac{dc}{dz} = \frac{z D}{(\bar{t}_- - t_-)} \frac{dc}{dz} \quad (19)$$

Since i , D and the transport numbers are constants, this confirms the previous conclusion that, within the range of applicability of the Nernst-Planck equations, the concentration gradient in the boundary layer is linear.

As the current is increased, the electrolyte concentration at the membrane interface decreases continuously. Hence the highest current carried by the ion fluxes J_+ and J_- is (for $dc/dz = -c_0/\delta$)

$$i_{lim} = \frac{z D}{(\bar{t}_+ - t_+)} \frac{c_0}{\delta} = - B c_0 / \delta \quad (20)$$

where c_0 is the bulk electrolyte concentration and $B \equiv -zD/(\bar{t}_+ - t_+)$.

Ohmic Potential Drop in the Boundary Layer

The complex hydraulic pattern is approximated by the simplified Nernst model of a boundary of uniform thickness, δ between the region of fast-flowing solution of uniform composition, c_0 , and the membrane surface. Mass transport in this boundary layer is by diffusion only

(Figure 3). The boundary layer thickness on the two membrane faces is assumed to be the same.

To calculate the resistance of unit cross section of this boundary layer, we perform an integration over its thickness, δ ,

$$\mathcal{R} = -\Delta E_b / i = \int_0^{\delta} \rho dz \quad (21)$$

The negative sign is introduced in Ohm's law because for positive potential drop the current is in the negative direction. The current density i is the same at any location z .

We can express the specific resistance ρ by the following expression (valid in dilute solution)

$$\rho = (c\lambda)^{-1} \quad (22)$$

where λ is the equivalent conductance of the electrolyte ($\text{ohm}^{-1} \text{cm}^2 \text{equiv.}^{-1}$),* and dz , from equation (19):

$$dz = - \frac{\mathcal{F} D}{i(\bar{t}_+ - t_+)} dc = (B/i) dc \quad (23)$$

where the constant B , which depends only on the nature of the dissolved electrolyte and of the membrane, is defined as

$$B \equiv - \mathcal{F} D / (\bar{t}_+ - t_+) = \mathcal{F} D / (\bar{t}_- - t_-) \quad (24)$$

Substituting the values for ρ and dz respectively in (21) we obtain

$$-\Delta E_b = \int_0^{\delta} \frac{B}{c\lambda} dc \quad (25)$$

*The formula given in most of the electrochemical literature is $\rho = 1000(N\lambda)^{-1}$ where N is the normality, equiv. liter^{-1} . Note that in our system of units, c is given in mole cm^{-3} , which, for a 1-1 electrolyte, is equal to equiv cm^{-3} . Hence $N/1000 = c$ and equation (22) is identical with the formulae in the literature.

For the left boundary, we integrate from c_o [at the (hypothetical) plane interface of bulk solution and boundary layer] to c_m^i at the membrane surface:

$$\Delta E_b^i = - (B/\lambda) \ln (c_m^i/c_o) \quad (26)$$

To eliminate c_m^i which is not accessible to direct measurement, we remember that the concentration gradient in the boundary layer is linear, and use equation (19):

$$\frac{dc}{dz} = \frac{c_m^i - c_o}{\delta} = - \frac{i(\bar{t}_+ - t_+)}{zD} = - \frac{i}{B} \quad (27)$$

We solve for c_m^i :

$$c_m^i = c_o + \delta i/B \quad (28)$$

and substitute this value in equation (26):

$$\Delta E_b^i = - (B/\lambda) \ln \left(1 + \frac{\delta i}{Bc_o} \right) = - (B/\lambda) \ln \left(1 - \frac{i}{i_{lim}} \right) \quad (29)$$

For the boundary on the right side we integrate equation (25) from c_m^n (concentration at the membrane surface) to c_o at the (hypothetical) plane interface between diffusion boundary and bulk solution on the right:

$$\Delta E_b^n = - (B/\lambda) \ln (c_o/c_m^n) \quad (30)$$

c_m^n is obtained in analogy with equations (27) and (28):

$$c_m^n = c_o - \delta i/B \quad (31)$$

and hence from equations (30) and (20):

$$\Delta E_b^n = (B/\lambda) \ln \left(1 - \frac{\delta i}{Bc_o} \right) = (B/\lambda) \ln \left(1 + \frac{i}{i_{lim}} \right) \quad (32)$$

In equations (29) and (32) the influence of the different process parameters has been clearly separated: δ is indicative of the hydraulic flow conditions; λ , B and c_o describe the physico-chemical properties of

solutions and membrane; i is the applied current density. Note that when negative ions flow from left to right, the current is counted negative. Hence both equations (29) and (32) yield positive electric ohmic drops, as they should. For $i \rightarrow 0$, the ohmic drop goes to zero. For $i \rightarrow i_{lim}$ [equation (20)] the ohmic drop tends to infinity.

Membrane Potentials

The potential difference across a membrane in contact with a 1-1 electrolyte solution of concentration c_m^i on the left and c_m^n on the right is⁽¹⁶⁾

$$\Delta E_m = (RT/\bar{z})(\bar{t}_- - \bar{t}_+) \ln (c_m^n/c_m^i) = \bar{c} \ln (c_m^n/c_m^i) \quad (33)$$

where
$$\bar{c} \equiv (RT/\bar{z})(\bar{t}_- - \bar{t}_+) \quad (34)$$

Here, again, potential differences are counted positive when the right side is more positive than the left.

If the hydraulic conditions on the left and right sides of the membrane are the same, the concentration excess (over the bulk concentration) on the concentrate side equals the concentration depletion on the diluate side.* This excess is calculated from equation (27):

$$c_m^n - c_o = c_o - c_m^i = -i\delta/B \quad (35)$$

Hence equation (33) can be written in terms of measurable quantities

$$\Delta E_m = \bar{c} \ln \frac{c_o - \delta i/B}{c_o + \delta i/B} = \bar{c} \ln \frac{1 - \delta i/(Bc_o)}{1 + \delta i/(Bc_o)} = \bar{c} \ln \frac{1 + (i/i_{lim})}{1 - (i/i_{lim})} \quad (36)$$

Junction Potentials

In addition to the membrane potentials (concentration potentials across the membrane), there exist also concentration potentials in the boundary layers, unless the electrolyte has equal positive and negative transport number (e.g. KCl).

*Because, for equal boundary layer thickness, the same driving force is necessary to remove ions from the membrane-concentrate interface as to transport them to the membrane-diluate interface.

The junction potentials are given by expressions similar to (33) with solution transport numbers, t , rather than transport numbers in the membrane, \bar{t} , however⁽¹⁶⁾. The sum ΔE_j of the junction potentials in the two boundary layers is

$$\Delta E_j = (RT/\bar{z})(t_- - t_+) [\ln (c_m^i/c_o) + \ln (c_o/c_m^n)] = -C(t_- - t_+) \ln (c_m^n/c_m^i) \quad (37)$$

where $C \equiv (RT/\bar{z})(t_- - t_+) \quad (38)$

Total Potential Drop

The potential drop between identical probe electrodes in the bulk solution phases on opposite sides of the membrane (Figure 1) is composed of (a) ohmic drops in the bulk solutions, the membrane and the boundary layers, and (b) membrane potential, junction potentials and electrode potentials.

The ohmic potential drops [listed under (a)] should vanish rapidly when the current is interrupted. The other potential drops are expected to relax more slowly, because the relaxation depends on ionic diffusion which is a slower process than the electronic processes which terminate the ohmic potential drop measured with well-reversible probe electrodes.

We have assumed that the solution flow past the electrodes is fast enough so that the difference in the bulk solution concentrations on the two sides of the membrane is negligible. Hence the electrode potentials cancel. It will also be assumed that the resistance of the membrane and the transport numbers \bar{t} in it are independent of the current density.* Hence the ohmic potential drop in the membrane, $-R_m i$ is proportional to the current. So is the drop, $-R_s i$, in the solution between each electrode and the adjacent boundary layer.

* While this assumption has been frequently made in the literature, some recent experiments indicate that it should not remain unquestioned.

The potential drop across unit cross section is [from equations (26), (30), (33), (37) and (35)]

$$\begin{aligned}
 \Delta E &= - (2R_s + R_m) i + (\Delta E_b^i + \Delta E_b^R) + \Delta E_m + \Delta E_j \\
 &= - (2R_s + R_m) i + (B/\lambda) \ln (c_m^R/c_m^i) + \bar{C} \ln (c_m^R/c_m^i) - C \ln (c_m^R/c_m^i) \\
 &= - (2R_s + R_m) i + [(B/\lambda) + \bar{C} - C] \ln \frac{1 - i\delta/(Bc_o)}{1 + i\delta/(Bc_o)} \\
 &= - (2R_s + R_m) i + [(B/\lambda) + \bar{C} - C] \ln \frac{1 + (i/i_{lim})}{1 - (i/i_{lim})} \quad (39)
 \end{aligned}$$

It is seen that the total potential drop is the sum of two terms, one linear in i and the other a logarithmic function of i . It is of interest that the ohmic drops in the boundary layers which are of dissipative nature are contained in the second term together with the membrane and junction potentials which are (at least partially) "reversible."

At low currents ($i \ll Bc_o/\delta$) equation (39) shows that the voltage is proportional to the current. Hence the initial slope of the E vs. $-i$ plot is

$$(-\Delta E/i) = 2R_s + R_m + [(B/\lambda) + \bar{C} - C][2\delta/(Bc_o)] \quad (40)$$

On the other hand, as i approaches the limiting current, the logarithmic term becomes dominant, $-\Delta E$ going to infinity as $i \rightarrow i_{lim}$ [equation (20)].

Numerical Example

It is of interest to consider the predictions of equation (40). Any deviations therefrom in the experimental results can then be attributed to the three main assumptions implicit in its derivation, namely (a) validity of the Nernst-Planck equations without interaction terms [equations (5) and (6)] and (b) assumption of a diffusion boundary layer of constant thickness (under conditions of forced flow) and (c) no polarization effects within the membrane. The equation is also based on conductance by a single $1-1$ electrolyte and can not be expected to hold

when an appreciable portion of the conductance is due to hydrogen and hydroxyl ions (at high voltages).

In the following numerical example, all parameters for the solution are adjusted to ideal-solution behavior (i.e. for intensive properties such as equivalent conductance and diffusion coefficient the values at infinite dilution are consistently taken). Reference is made to the situation shown in Figure 3, i.e. an anion exchange membrane with negative ion flux from left to right. Therefore the current is negative.

Temperature: 25°C (298°K)

Solution: KCl , 0.03N , ($c = 3 \times 10^{-5}$ mole cm^{-3})

$$\lambda = 150 \text{ ohm}^{-1} \text{ cm}^2 \text{ mole}^{-1}; \text{ spec. conductance}$$

$$= 4.5 \times 10^{-3} \text{ ohm}^{-1} \text{ cm}^{-1}$$

$$t_+ = 0.50 \quad (t_- = 0.50)$$

$$D = 2.0 \times 10^{-5} \text{ cm}^2 \text{ sec}^{-1}$$

Membrane: Resistance of unit area $R_m = 11 \text{ ohm cm}^2$

$$\bar{t}_- = 0.98 \quad (\bar{t}_+ = 0.02)$$

Boundary Layer: $\delta = 0.02 \text{ cm}$

Solution between Probe Electrode and Boundary Layer:

Assume resistance is equivalent to layer of 0.1 cm thickness

$$\text{i.e. } R_s = \rho \times 0.1 = [1 / (0.0045 \text{ ohm}^{-1} \text{ cm}^{-1})] \times 0.1 \text{ cm} = 22.2 \text{ ohm cm}^2$$

Universal Constants:

$$R = 8.32 \text{ watt sec mole}^{-1} (\text{°K})^{-1}$$

$$\mathcal{F} = 0.96 \times 10^5 \text{ coul mole}^{-1}$$

Other Expressions:

$$B = zD/(\bar{f}_- - t_-) = 0.96 \times 10^5 \text{ coul mole}^{-1} \\ \times 2 \times 10^{-5} \text{ cm}^2 \text{ sec}^{-1} / (0.98 - 0.5) \\ = 4.00 \text{ amp mole}^{-1} \text{ cm}^2$$

$$\bar{C} = (RT/z)(\bar{f}_- - \bar{f}_+) = 0.0258 (0.96) = 0.0248 \text{ volt}$$

$$C = (RT/z)(t_- - t_+) = 0$$

$$-(i/i_{lim}) = (i\delta/Bc_0) = \frac{0.02 \text{ cm} \times i \text{ amp cm}^{-2}}{4.00 \text{ amp mole}^{-1} \text{ cm}^2 \times 3 \times 10^{-5} \text{ mole cm}^{-3}} = 167 \times i$$

Using these values, equation (39) becomes

$$\Delta E = - (2R_s + R_m) i + [B/\lambda] + \bar{C} - C \ln \frac{1 - [\delta/(Bc_0)] i}{1 + [\delta/(Bc_0)] i}$$

$$\Delta E = - (44.4 + 11) i + 10^{-3} (26.7 + 24.8) \ln \frac{1 - 167 i}{1 + 167 i} \\ = - 55.4 i + 51.5 \times 10^{-3} \ln \frac{1 - 167 i}{1 + 167 i}$$

A plot of the first and the second terms of this equation, as well as their sum is shown in Figure 4. Note that the limiting slope, $\lim_{i \rightarrow 0} \Delta E/(-i)$

does not represent the ohmic drop $-(R_s + R_m) i$, but contains, in addition, a sizeable contribution from the membrane potential in the second term. It is also of interest that for the case calculated the ohmic drop contribution B/λ (= 26.7 millivolt) in the prelogarithmic term is about the same as the membrane potential contribution (\bar{C} = 24.8 millivolt). This means that the ohmic drop in the boundary layer contributes only about one half as much to the polarization potential as the membrane potential. This remains true when the boundary layer thickness and/or current density are changed (as long as there is no appreciable water splitting), because neither B/λ nor \bar{C} depends on J and i . On the other hand, the ratio $\Delta E_b/\Delta E_m$ of the contributions of ohmic drop in the boundary

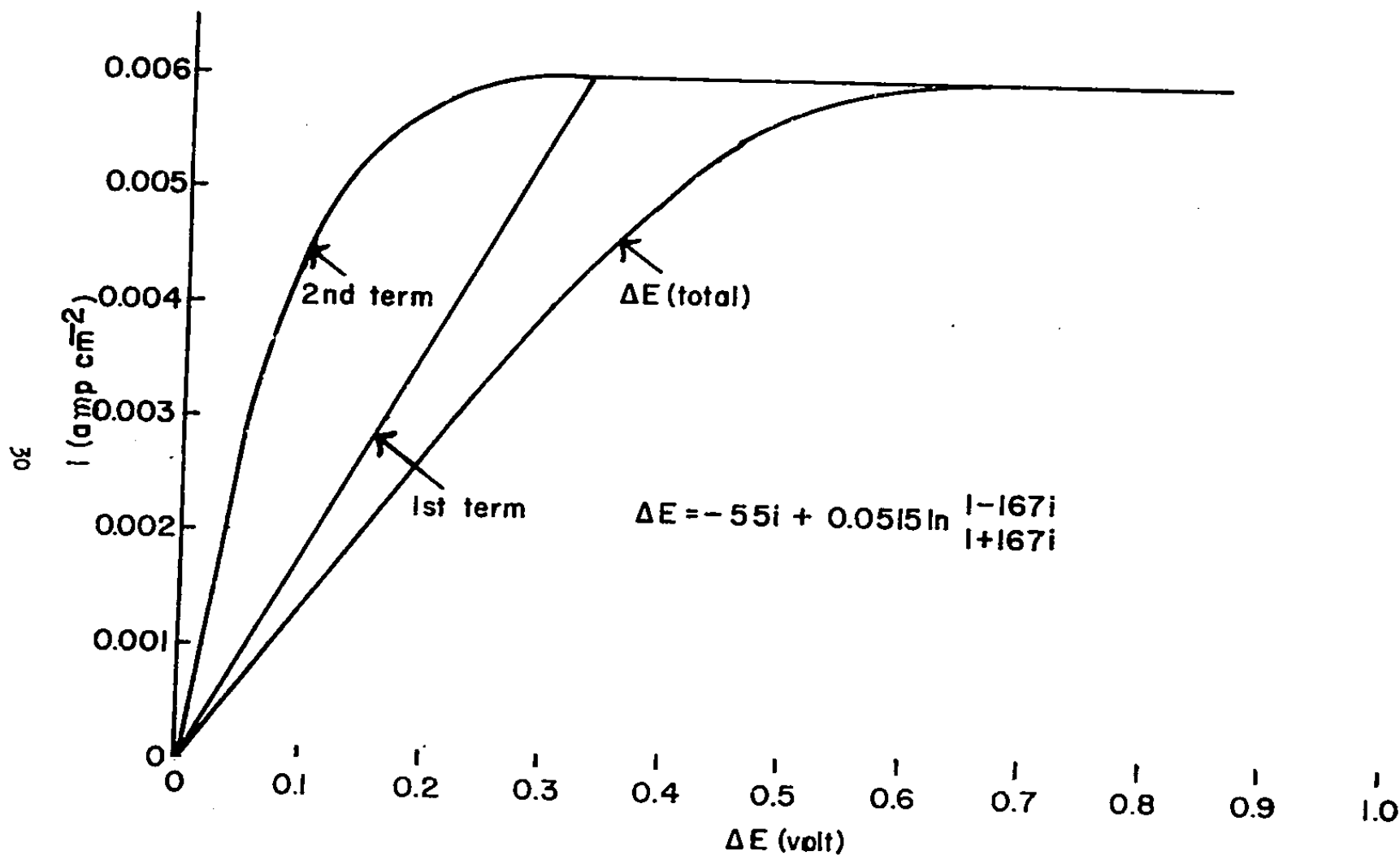


FIGURE 4. CALCULATED CURRENT-VOLTAGE CURVE IN ABSENCE OF "SUPPORTING" ELECTROLYTE; EQUATION (39)

layer and membrane potential to the total polarization ΔE does depend on the transport number of the electrolyte and the membrane selectivity. [See the definitions of B and \bar{C} equations (24) and (34) respectively.] In spite of this fact, $\Delta E_b / \Delta E_m$ does not vary radically for most electro-dialysis systems, since the most common electrolytes found in brackish waters have similar diffusion coefficients and ionic transport numbers, and since most modern electro-dialysis membranes have similar permselectivity (i.e. similar \bar{t}_+ and \bar{t}_- for dilute solutions). Therefore we may generalize our conclusion from the numerical example above and state that in most cases ohmic drop in the boundary layer, ΔE_b , and membrane potential, ΔE_m , make contributions of similar order of magnitude to the total polarization potential, ΔE .

Current-Voltage Curves in the Presence of Supporting Electrolyte

In some experiments, an excess of soluble polyelectrolyte is added to the solutions. The polymeric ion has the same charge as the counterion, but it is assumed that because of its large size, it can not pass through the membrane in significant amounts. For instance, in our experiments with anion-exchange membranes, we added polystyrene sulfonate of molecular weight 30,000 (PSS) to the solution.*

Consider solutions containing low-molecular weight anions (e.g. Cl^-) of concentration c_- , large anions (equivalent concentration c_-) and a single kind of cations (e.g. K^+), concentration c_+ . We can write three flux equations of the type of equations (5) and (6), an electroneutrality condition, a continuity equation for the electric current, and we can also set the flux ratio in the solution equal to the flux ratio in the membrane, as in equation (7):

$$J_+ = -D_+ \left[\left(\frac{z}{RT} \right) c_+ \left(\frac{dE}{dz} \right) + \left(\frac{dc_+}{dz} \right) \right] \quad (41)$$

$$J_- = -D_- \left[\left(-\frac{z}{RT} \right) c_- \left(\frac{dE}{dz} \right) + \left(\frac{dc_-}{dz} \right) \right] \quad (42)$$

* Kindly supplied by Dow Chemical Company, Midland, Michigan

$$J_{\pm} = 0 = -D_{\pm} [-(z/RT) c_{\pm} (dE/dz) + (dc_{\pm}/dz)] \quad (43)^*$$

$$c_{+} = c_{-} + c_{\pm} \quad (\text{electroneutrality}) \quad (44)$$

$$J_{+} - J_{-} = i/z \quad (\text{continuity of electric current}) \quad (45)$$

$$J_{+}/J_{-} = -\bar{f}_{+}/\bar{f}_{-} \quad (46)$$

The six unknowns are J_{+} , J_{-} , c_{\pm} , c_{+} , c_{-} and dE/dz . The first three can be readily expressed in terms of the others by first solving equations (44) to (46):

$$J_{+} = i \bar{f}_{+}/z \quad (47)$$

$$J_{-} = -i \bar{f}_{-}/z \quad (48)$$

$$c_{\pm} = c_{+} - c_{-} \quad (49)$$

and then substituting these three expressions in equations (41) to (43):

$$(i \bar{f}_{+}/z D_{+}) + c_{+} (z/RT)(dE/dz) + (dc_{+}/dz) = 0 \quad (50)$$

$$- (i \bar{f}_{-}/z D_{-}) - c_{-} (z/RT)(dE/dz) + (dc_{-}/dz) = 0 \quad (51)$$

$$- (z/RT)(c_{+} - c_{-})(dE/dz) + (dc_{+}/dz) - (dc_{-}/dz) = 0 \quad (52)$$

This is a set of three simultaneous differential equations to be solved for the variables c_{+} , c_{-} and E .

If the equivalent concentration of polyelectrolyte is substantially larger than that of the low-molecular weight electrolyte, we can simplify the solution by the following approximation: in equations (51) and (52) we drop the terms containing $c_{\pm}(dE/dz)$, because both c_{\pm} and (dE/dz) are small compared to the other terms** in the sums, and the product of these

*The diffusion coefficient in this equation also refers to the equivalent of the polyion, but since D_{\pm} cancels anyway, the exact definition is not discussed here.

** (dE/dz) is small because addition of neutral electrolyte suppresses the electrical potential drop in the boundary layer.

two small terms is considered negligible. In other words, we neglect transport of Cl^- in the boundary layer by electromigration compared with transport by diffusion.

With this approximation we obtain from equation (51)

$$i/\bar{x} = (D_-/\bar{t}_-) dc_-/dz \quad (53)$$

which is an expression of the type of Fick's law because $-\bar{t}_- i/\bar{x} = J_-$ [equation (48)].

The gradient of the concentration of c_+ can be calculated by combining equations (50) and (52), in which the term containing $c_-(dE/dz)$ has been neglected:

$$\frac{dc_+}{dz} = \frac{1}{2} \left(\frac{dc_-}{dz} - \frac{i \bar{t}_+}{\bar{x} D_+} \right) = \frac{1}{2\bar{x}} \left(\frac{\bar{t}_-}{D_-} - \frac{\bar{t}_+}{D_+} \right) \quad (54)$$

Comparing (53) to (54) we find that

$$\frac{1}{\bar{x}} = \frac{D_-}{\bar{t}_-} \frac{dc_-}{dz} = 2 \frac{dc_+}{dz} \left(\frac{D_+ D_-}{D_+ \bar{t}_- - D_- \bar{t}_+} \right) \quad (55)$$

and hence

$$\frac{dc_+}{dz} = \frac{1}{2} \frac{dc_-}{dz} \left(1 - \frac{\bar{t}_+ D_-}{\bar{t}_- D_+} \right) \quad (56)$$

The significance of the last equation is illustrated for the case of KCl ($D_+ = D_-$) at an ideally anion-selective membrane ($\bar{t}_+ = 0$). It is seen that in this case the gradient of the K^+ concentration in the boundary layer is only half that of the Cl^- concentration, and that because of electroneutrality [equation (44)] there exists a PSS concentration gradient also of half the magnitude of the Cl^- gradient, but in the opposite direction:

$$\frac{dc_-}{dz} = - \frac{1}{2} \frac{dc_-}{dz} = - \frac{dc_+}{dz} \quad (57)$$

In other words, both K^+ and Cl^- concentration decrease from bulk solution to membrane surface while the PSS concentration increases (see Figure 5).

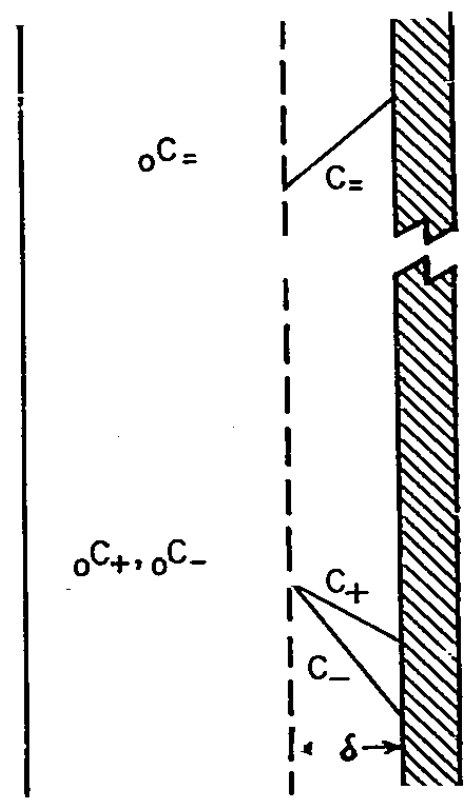
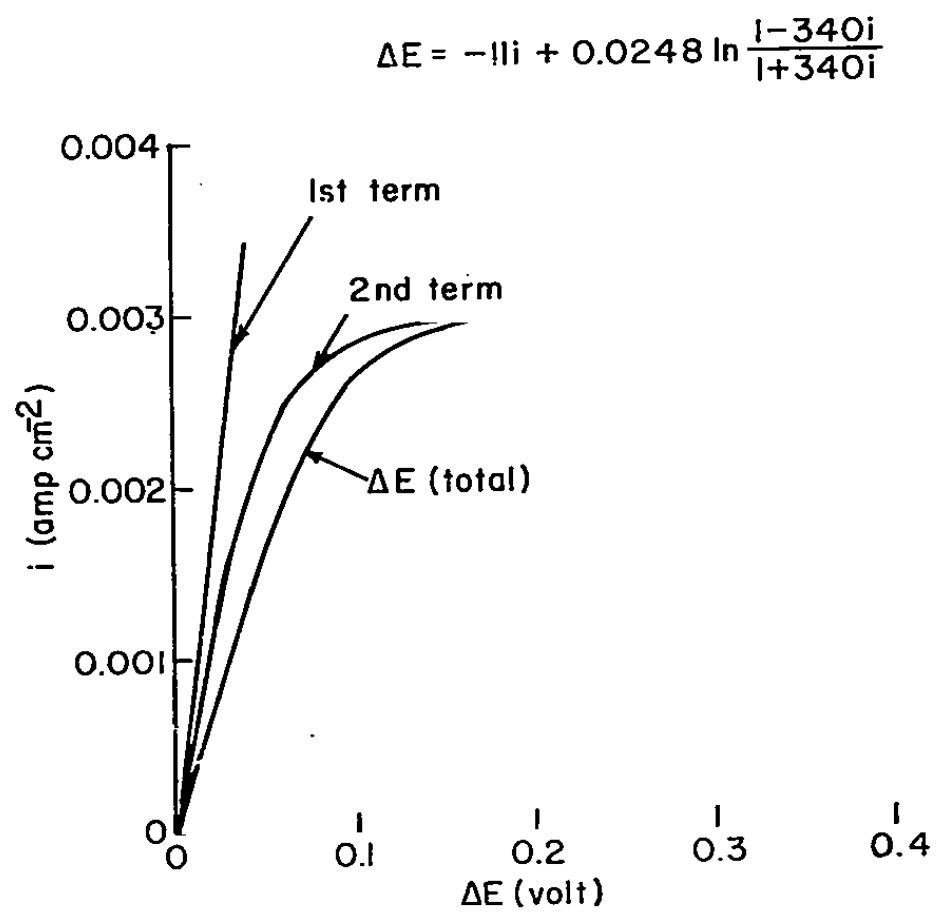


FIGURE 5. CALCULATED CURRENT-VOLTAGE CURVE IN PRESENCE OF "SUPPORTING" ELECTROLYTE; EQUATION (62)
 INSERT SHOWS SCHEMATIC OF CONCENTRATION PROFILES; EQUATION (57)

Returning to equation (53), we see that the limiting current in the presence of supporting electrolyte is

$$i_{lim} = - (\mathfrak{D}_- / \bar{f}_-) {}_o c_- / \delta \quad (58)$$

(where ${}_o c_-$ is the concentration of Cl^- in the bulk solution) because the largest possible numerical value of dc_-/dz is $- {}_o c_- / \delta$.

Comparing equation (58) to the analogous equation in the absence of supporting electrolyte [equation (20)] we see that the presence of the supporting electrolyte depresses the limiting current.

To express the concentration of Cl^- at the membrane surface, ${}_s c_m^i$ as a function of the current density, we substitute in equation (53) $dc_-/dz = ({}_s c_m^i - {}_o c_-) / \delta$, and solve for ${}_s c_m^i$:

$${}_s c_m^i = {}_o c_- + i \bar{f}_- \delta / (\mathfrak{D}_-) = {}_o c_- + i \delta / B_- \quad (59)$$

where $B_- \equiv \mathfrak{D}_- / \bar{f}_-$ (60)

[Comparison of B_- with B as defined in equation (24) shows that for KCl at a perfect anion-exchange membrane $B_- = B/2$.]

The total potential drop across the probe electrodes consists again of ohmic drops, membrane and junction potentials as in the absence of supporting electrolyte [equation (39)]. Because of the presence of a large excess of supporting electrolyte, however, the resistance sum, $2R_{sp}$, in the solutions including the boundary layers, is expected to be very small, and the junction potentials in the solutions are small, too. The membrane potential is $\bar{C} \ln ({}_s c_m^n / {}_s c_m^i)$ [see equation (33)], where ${}_s c_m^i$ is given by equation (59) and ${}_s c_m^n$ is determined in analogy with equation (35):

$${}_s c_m^n - {}_o c_- = {}_o c_- - {}_s c_m^i = - i \delta / B_- \quad (61)$$

Hence the total potential drop between the probe electrodes is*

$$\begin{aligned} \Delta E_s &= - (2R_{SP} + R_m) i + \Delta E_m = - (2R_{SP} + R_m) i + \bar{C} \ln \frac{1 - i\delta/(B_{O_2} c_{O_2})}{1 + i\delta/(B_{O_2} c_{O_2})} \\ &= - (2R_{SP} + R_m) i + \bar{C} \ln \frac{1 + (i/i_{lim})}{1 - (i/i_{lim})} \end{aligned} \quad (62)$$

where R_{SP} is small. If any additional series resistances exist (for instance by creation of "poisoned" surface layers on the membrane), their influence will appear as an additional term in the expression $(2R_{SP} + R_m)$ in equation (62).

A numerical example for the same conditions as those described before (Figure 4) is shown in Figure 5. Here equation (62) is plotted under the assumption that the excess of supporting electrolyte is so large that R_{SP} is entirely negligible.

*entirely neglecting the junction potentials (this is a crude approximation which can be refined when the transport numbers in PSS solutions are known)

III.A.4 Results and Discussion

Figure 6 shows current-voltage curves of 0.01N KCl solutions for two series of experiments with membrane III BZL 183, viz. in the presence and absence of PSS (5% by weight). V_p is the potential difference measured between the two probe electrodes (Figure 1). Different curves on the same graph refer to different solution flow rates past the membrane (flow rates past the two membrane faces were held equal). These curves describe early experiments in which the microelectrode distance in different series was not easily reproducible. No quantitative conclusions should, therefore, be drawn from comparisons of the absolute values of the currents in the two graphs.* On the other hand, the figures illustrate a basic difference in the shape of the curves: in the absence of PSS, the limiting currents are not well defined - in fact there is merely a gradual change of slope with an inflection. In the presence of PSS, however, two well-distinguished regions can be seen, viz. a low-resistance region at low voltages and a high-resistance region of voltage-independent slope at higher voltages. It is significant that the latter slope depends very little on the flow rate. The same picture emerges from experiments at higher flow rates and at different chloride concentrations (Figure 7), and from similar experiments with membranes CA 1 (Figure 8) and A 101 B (Figure 9). In all cases the shape of the curves suggests the presence of two superimposed phenomena, namely: (1) a limiting current which increases with increasing KCl concentration and solution flow rate, (2) an additional current which seems to be due to a parallel conductance, is independent of the flow rate and causes the (hypothetical) limiting current plateaus to degenerate into low-slope plateaus. Current (2) increases slightly with increasing chloride concentration.

*The viscosity of the solutions containing PSS + 0.01N KCl is considerably higher than of the 0.01N KCl solutions. Hence experiments at equal flow rates do not represent equal Reynolds or Sherwood numbers.

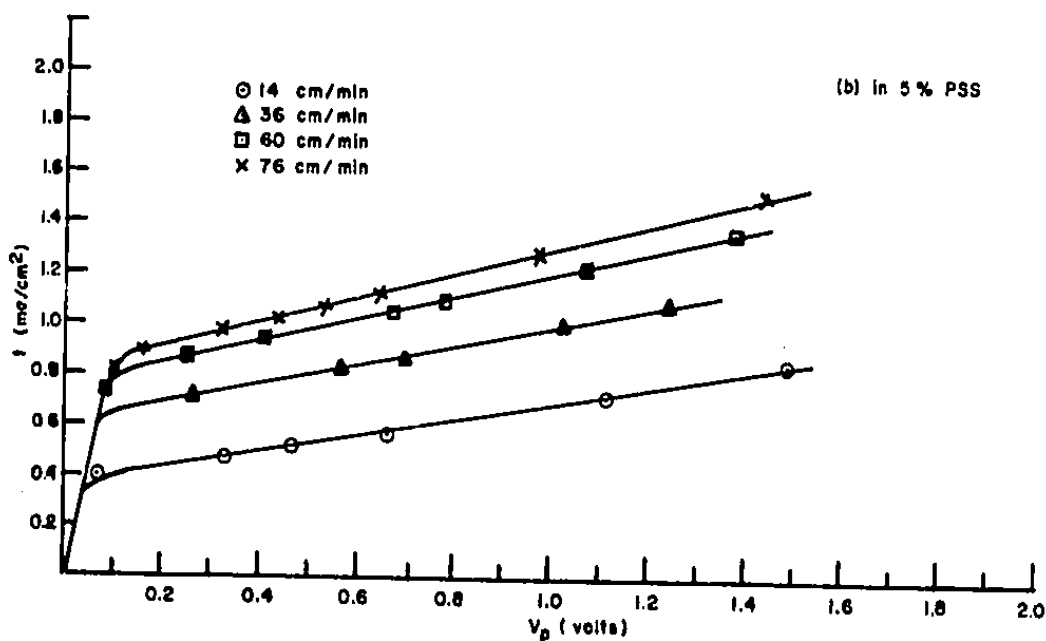
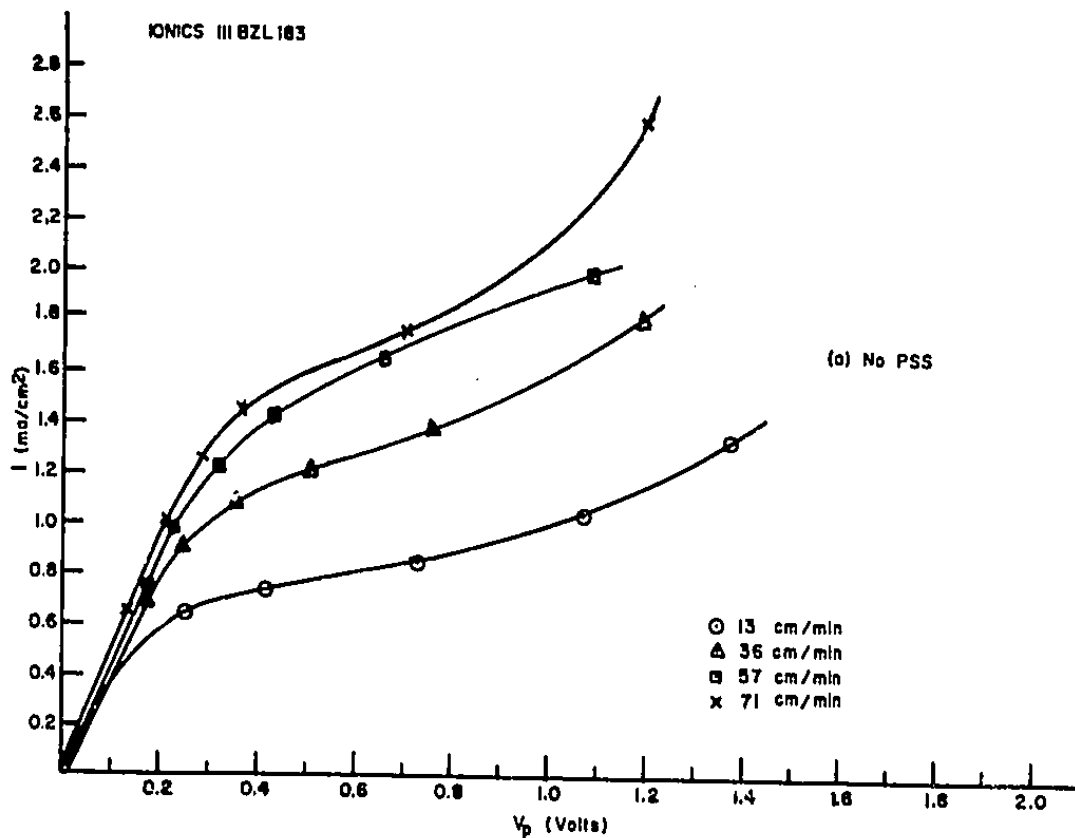


FIGURE 6. CURRENT-VOLTAGE CURVES OF 0.01N KCl SOLUTION
 LOW FLOW RATES. MEMBRANE III BZL 183 (A.E.)
 (a) No PSS. (b) 5% PSS added.

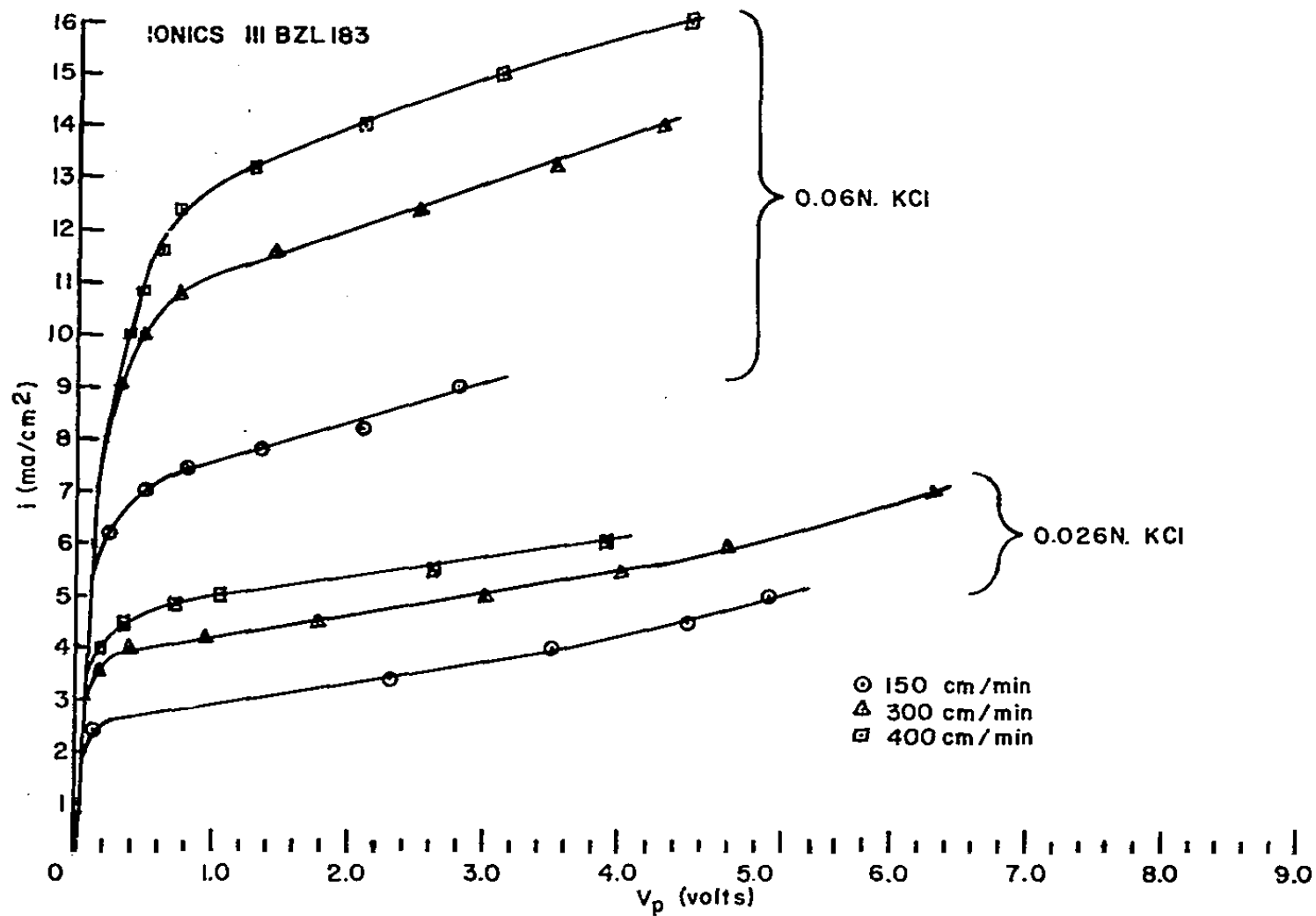


FIGURE 7. CURRENT-VOLTAGE CURVES OF 0.026 AND 0.06N KCl SOLUTIONS IN 5% PSS MEMBRANE III BZL 183 (A.E.)

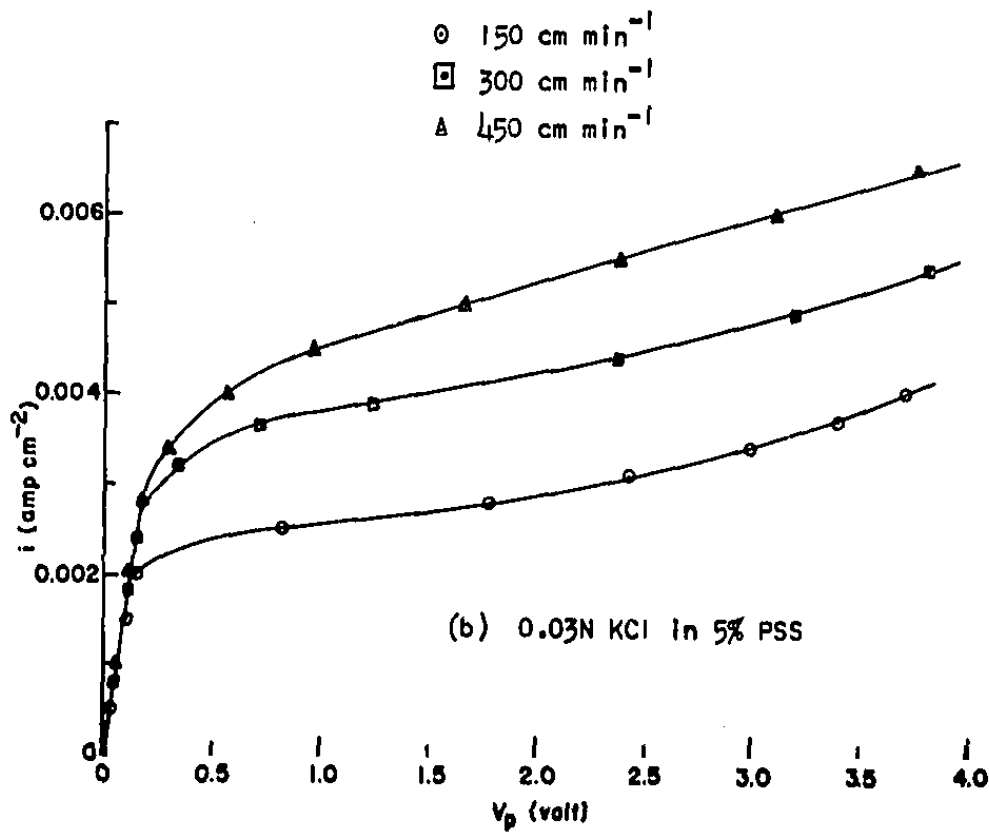
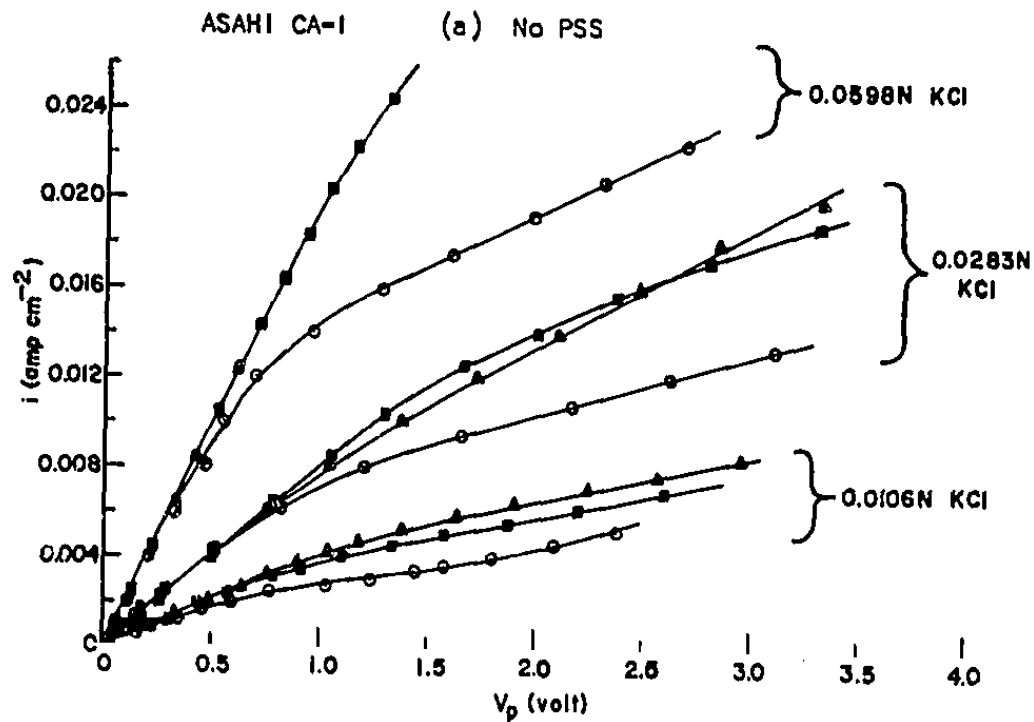


FIGURE 8, CURRENT-VOLTAGE CURVES FOR MEMBRANE CA-1
 (a) No PSS (b) 5% PSS

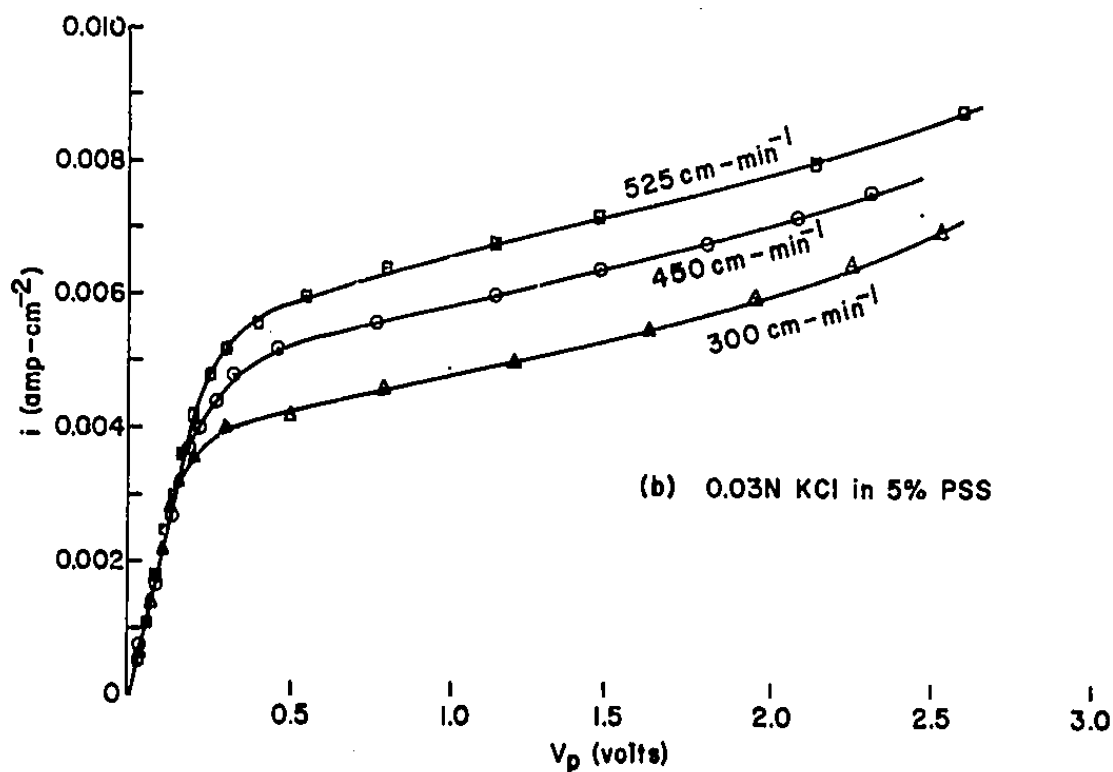
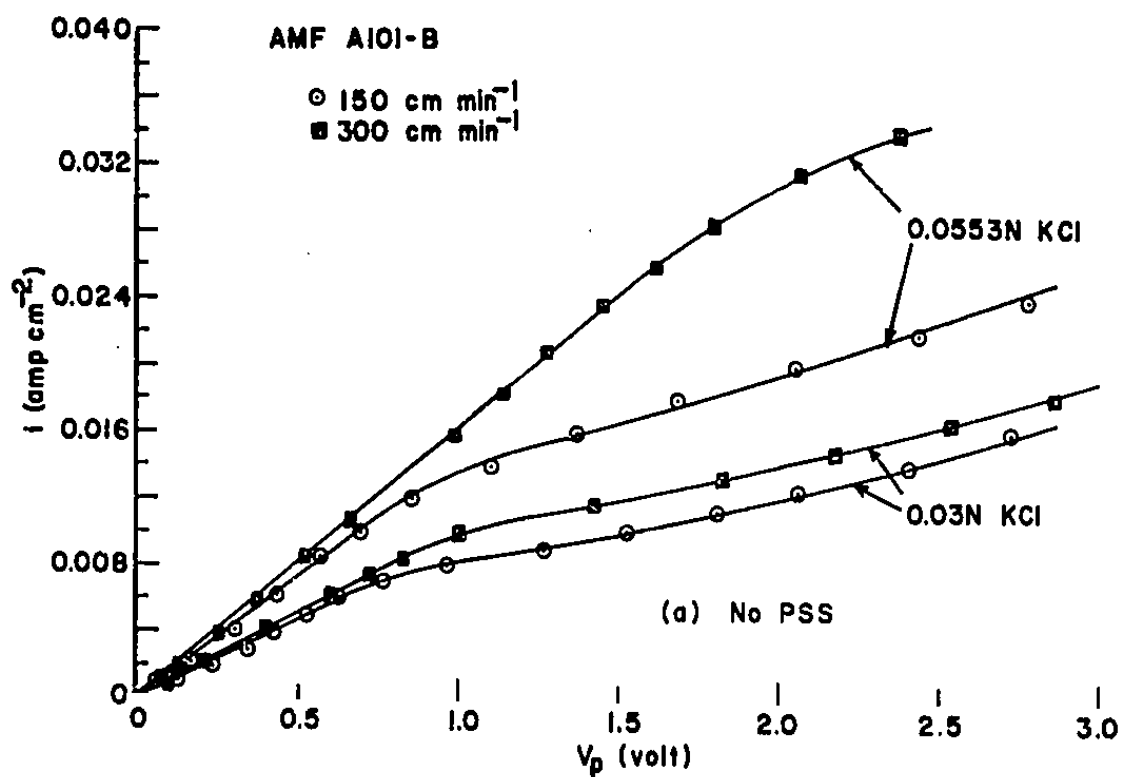


FIGURE 9, CURRENT-VOLTAGE CURVES FOR MEMBRANE A-101-B
 (a) No PSS. (b) 5% PSS added.

Figure 10 shows current-voltage curves for membrane MA 3236 (Ionac Co.). This membrane is supplied by the manufacturer between two plastic sheets that could be peeled off when the sandwich was soaked. The curves in Figure 10a were obtained without surface treatment of the membrane. It is seen that the resistance between the probe electrodes was high and there was relatively little difference between experiments at different flow rates. Abrasion of the surface with fine sandpaper decreases the resistance (Figure 10b), but there is again little influence of flow rate on the current-voltage curves. In the presence of PSS, however, (Figure 10c), "sloping plateaus" appear. At any given probe electrode voltage in the "sloping plateau" region, the currents are, as usual, lower than in the absence of PSS. This is probably due to the high viscosity of the PSS solutions which increases the thickness of the (hypothetical) boundary layer.

Similar results were obtained with membrane Ionac MA 3475 XL (Figure 11). For both of the latter membranes, no limiting current plateau at all can be distinguished in the absence of polystyrene sulfonate. Addition of polystyrene sulfonate causes at least some differentiation of "sloping plateaus."

In the preceding paragraphs, emphasis was placed on the occurrence (or lack of occurrence) of true limiting currents; i.e., regions of the current-voltage curve with a clear current plateau.* The importance of these plateaus lies in their use as mass transfer criteria; in fact, much modern mass transfer research is being done by electrochemical methods and the magnitude of the limiting current at metal-solution interfaces serves to calculate the mass transfer rate (12,18-21). The experiments described in Figures 6 through 11 show that contrary to results at

*Note that the practical plant definition of "limiting current"⁽⁶⁾ refers to the minimum of a plot of E/I vs. $1/I$ (E = voltage, I = current).

This minimum is not indicative of a current plateau, which is the usual electrochemical meaning of a "limiting current." The E/I vs. $1/I$ curve will often have a minimum, whether there exists a true limiting current (i.e., a current plateau) or not.

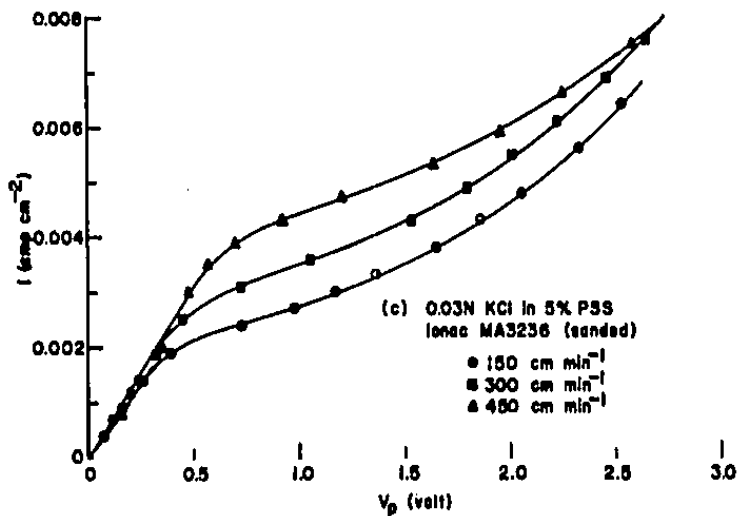
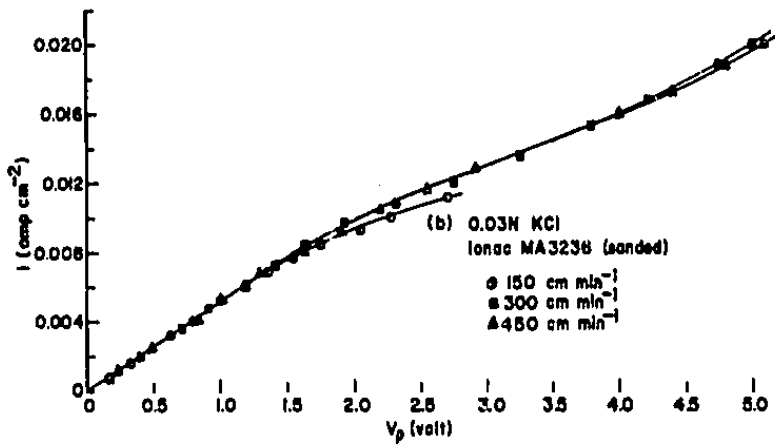
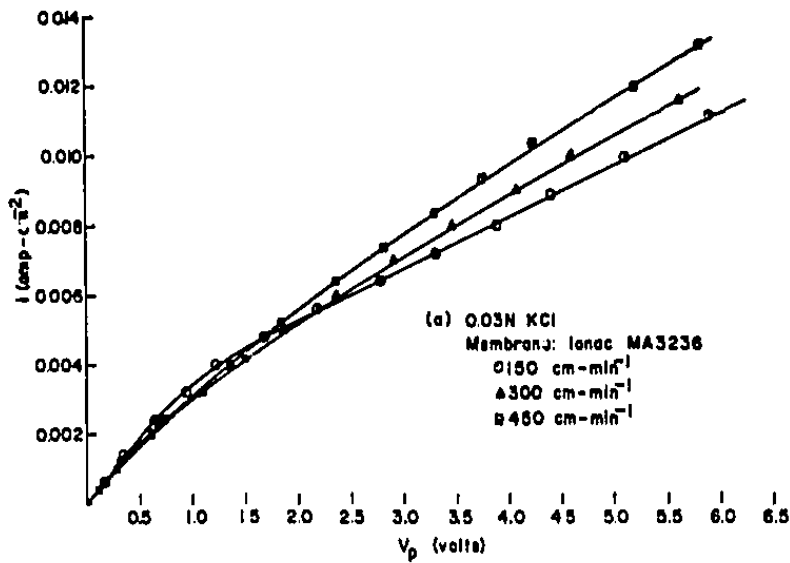


FIGURE 10. CURRENT-VOLTAGE CURVES FOR MEMBRANE MA 3236
Average time after first exposure of membrane to PSS: 22 hrs.
(a) No surface treatment, no PSS. (b) Surface sanded, no PSS.
(c) Surface sanded, 5% PSS added.

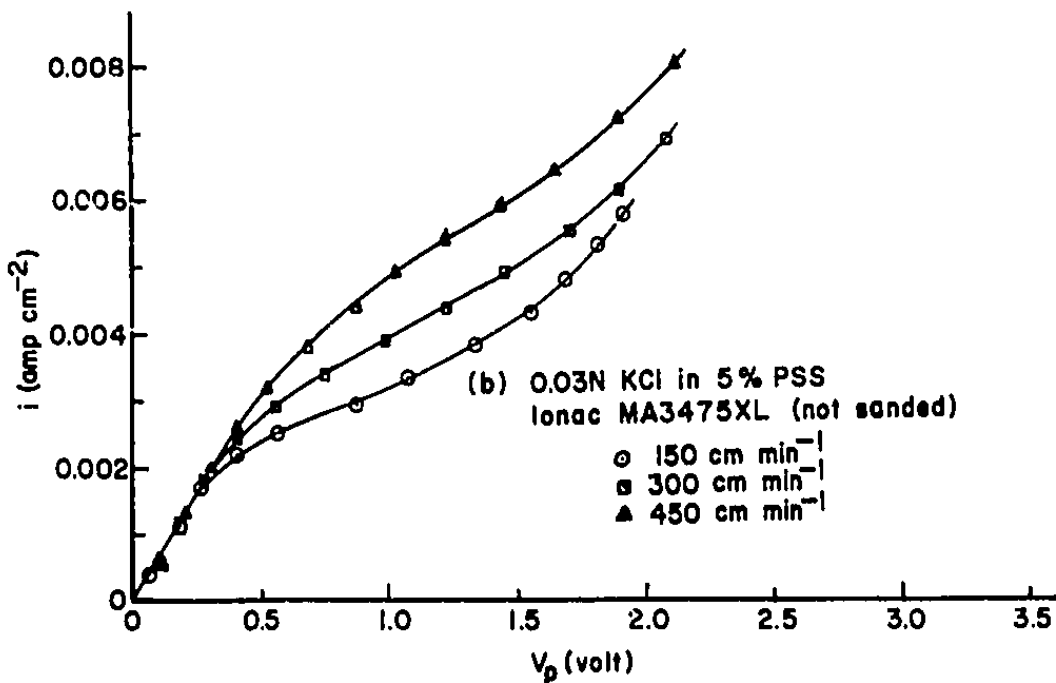
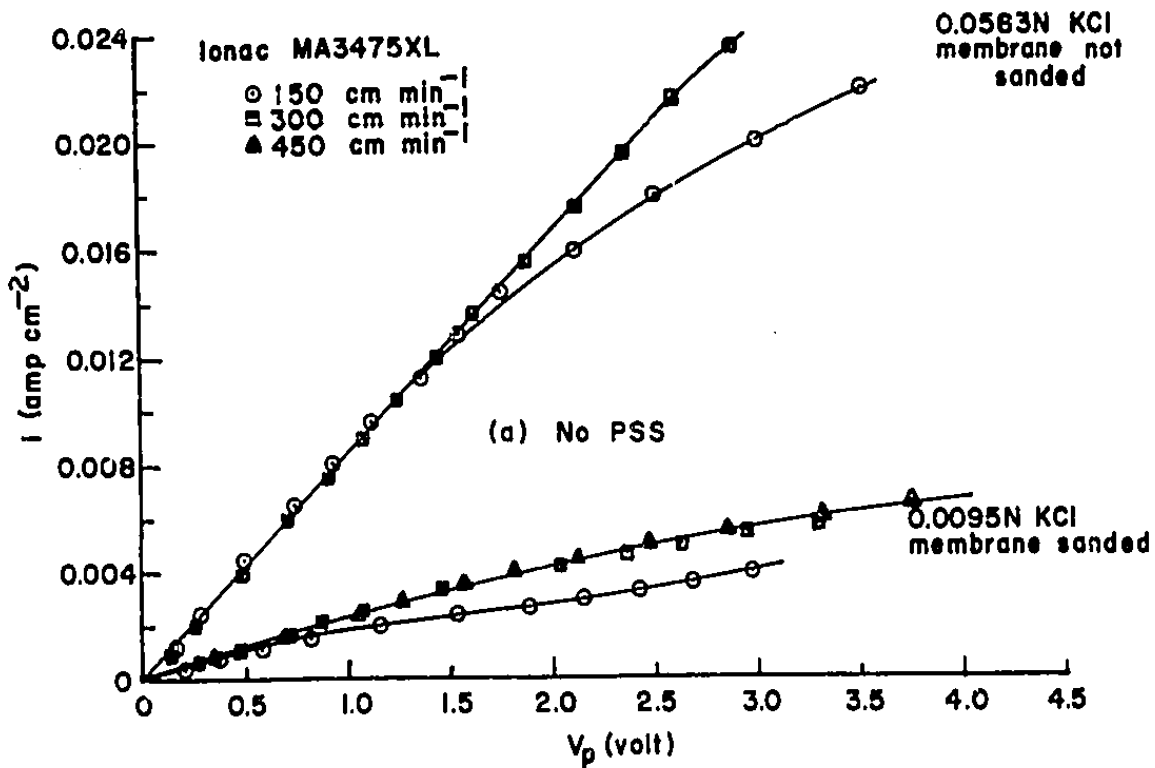


FIGURE 11. CURRENT-VOLTAGE CURVES FOR MA 3475 XL

(a) No PSS. (b) 5% PSS added.

Curves for 150, 300, and 450 cm min⁻¹ measured 5, 1.5, and 6 hr respectively after first exposure of membrane to PSS.

metal-solution interfaces, regions of constant current are not found in current-voltage curves at membrane-solution interfaces. The addition of PSS improves the situation, however, in that one can at least distinguish two regions of the current-voltage curves, viz. a steep rise and a more or less linear "sloped plateau." The slope of the "plateau" varies from membrane to membrane, some resembling almost horizontal plateaus, while others have pronounced slants.

It is of interest to study the trends of "limiting" currents with flow rate and chloride concentration. As a first approximation, the extrapolation of the low-slope portion of the current-voltage curve to zero voltage was taken as an index for the limiting current (in accordance with the current superposition model) and plotted against linear flow rate on log-log paper. This type of evaluation of the results for the Ionics membrane is shown in Figure 12. The results are not extensive enough to permit any accurate correlations between mass transport and Reynolds number, and it should also be borne in mind that several changes in apparatus and procedure were made between the early low-flow rate and the later high-flow rate experiments, so that the former series can not be readily compared to the latter. But even the fragmentary information summarized in Figure 12 permits the following conclusions: (a) limiting currents increase with increasing flow rate; in the higher flow-rate range the exponent n in the correlation:

$$\text{Limiting current} \propto (\text{flow rate})^n$$

is probably larger than 0.5; and (b) at a given flow rate, the limiting current increases monotonously, and perhaps in direct proportion, to the low-molecular weight electrolyte (KCl) concentration.*

*It is of interest to consider the experiments described in the light of molecular separations on polymer-solution surfaces which do not involve electric phenomena, e.g., the phenomenon of "Gel Permeation Chromatography" (22,23). In analogy, the type of electrical measurements outlined might prove useful for the analysis of polyelectrolyte mixtures by means of membranes of well-defined pore size (or vice-versa) in an analogous operation of "gel permeation polarography."

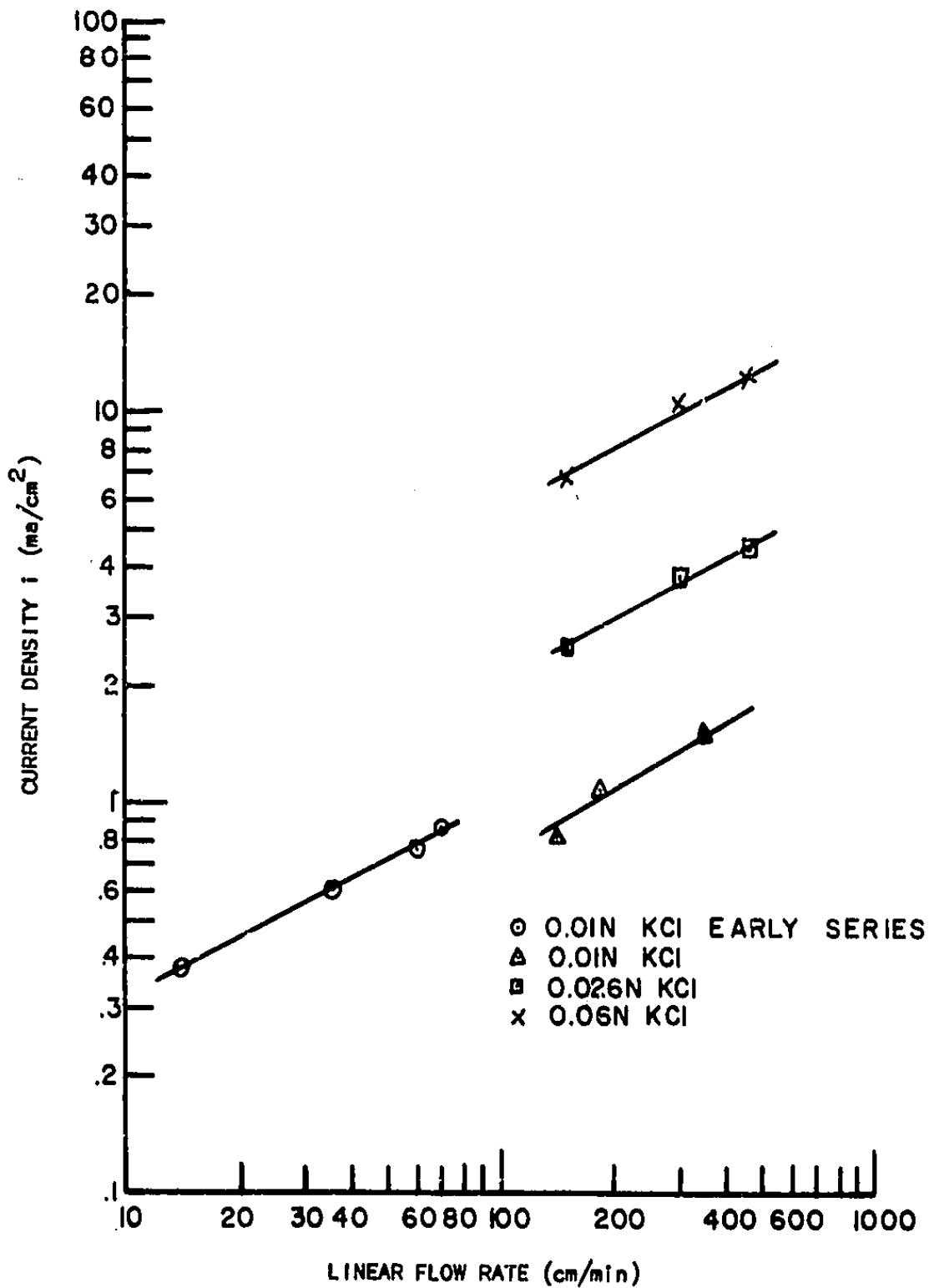


FIGURE 12, EXTRAPOLATED "LIMITING" CURRENT VS. FLOW RATE
SUMMARY OF RESULTS. MEMBRANE III BZL (A.E.)

In order to verify that the absence of "plateau" regions in our experiments was not due to hydrodynamic effects, a number of experiments were performed in which rapid stirring along the whole membrane surface was carried out simultaneously with slow flow. Cooke and Van Der Walt⁽³⁾, have demonstrated considerable variability of the diffusion layer thickness in simple electrolyte solutions under certain conditions, with resulting variability of polarization conditions along the membrane. In other words, "limiting" current conditions do not occur uniformly across the whole membrane (not even across small membrane samples) and the result was found to be a current-voltage curve which never exhibits a well-defined plateau.* It seemed unlikely that the long low-slope regions of the current-voltage curves in Figures 6-8 could be explained by such hydrodynamic factors, and it was, therefore, deemed of interest to test this point. It was indeed found that in spite of even stirring along the whole membrane surface, which should ensure uniform diffusion layer thickness, no flat plateaus were evident.

If the membrane consisted of macroscopic regions of different character, the current-voltage curves could be readily explained. Suppose that there were perfectly permselective patches in parallel with non-permselective ones. The observed current would then be the sum of the contributions of the two types of patches, namely: (a) a polarographic "wave" (plateau) type and (b) a superimposed ohmic current. Since current (a) is a polarization phenomenon, it should increase with increasing flow rate and concentration, as found; current (b) should be independent of the flow rate, again as found.

While it is true that many properties of ion-exchange membranes can be understood from their heterogeneous nature⁽²⁴⁻²⁶⁾, which seems to exist even in membranes labeled "homogeneous" from a macroscopic standpoint, it should be borne in mind that these heterogeneities are of colloid dimensions. It is, therefore, of considerable interest that the current-voltage curves exhibit the shape expected from the macroscopic

* It should be noted that Cooke and Van Der Walt used "overpotential" rather than straight probe electrode voltage as a parameter. Overpotential is the measured probe electrode potential minus the ohmic drop, and was determined by an interruption method^(2,3).

heterogeneous model. The relative amount of imperfections necessary to account for the observed slopes (Figure 6) is small: less than 3 percent of the membrane area would have to be non-permselective, with the remainder entirely ideal.

The behavior of the polyelectrolyte solutions thus focuses attention on the relationship between membrane heterogeneity and polarization. It is of interest that Block⁽²⁷⁾, who studied a large number of commercial membranes and found micro heterogeneities in many of them related their polarization behavior at high current densities to the (yet unmeasured) influence of micro heterogeneity on H^+ and OH^- conductivity in the membrane. Some aspects of the heterogeneity problem are discussed in Section IV of this report dealing with radio-frequency measurements which often provide some indication of these heterogeneities.

It has not been definitely proven, however, that membrane heterogeneities are primarily responsible for the lack of the genuine limiting currents predicted from the solution of the Nernst-Planck equations. It should be noted that this theory does not make allowance for any rate-controlling influence of reactions near the membrane-solution interface, e.g. desolvation of the ions or other changes in the solvent structure when the ion passes across the phase boundary. Such reactions have been studied extensively in the electrochemistry of metal-solution interfaces, and it might prove worthwhile in the future to investigate their possible influence on mass transfer at membrane-solution interfaces, rather than assuming a priori that they are so fast as to be negligible as rate-controlling factors.

Comparison of Results with Different Membranes

To "normalize" the curves for different membranes, i.e. to correct for different membrane resistance terms, R_m , and for different solution resistances, R_s , between the probe electrodes (due to slightly different positioning of the electrodes in different experiments), a number of current-voltage curves at 300 ml/min were replotted, by deducting or adding a linear term, $i \propto E$, such that the initial slopes of all curves coincide (Figure 13). For a justification of this procedure, see equation (39) of Section III.A.3. Having thus eliminated the differences of ohmic resistances in the membrane and in those parts of the solution

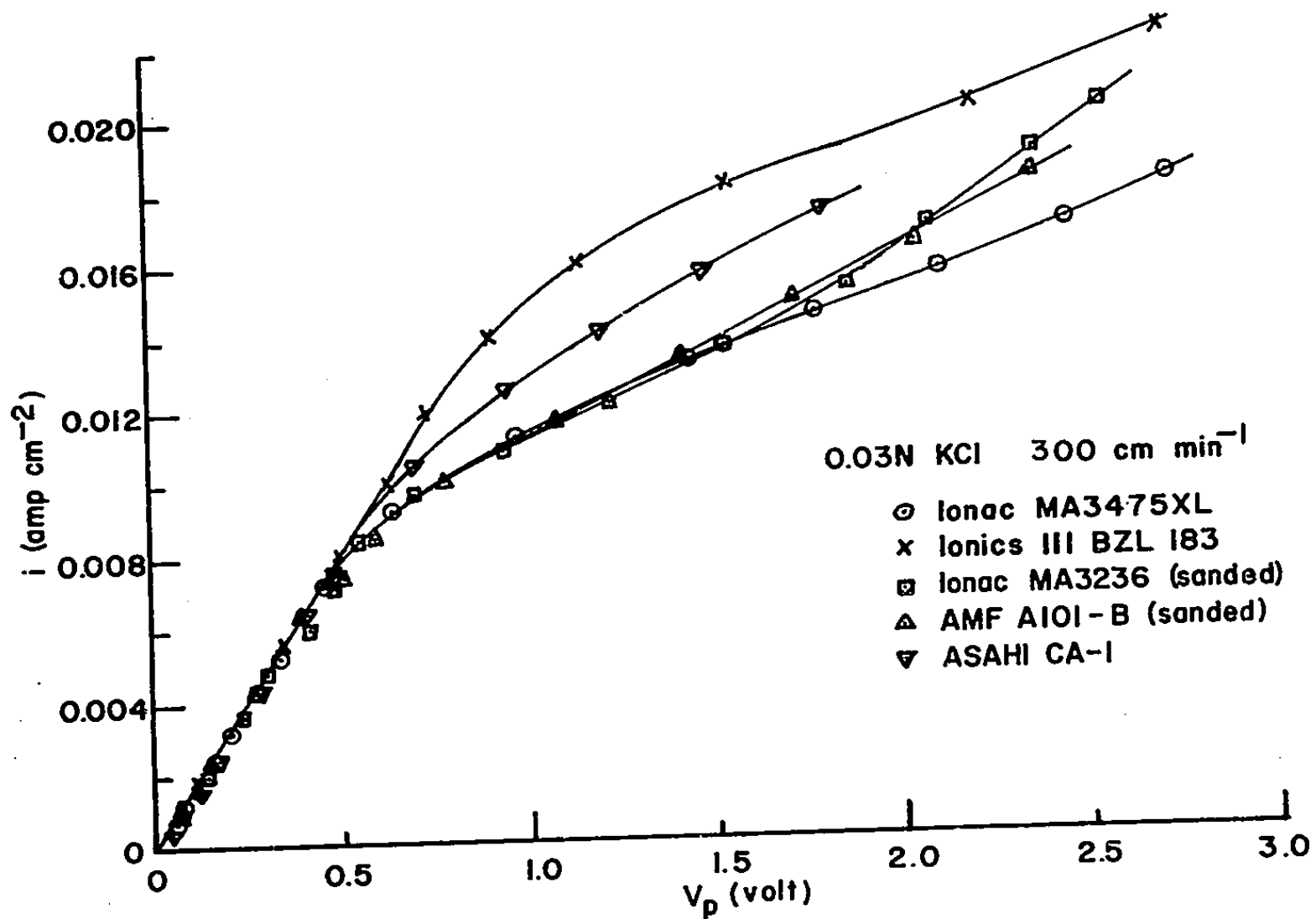


FIGURE 13. "NORMALIZED" CURRENT-VOLTAGE CURVES FOR DIFFERENT MEMBRANES

which are outside the bounds. We should expect all curves to be alike because presumably the boundary layer resistance is the same for all membranes at a given current density.* Figure 13 shows, however, that the normalization does not make all curves coincide. Therefore it seems that in addition to the resistances to ion transfer in the bulk solution and the linear ohmic resistance of the membrane, other resistances which the theory does not take into account, come into play. These effects increase in the series Ionics A III BZL < Asahi CA I < (AMF A 101-B, Ionac MA 3236, Ionac MA 3475 XL). At this stage, one can merely speculate about the reasons for the differences between these curves. Again, heterogeneities within the membrane might give rise to internal polarization effects which differ in accordance with the structure of the membrane. It is also possible that at least some part of the differences is due to individual differences of "water splitting" at the solution side of the membrane.

Since the Ionics A III BZL membrane seems to conform best with the simplified Nernst layer theory, its current-voltage curve in the presence of PSS is compared with the theoretical curve in Figure 14. The theoretical curve was calculated from equation (62) of Section III.A.3 with $R_m = 11 \text{ ohm cm}^2$, $i_{lim} = 0.0048 \text{ amp cm}^{-2}$, and $R_{sp} = 11 \text{ ohm cm}^2$, the latter value having been selected to make the initial slope of the calculated and experimental curves coincide. (This was necessary because the exact distance of the probe electrodes from the membrane surfaces was unknown; the value of 11 ohm cm^2 is entirely reasonable, corresponding to a distance of 1.5 to 2 mm.)

The discrepancies below the theoretical limiting current are not surprising in view of the change of the diffusion thickness layer along the membrane. The continuous linear increase of the "limiting" current is not readily understood, however. Since practically no pH change in the bulk solutions was detected, it is unlikely that H^+ and OH^- carry the current ("no water splitting"). It is of interest, however, that about the

*Some differences in the current-voltage curves might be due to surface roughness differences (which are described in Section III.D). It is not likely, however, that the differences in Figure 13 are merely surface roughness effects.

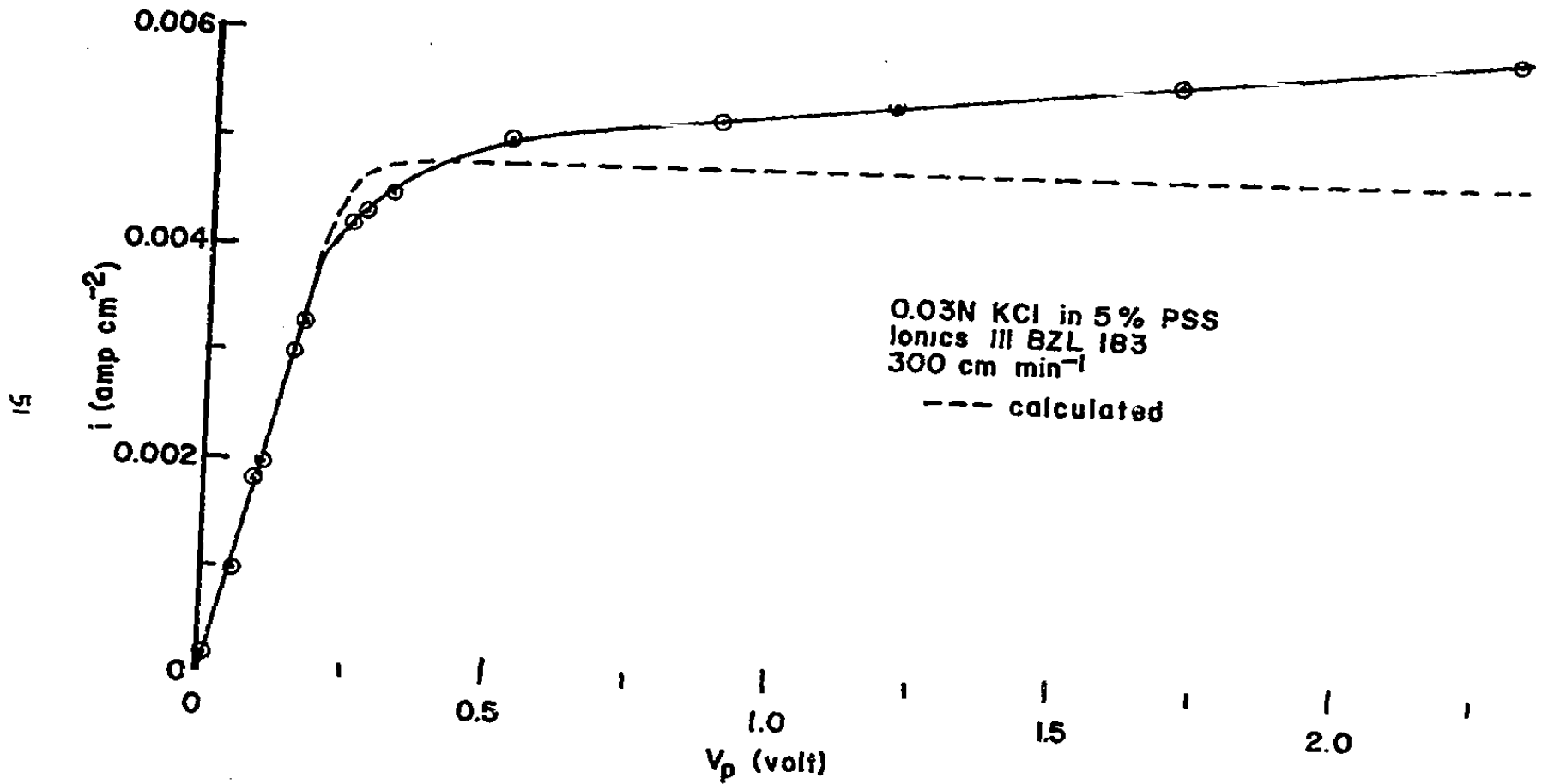


FIGURE 14. COMPARISON OF EXPERIMENTAL CURRENT-VOLTAGE CURVE WITH CALCULATED CURVE

same slope is obtained in PSS solutions which contain only traces of KCl. Figure 15 shows i vs. V_p curves in such solutions for two membranes on an expanded scale. If the membranes were completely impermeable to PSS, they should pass practically no current. The results show, however, that for both membranes, a linear current increase occurs where there should be a limiting current. The slopes are 0.39 and 0.9 $\text{ma cm}^{-2}/\text{volt}$ for Ionics and AMF membranes respectively as compared to 0.39 and 0.64 (Ionics) and 1.2 (AMF) observed in different experiments with 10 to 50 times higher KCl concentrations. Since the slope of the plateaus is not much dependent on the KCl concentration, the excess current might be due primarily to a parallel "leak" conductance of some PSS through the larger "pores" of the membrane. Since the PSS solutions had been carefully dialyzed before the experiments, it is not at all clear whether PSS molecules sufficiently small to be able to get through the membrane were present, but note that a relatively minor percentage of "leak" area could explain the results for these two membranes.

Interaction between Membranes and PSS

Polyelectrolytes of opposite charge generally interact very strongly; therefore, it is not a priori clear whether the addition of negatively charged soluble polystyrene sulfonate would not "poison" the positively charged anion-exchange membrane matrices. While strong "poisoning" of anion-exchange membranes by multivalent cations has been observed^(8,28), this type of interaction does not necessarily impede the migration of small ions to a very large extent, provided the molecular size of the soluble polyelectrolyte is kept within certain limits. Small⁽²⁹⁾ has shown that certain polyelectrolytes adsorb strongly on the surface of ion-exchange resin granules, and yet do not materially impede the rate of exchange of small ions; Small's results encouraged us to use PSS in our systems. The results (Figures 6-11) show that while the presence of PSS decreased the current density, as compared to corresponding membrane-solution systems which did not contain PSS (partly due to the higher viscosity of the PSS solutions), "poisoning" in the customary sense of the word did not occur in these systems.

This conclusion was borne out by a study of the change of current-voltage curves with time (Figure 16). Considerable differences of interaction behavior were observed for the different membranes. For

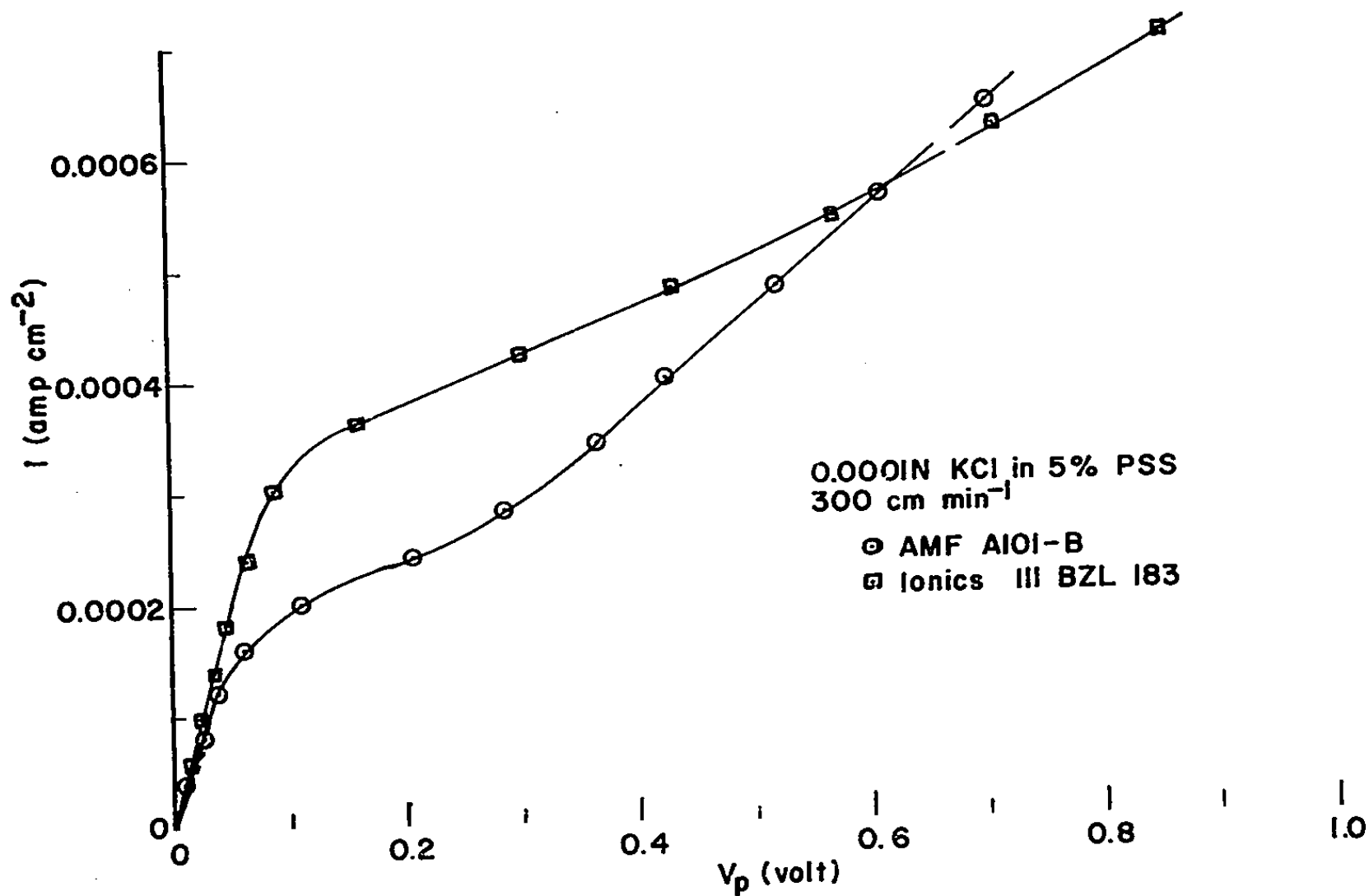


FIGURE 15. CURRENT-VOLTAGE CURVES IN PSS SOLUTIONS CONTAINING ONLY 0.0001N KCl

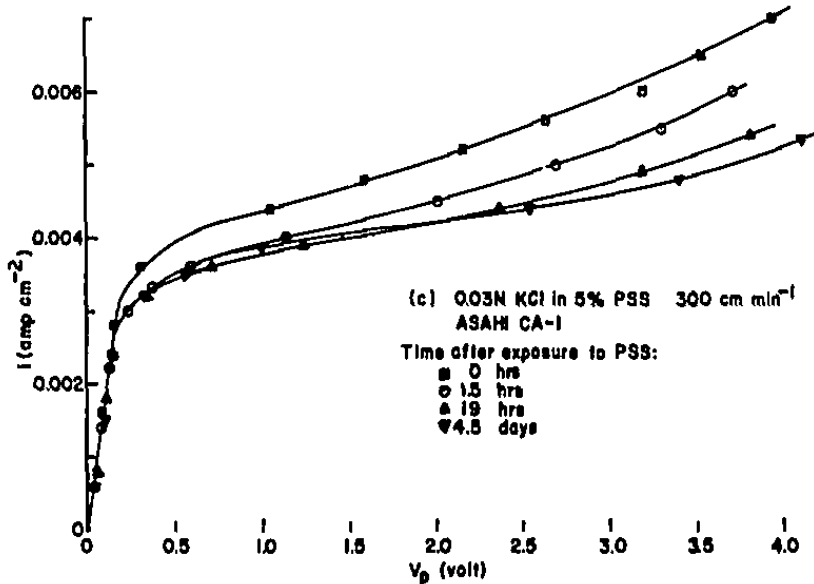
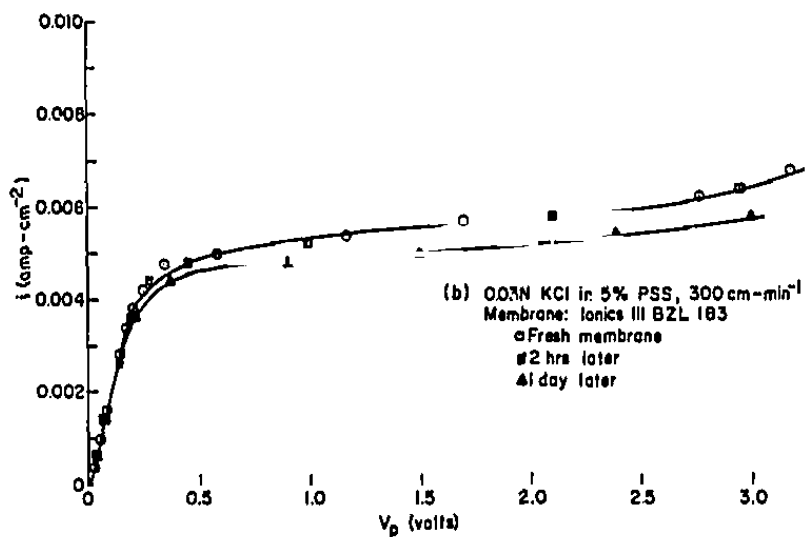
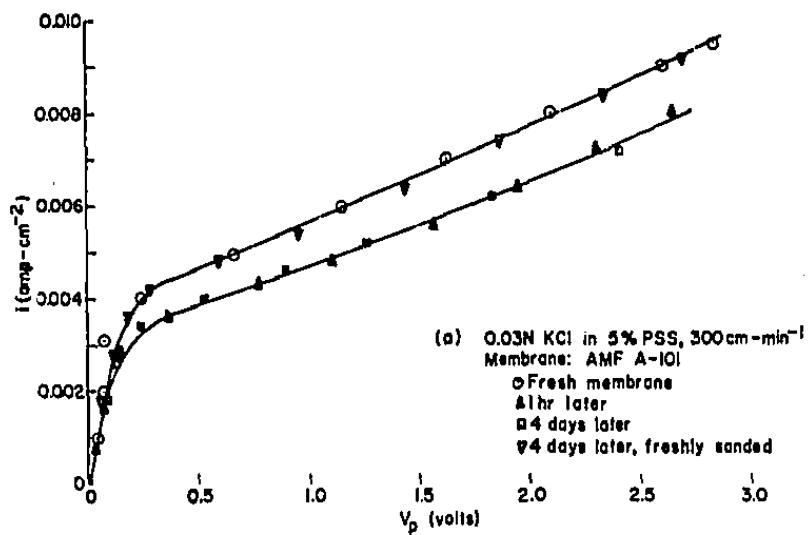


FIGURE 16, CHANGE OF CURRENT-VOLTAGE CURVES WITH TIME

membrane ANF A-101 current-voltage curves were repeated after abrasion of the surface four days after exposure to PSS. It is seen that this procedure restored the current densities to the same state as for fresh membranes. Therefore, at least for this membrane, the interaction occurs only at the surface; it does not drastically "poison" the interior of the membrane.

The experiments with PSS described in Figures 6-11 were all carried out at a time when the interaction with PSS causes only very slow changes of the current with time.*

*Although we have no data for the Ionac membranes corresponding to the data for the other membranes (shown in Figure 16), several indirect observations indicate that no rapid changes occurred in the Ionac membranes either.

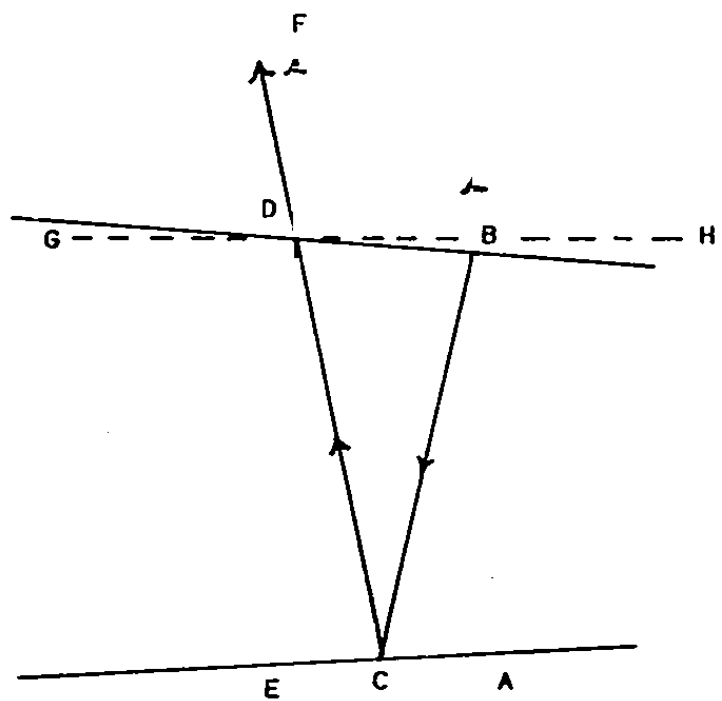
III.B. Laser Interferometry of Membrane-Solution Interfaces

III.B.1 Principle

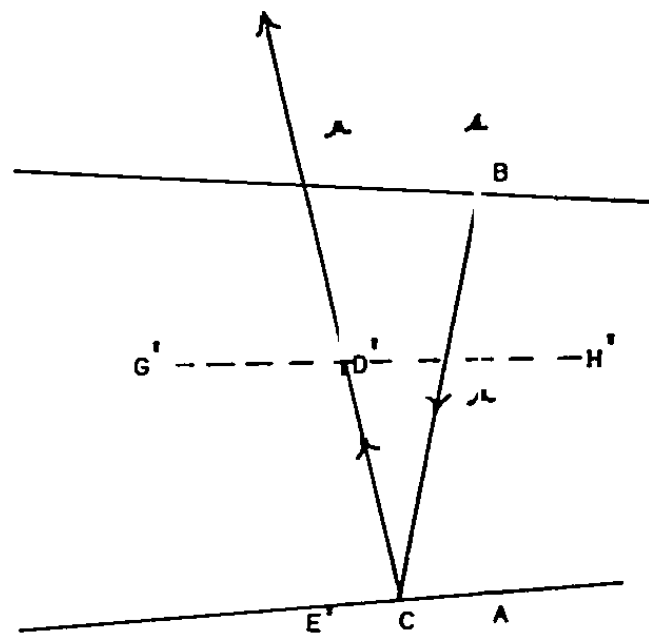
Concentration polarization at membrane-solution interfaces was also studied by laser interferometry. A small interferometer cell was developed which enabled us to observe the formation of concentration polarization layers at membrane-diluate interfaces under natural convection conditions. Several movies of the development of these layers were produced. This technique proves to be very useful for the study of both transient and steady-state polarization phenomena at the membrane-solution interfaces. Experiments were also carried out under conditions of laminar and turbulent flow in the diluate compartment. Because of the shrinkage of the diffusion layers under these conditions, the optical requirements are more stringent than those achievable in our original cells; it is believed that these requirements can be met in more sophisticated cells which are now being designed. It is important, however, that the principle of the applicability of this method to electro dialysis systems was confirmed in the first stage of this research.

These experiments were carried out jointly with R. N. O'Brien and K. Beach of the Lawrence Radiation Laboratory, Berkeley. The membranes, electrodes, and solutions were placed into a wedge interferometer. This type of interferometer is discussed in some detail in References 30 and 31. Briefly, as shown schematically in Figure 17, a parallel beam of light impinges on a wedge formed of two glass flats with partially reflecting surfaces, normal to the bisector plane of the wedge. If the camera focuses on a plane G-H (Figure 17a) intersecting the back window of the cell (the upper wedge plane) at D, then the interference of the two coherent rays ABCD and EF at D will be observed. (The path length difference BCD between the two interfering rays is almost double the average wedge thickness, t' , because the wedge angle is very small; typical dimensions are $t' = 3\text{mm}$ and wedge angle $\beta = 2$ minutes.) Any displacement of the focal plane e.g. to G'-H' (Figure 17b) leads to the observation of the interference of a different ray (E'D') with ray ABCD'. In other words, the interference at D'

$$2t' = \overline{AB} + \overline{DE} \quad (\text{Figure 17})$$



(a)



(b)

FIGURE 17. SCHEMATIC OF LIGHT PATH IN WEDGE INTERFEROMETER

(Figure 17b) rather than at D (Figure 17a) is now observed. Note, however, that when rays AB and ED or AB and E'D' are quite close together (which is the case at near-normal incidence), the average wedge thickness, t' , for cases (a) and (b) is almost the same. Since the path length differences between the interfering rays $\overline{ABCD}-\overline{DE}$ and $\overline{ABCD'}-\overline{E'D'}$ are in both cases twice the average wedge thickness in the regions considered here, the interference at D' will be almost the same as at D. In other words, we can refocus the camera (in a vertical direction in Figure 17) at any plane parallel to G-H within the wedge without changing the fringe position appreciably. On the other hand, moving substantial distances to or from the fulcrum of the wedge (horizontally in Figure 17), one will alternately obtain reinforcement and extinction in accordance with the variation of the phase difference caused by the more substantial change of the wedge thickness in the observed region.

This discussion presupposes that the interfering rays ABCD and ED (or ABCD' and E'D') are in phase. Lateral coherence of the incident parallel beam of light is therefore necessary--at least over a distance of the order AE or AE'. In addition, axial coherence of at least $2t'$ is required (axial coherence is coherence in the direction of light propagation). These coherence requirements together with the desired high intensity for fine-grained motion picture film, are conveniently met by lasers. In fact, in this case the good coherence obtains even over much wider regions.

The magnitude of the wedge angle in Figure 17 was exaggerated for the purpose of illustration only. In practice this angle is quite small, and the incidence is almost normal to either wedge plane. In this case an approximate interference formula may be used⁽³⁰⁾: interference occurs when

$$2\mu' t' \approx n\lambda$$

where μ' is the index of refraction of the fluid in the wedge, t' (cm) the average thickness of the wedge section shown in Figure 17, n the order of interference, and λ the wavelength of the light (cm); n is an integer for constructive interference. It is seen that for a monochromatic interference fringe (which is a line of constant n), the product of the refractive index, μ' , and the path-length difference, $2t'$, is a constant.

If a refractive index gradient arises in the direction normal to the plane of drawing, the interference spots must move up or down the wedge⁽³¹⁾. In other words, fringes which were originally straight must curve toward the wedge apex when the index of refraction, μ' , increases, and away from the apex when μ' decreases. The observed fringe shift makes it possible to calculate the changes of index of refraction and hence the concentration changes.

Although conventional monochromatic light sources have been successfully used for quantitative wedge-interferometry, the ready commercial availability of uniphase output continuous gas lasers has greatly amplified the application of this technique because of the coherence and high intensity of these strictly monochromatic light sources which makes it possible to work with fairly large cell thicknesses, t' , and to obtain high enough light intensities for convenient normal-speed motion picture photography with fine-grained film (ASA speeds 50-80)⁽³²⁾. The camera used was a Bolex H-16 RX-4 16 mm with Switar 1:1.4, $f=25$ mm lens.

III.B.2 Interferometer Cell

An assembly view of the cell used in these experiments is shown in Figure 18.† Figure 19 is a drawing of the "Plexiglas" membrane and electrode holder which fits inside the cell, as designed by K. Beach. The interferometer and microelectrodialysis cell are an integral unit. The current is introduced through two small Ag/AgCl electrodes and passes through the cation and anion-exchange membranes which border the solution channel. The small membrane strips were stretched taut over the openings between the electrode compartments and the central solution channel. As shown in Figure 19, the membrane strips are tightly held between two "Plexiglas" sections; the strips protrude into the small cylindrical openings, f. The two "Plexiglas" pieces holding the membrane fit into the inside of a hollow "Teflon" cylinder, and are pressed together and held in place by insertion of "Teflon" retainers (which act as solution ducts) in notches e (Figure 19).

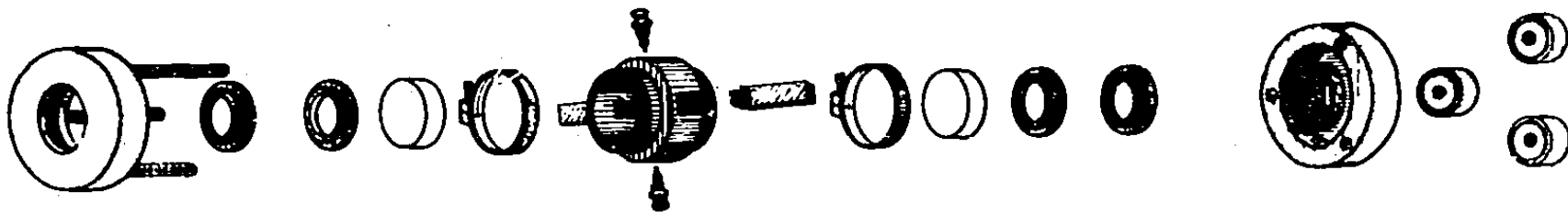
Laser radiation* was passed perpendicular to the plane of the drawing through a pair of optical flats with mirror surfaces on the inside (Optical Coating Laboratories, Santa Rosa, California). The reflection was about 90 percent.** The flats were 1/4-inch thick and 1 1/8-inches in diameter. The seal between the flats and the "Teflon" cylinder was effected by compression rings (Figure 18). The mirrored flats were held in place by axial pressure exerted by screws in a cylindrical brass frame of expandable thickness into which the whole cell assembly fits. The wedge was produced by tightening the top or the bottom screw more than the two other screws. This creates enough pressure on the relatively soft "Teflon" to produce the desired wedge effect.***

† Courtesy of Lawrence Radiation Laboratory, Berkeley, California.

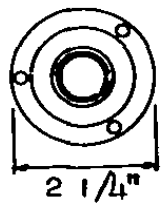
* Model 130, Spectra-Physics, Mountain View, California. This continuous-wave gas laser has a rated output power of 0.75 milliwatt (hemispherical). A telescope expanded the beam from a diameter of 1.2 mm to any desired diameter up to 60 mm. $\lambda = 6328 \text{ \AA}$.

** This reflectivity was specified by the manufacturer for the air-glass interface. It is different for the solution-glass interface.

*** Note that due to the wedge angle the distance between the optical flats thus varied in the vertical direction, while Figure 17 shows a variation in the horizontal direction. In other words, the apex of the wedge was perpendicular to the membrane surfaces.



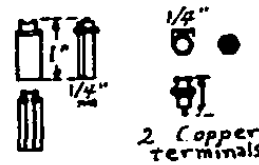
61



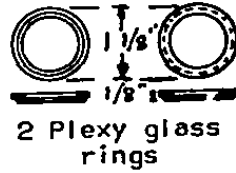
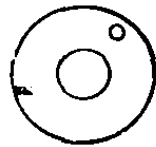
2 Aluminum rings



2 Brass tightening rings



2 Copper terminals



2 Plexy glass rings



2 Electrodes



3 Steel tightening 3/8" nuts

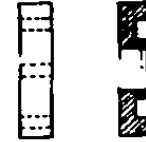
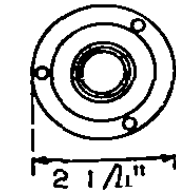
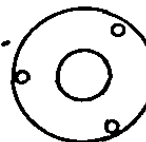


FIGURE 18. ASSEMBLY VIEW OF O'BRIEN INTERFEROMETER

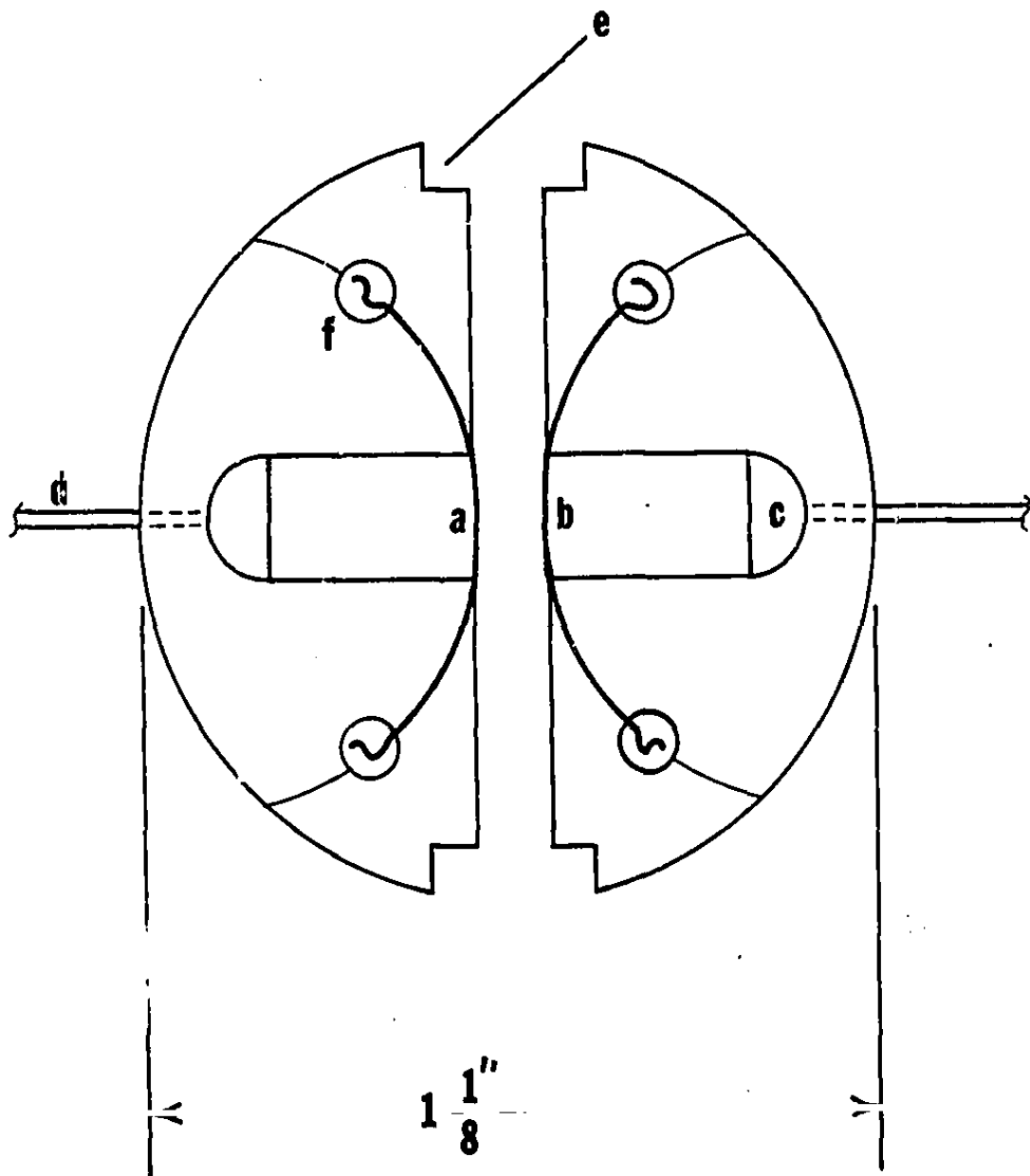


FIGURE 19. MEMBRANE HOLDER FOR CELL

- a. Anion-exchange membrane
- b. Cation-exchange membrane
- c. Ag/AgCl electrode
- d. Electrode lead
- e. Notch for retainer located on entry and exit channels (see Figure 18)
- f. Membrane tightening hole

The wedge angle was adjusted until the fringes were about 1 mm apart; concentration changes can be calculated from the fringe shifts, provided the relation between refractive index and concentration is known⁽³¹⁾. This relation is almost exactly linear.

III.B.3 Procedure and Results

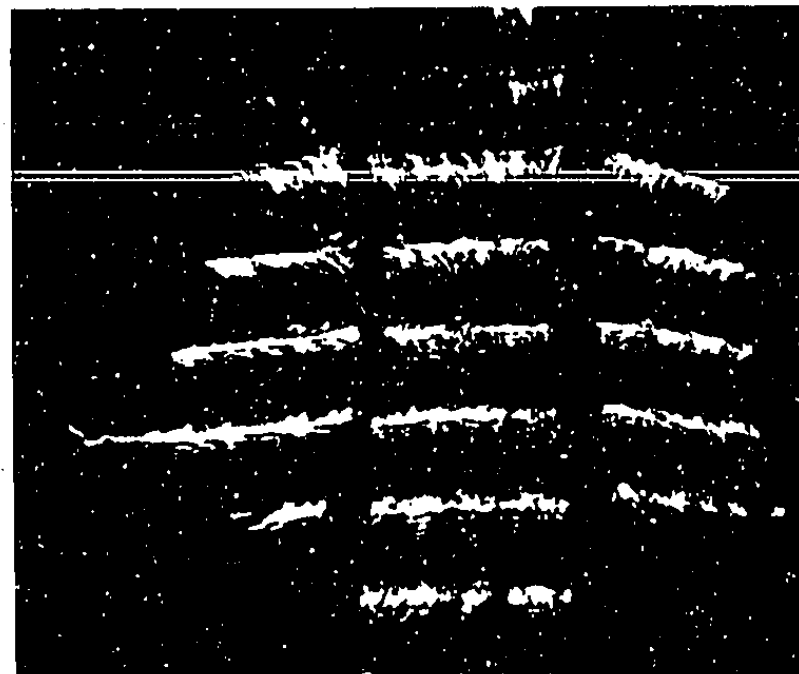
The laser, cell, and camera were mounted in line with suitable clamps (an optical bench did not prove essential for this purpose, but it is useful) and movies taken of the development of the fringe pattern as a function of time, current density, nature of the solutions, and solution flow rate in the channel between the membranes. The anion and cation-exchange membranes were A-101 and C-103 respectively (American Machine and Foundry Company, Springdale, Connecticut). All experiments were carried out at $23 \pm 1^\circ\text{C}$. Originally a simpler cell was used which provided large recesses from the main channel near the membrane surfaces. While this cell had the advantage of very simple design, the hydraulic conditions are complex; therefore, we used the cell shown in Figure 18 in later experiments.

Current was drawn from a galvanostatically controlled power source (Model C63A, Electronic Measurements Corporation, Eatontown, New Jersey); voltage and current were continuously read. The current density was calculated with respect to the exposed membrane area.

Figure 20 shows a pair of frames before the passage of current and in the quasi-stationary* state respectively (i.e.) about one minute after the current was switched on) under conditions of natural convection. The details of the experimental results are embodied in the movies and are briefly summarized as follows:

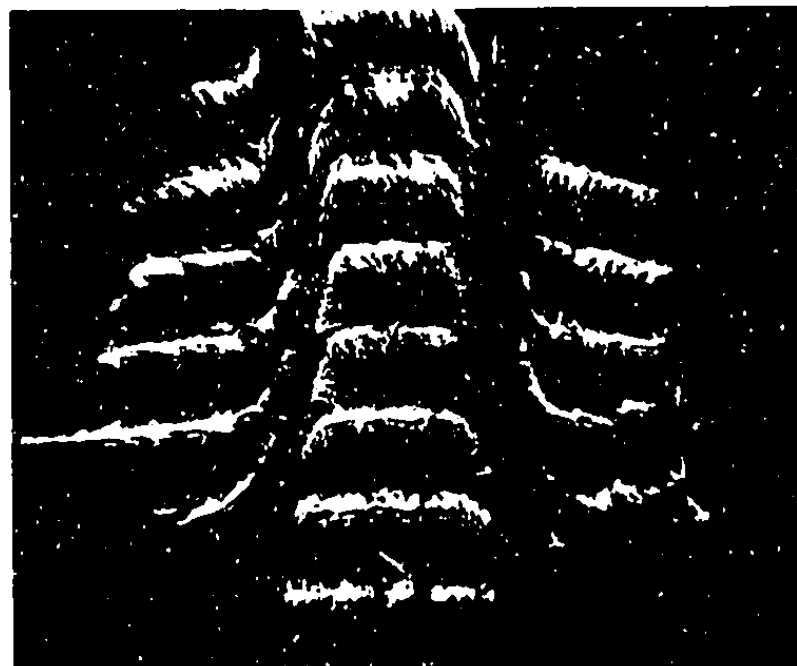
- (1) The time for the establishment of a quasi-stationary state is of the order of 20 seconds for the conditions shown in

* The term "quasi-stationary" is used here to indicate that in the absence of flow, no stationary state can be reached. There is a rapid change of the concentration profiles when the current is switched on, followed by a state of slow change. The beginning of this latter state is termed "quasi-stationary."



(a)

Reproduced from
best available copy.



(b)

FIGURE 20. LASER INTERFEROGRAMS OF MICROELECTRODIALYSIS CELL

Interference lines show concentration distribution before (a) and during passage of current (b). Solution 0.03 N KCl. Vertical shadows are anion exchange membrane (left) and cation exchange membrane (right). Positive current, 10 milliamp cm^{-2} from left to right in (b). Natural convection. Distance between membranes 0.3 cm.

Figure 20. This is of the same order as calculated for similar conditions⁽⁵⁾.

- (2) The thickness of the natural-convection diffusion layer varies somewhat with position; for the conditions studied here, values of 0.02 - 0.05 cm were found.
- (3) As expected from the theory, the relaxation time after switch-off of the current is roughly the same as the time necessary for the establishment of the diffusion layer. This is of importance for the evaluation of pulsing methods in electrodialysis.

Some experiments were carried out under flow conditions. The results are not amenable to quantitative interpretation because various sources of error including leakage of solution between membrane and glass flat tend to obscure the concentration changes in the boundary layer. It was concluded that the method is potentially very valuable, but requires the development of more sophisticated cells. These are now being developed.

III.C. Microelectrode Development

Microelectrodes are important for the local probing of potential differences across membranes and for the determination of ion concentrations. In this research, microelectrodes for the first purpose were prepared and used. In addition, development was carried out for micro pH electrodes suitable for the mapping of local pH changes. The electrodes prepared in this research have diameters of the order of 0.1 mm. This is much larger than some of the microelectrodes used in biological and medical applications, but the purpose of the electrodes and the conditions of use are quite different. The recent development of several types of very small microelectrodes for biophysical studies⁽³³⁾ and of the associated electronics, and the development of small conductivity probes (which are based on a different principle, however, and serve a different purpose)^(34,35) encourages us to believe, however, that a further size reduction in our electrodes below 1 mm is possible.

Silver-Silver Chloride Electrodes

These electrodes were first prepared by standard electrolytic and thermal methods⁽³⁶⁾. It was soon found, however, that "hybrid" microelectrodes of the Cole-Kishimoto type⁽¹⁴⁾ gave stabler potentials than the conventional electrodes. The "hybrid" electrodes contain platinized platinum, silver and silver chloride. It is probable that their specific surface is larger than that of the more conventional silver-silver chloride electrodes and that this accounts for their high stability.

The plating circuit consists of the electrolytic cell, a 100,000 ohm potentiometer, milliammeter, and three volt battery in series. Twenty-two gauge silver wire (anode) is plated with AgCl for about eighty minutes at 0.04 milliamperes. The electrolyte is 0.5M KCl and the cathode a platinum wire. The silver wire is completely sheathed in plastic tubing, except for its tip. After rinsing both electrodes, polarity is reversed, and they are immersed in Kohlrausch solution (H_2PtCl_6 with a small amount of lead acetate)⁽³⁷⁾. Platinizing is carried out at a current of 0.04 ma for 17 minutes. The electrodes are rinsed, polarity reversed again, and the electrodes returned to the KCl solution, where an additional amount of AgCl is deposited for one minute at 0.04 ma.

These electrodes proved to be stable microprobes for electrical potential sensing in chloride solutions. Their potential depended on the chloride concentration as predicted by the Nernst equation.

These electrodes were used as potential probes in most of the experiments described in Section III.A and proved stable and reliable. Because of the relatively small amount of ions migrating through the ion-exchange membranes under rapid flushing of the cell compartments with identical solutions, the potential drop between the electrodes and the solutions in which they are immersed was almost equal for each electrode pair, and constant with respect to time. Asymmetry potentials were determined outside of the cell and were found to be smaller than other errors and fluctuations in the potential differences measured under current flow.

pH-Electrodes

The development of microelectrodes for the detection of pH changes near the membrane surfaces presented more difficulties, but some encouraging progress was made with antimony electrodes. It is possible to make and/or obtain commercially⁽³⁸⁾ experimental glass electrodes with characteristic tip dimensions of about 1 mm, and it may be possible to develop smaller ones. The impedance of these electrodes is very high, however, and further scale-down would involve special instrumentation; because of the very high impedance one expects also slow response in that case. We therefore concentrated our efforts on antimony electrodes. Large antimony electrodes were in common use in analytical laboratories before the large-scale commercial availability of sturdy glass electrodes. While they are not as stable and reliable as glass electrodes, they give reasonably accurate results if calibrated properly^(36,39), and are in principle more amenable to miniaturization because of their much lower impedance. Small antimony electrodes are being used for dental research.*

Several pairs of micro pH-probes were prepared. They consist of micro-antimony electrodes and micro KCl-bridges (Luggin capillaries) leading to calomel electrodes. The outer diameter of either of these

* The author thanks Dr. I. Kleinberg, University of Manitoba, Winnipeg, Canada, for his advice and the gift of a dental research electrode.

probes is about one millimeter. They were inserted into the cell and their potential measured as a function of the cell current, after their position had been adjusted properly in an equipotential plane. In other words, the position of the electrodes was adjusted so that they did not register an IR drop at low current densities. It was assumed that any change in the potential difference between the electrodes is due to pH changes. A calibration curve had been prepared previously for each electrode pair by electrometric titration of a universal buffer solution. It was found that while the microelectrodes performed very well under the calibration conditions outside the cell, their performance within the cell during the passage of current was frequently unstable and erratic. On the other hand, certain 3-electrode assemblies showed promising results within and outside the cell. These assemblies contain two antimony electrodes and a Luggin capillary mounted flush in epoxy resin. The area defined by the tips of these electrodes is placed parallel to the membrane. One antimony electrode (the "auxiliary electrode") serves to pass periodically a polarizing current through the other. After this current is switched off, the potential difference between the second antimony electrode and the Luggin capillary is allowed to reach a steady value which was found to indicate the pH in the vicinity of the (second) antimony electrode. The periodic polarization-depolarization thus seems very useful.

This method was discovered and tested only toward the end of the contract period; thus only preliminary (and promising) results were obtained. This aspect of the work is being continued under a new grant.

III.D. Membrane Roughness Measurements

Because of the importance of hydrodynamic conditions at the membrane-solution interface for polarization phenomena, the surface roughness of three membranes used in our polarization studies was measured. It is known from other mass transfer studies that surface roughness can be a significant factor in determining the turbulent flow pattern near the interface. Therefore we wanted to determine the magnitude of the roughness for different membranes used in our previous measurements. These membranes had exhibited different polarization behavior.

The roughness was measured with a profile meter, Model V "Mototrace" (Physicists Research Company, Ann Arbor, Michigan). The membranes were measured in a wet state, after having been superficially dried with a paper towel. The results are shown in Figure 21.

It is seen that the membranes vary appreciably in surface roughness. The roughness of the American Machine & Foundry Company (A.M.F.) membrane shows no distinct periodicity whereas the Ionics membrane does. This periodicity reflects the mesh of the fabric backing the membrane whose threads are on the average about 1 mm apart. The Ionac membrane is also backed by a fabric, but the weave is much tighter; it is not clear whether the appreciable surface roughness of this membrane is entirely due to the backing material.

With regard to the hydrodynamic aspects of this research, the surface roughness shown in Figure 21 might prove to be quite significant. The larger protrusions are of the order of 0.1 mm, which is larger than the boundary layer thickness. Therefore we might expect the membrane itself to disrupt to a certain extent the development of the boundary layer and to promote turbulence.

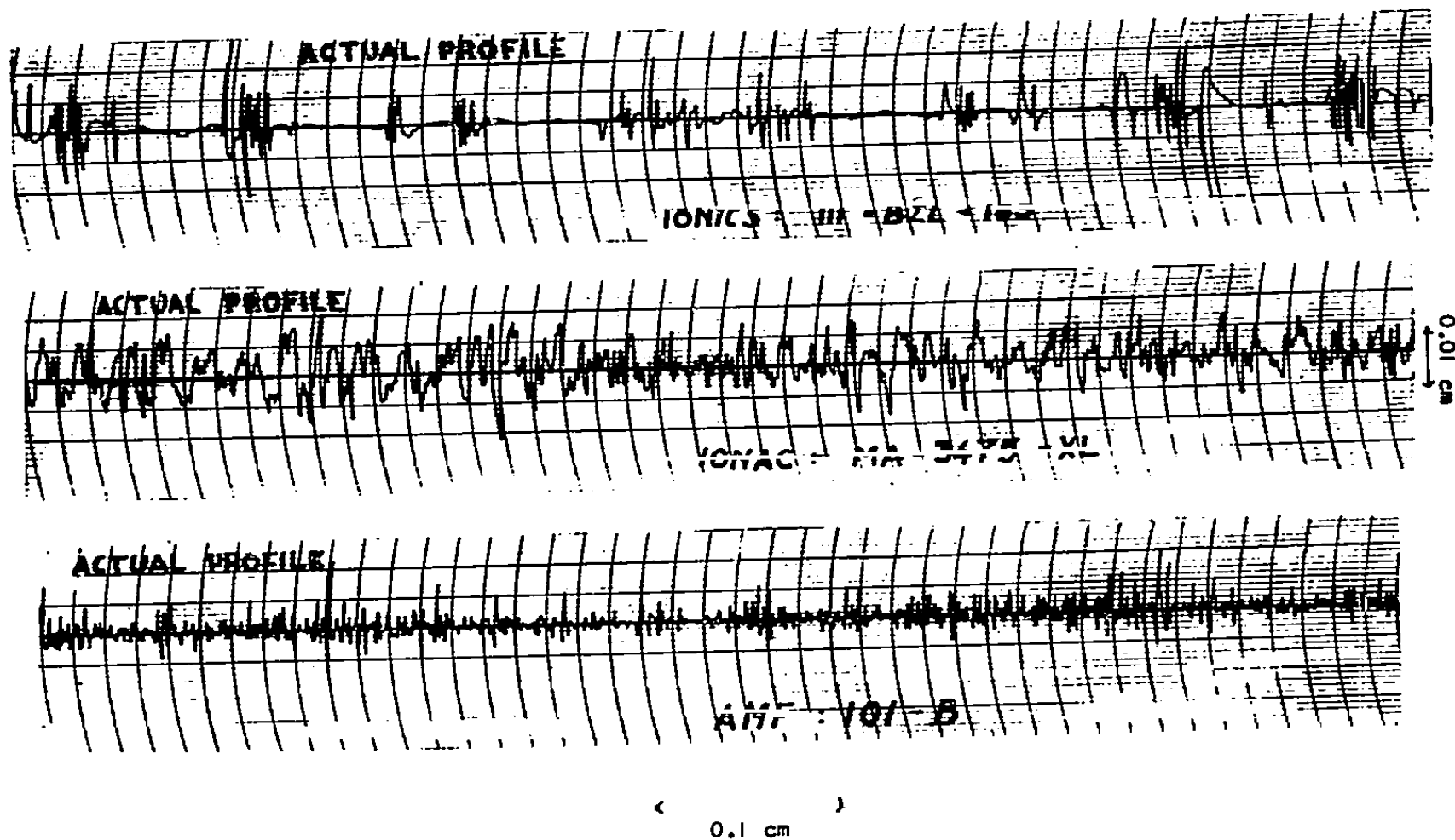


FIGURE 21. SURFACE ROUGHNESS MEASUREMENTS OF THREE ION-EXCHANGE MEMBRANES

III.E. Pilot-Size Cell

The findings of the laboratory experiments were utilized in the design of a large cell for the study of polarization at single anion-exchange membranes of size 1.5 foot x 1.5 foot. While this cell was designed and built during the period of grant 14-01-0001-652, there was not enough time to perform experiments with it during the grant period. Therefore no more than a brief description is given here. The experiments are being continued under a new grant 14-01-0001-1295.

The large cell was designed for the measurement of current-voltage curves at different locations of electro dialysis membranes, and in the presence of different spacers. Current can be measured in eight sections separately; provision is also made for the insertion of micro-electrodes. Redox solutions can be used in the electrode compartments in order to reduce the voltage drop in them; laboratory experiments in a small cell indicated that a sufficiently high voltage drop reduction is indeed possible.

III.F. Radio-Frequency Measurements

III.F.1 Introduction

In experiments described in Section III.A.4 we found that for some ion-exchange membranes the current-voltage curves are almost independent of the solution flow rate. This indicates that under the conditions of these experiments the solution-boundary layer at the membrane-solution interface is not controlling the rate of mass transfer, and raises the question of internal polarization phenomena within the membrane, brought about by heterogeneities. Moreover, the appearance of linear "slanted plateau" regions observed with some membranes also suggests heterogeneity. In fact, a similar phenomenon has recently been claimed to exist in membranes into which macroscopic heterogeneities were incorporated on purpose⁽⁴¹⁾.

Therefore we are interested in quantitative methods characterizing membrane heterogeneity. Electron micrographs have been used for a considerable time to study heterogeneities in ion-exchanger granules^(42,43) and membranes^(27,44), and have indeed demonstrated the existence of heterogeneities on membrane surfaces, as well as very considerable differences between different ion-exchange membranes with respect to the type and characteristic size of the heterogeneities. The interpretation of Donnan uptake data in ion-exchange materials also leads to the conclusion that submicroscopic heterogeneities exist in them^(25,26,45) and similar conclusions were reached from the detailed evaluation of diffusion data⁽⁴⁶⁾.

We thought that the measurement of the radio-frequency properties of ion-exchange membranes should provide a quantitative indication of membrane heterogeneity, because it is well known that a heterogeneous mixture of conductors shows a dispersion of the dielectric constant and conductivity ("Maxwell-Wagner effect") which for materials of the type of our membranes should be located in the radio-frequency range^{(47)*}, and has indeed been found in columns containing ion-exchanger-solution systems which are macroscopically heterogeneous in that range⁽⁴⁸⁾, and

*For the purpose of this discussion, the "radio-frequency range" is taken as about 1-100 megacycle sec⁻¹.

quantitatively interpreted as a consequence of their heterogeneity. If this interpretation is correct, one should expect a similar dispersion in the radio-frequency range due to microscopic and, perhaps, submicroscopic heterogeneities. While it is not always possible to determine the characteristic dimension of the heterogeneities from such measurements,* the detection of such dispersions is of relevance to membrane performance, since the dispersion in this range attests to the deviation of the membrane from the single-phase ("chemically homogeneous") model⁽⁴⁹⁾ on which the most common membrane concepts and equations are based.

We have indeed found such dispersions with six membranes and will describe our results in the following. Since the technique of measurement is not a simple one, however, much of the work during this grant period consisted of the development of the methods of measurement. The results should be considered preliminary, and no quantitative theories based on them, nor far-reaching hypotheses reached from them before this work has proceeded through further stages of refinement of method and evaluation. We do believe, however, that the appearance of the dispersion in the radio-frequency range in all six cases is noteworthy; and it is for this reason that the present stage of the method development and the preliminary results are reported here. If these are borne out by future work, these findings would open the way to a non-destructive method for characterizing membrane heterogeneities by the frequency dispersion characteristics of the membranes.

III.F.2 Principle

The use of radio-frequency measurements for the determination of membrane heterogeneity will be illustrated by the simple example of a "half-sandwich" membrane, consisting of two different layers, 1 and 2, respectively in series, each of which has different transport coefficients. If the resistances and capacitances of these layers are designated by R (ohm) and C (absolute farad) respectively, it is found that the apparent

*For instance, the evaluation of the dispersion observed for ion-exchange resin-solution systems [described in reference (48)] is independent of the particle size of the resin. Even submicroscopic heterogeneities, such as double layers of colloids, can indeed give rise to dispersions in this frequency range.

resistances, R_a , and capacitances, C_a , as measured with a Schering bridge (or any similar instrument) are strongly dependent on the frequency.

Elementary network theory leads to the following expressions:

$$R_a = (C' + E) \left[1 + \omega^2 \frac{(D + F)^2}{(C' + E)^2} \right] \quad (63)$$

$$C_a = (D + F) / \left[1 + \omega^2 \frac{(D + F)^2}{(C' + E)^2} \right] \quad (64)$$

where $\omega = 2\pi f$ (65)

$$C' \equiv \frac{R_1^2 C_1}{1 + \omega^2 R_1^2 C_1^2}; \quad E \equiv \frac{R_2^2}{1 + \omega^2 R_2^2 C_2^2} \quad (66)$$

$$D \equiv \frac{R_1^2 C_1}{1 + \omega^2 R_1^2 C_1^2}; \quad F \equiv \frac{R_2^2 C_2}{1 + \omega^2 R_2^2 C_2^2} \quad (67)$$

Even without going into a detailed discussion of these formulae,* one can easily calculate in what approximate frequency range the dispersion may be expected: It is readily seen from the formulae that maximum changes of C_a and R_a occur when $\omega^2 C^2 R^2 (= \omega^2 C^2 / K^2$, where K is the layer conductance) becomes unity. Now the ratio C/K is equal to

$$C/K = 0.0885 \times 10^{-12} \epsilon / K \quad (68)$$

where ϵ is the dielectric constant and K the conductivity ($\text{ohm}^{-1} \text{cm}^{-1}$) of the respective layer. Taking values of $\epsilon=38$, $K=2 \times 10^{-3}$ mho cm^{-1} as

*Some discussion may be found in references 47 and 50.

rough estimates, we obtain for the frequency, f' , at which $\omega^2 C^2 R^2$ becomes unity:

$$f' = \frac{\omega'}{2\pi} = \frac{1}{2\pi} (C/K)^{-1} = \frac{1}{6.28} \left(0.0885 \times 10^{-12} \times \frac{38}{2 \times 10^{-3}} \right)^{-1} = 95 \times 10^6 \text{ cycle sec}^{-1}$$

Depending on the exact values of the capacitances and conductances of the different layer regions of the membrane, the frequency characteristic of the dispersion can vary accordingly. If element 1 is primarily a capacitance (very large R_1) and element 2 primarily a conductance (very small C_2) and if the thickness of layer 1 is one order of magnitude less than that of layer 2, one would expect the dispersion to occur roughly at 10 megacycle sec^{-1} . At any rate this rough calculation shows that dispersions in the radio-frequency range should be quantitative indicators of membrane heterogeneity. This conclusion is in line with previous radio-frequency work on systems containing electrolyte solutions and granular ion-exchange resins⁽⁴⁸⁾, and with work on biological membranes.

In order to stay within the range of conventional bridge instruments for the radio-frequency range, we measured the complex impedance of a stack of 10 membranes separated by thin solution layers of well-defined thickness (0.0625"), followed by the measurement of a stack of 5 membranes.* The solution layers were introduced because it is possible to obtain well reproducible membrane-solution contact, while irreproducible contact resistances are liable to develop if one just places one wet membrane on top of the other between a pair of electrodes. It is necessary to have a number of membrane thicknesses in series, because the conductance of a single membrane of reasonably representative area is generally too high for the range of available instrumentation. By measuring the impedance at two different sample thicknesses in this manner, one can correct for the impedance of the transmission line which is considerable (especially

*In the first stack there are 9 solution layers between the membranes, one between the bottom membrane and bottom electrode, and a double solution layer between top membrane and top electrode (altogether 12 solution spaces, i.e. 0.750" = 1.905 cm solution thickness). In the second stack there are 4 solution layers between the 5 membranes, and one each between the electrodes and adjacent membrane. Hence both membrane and solution total thickness are halved in the second stack.

at the higher frequencies) and is left with the impedance of a series combination of membrane and solution.

The impedance of the solution alone is then computed from measurements of the solution impedance at two electrode distances, and subtracted from the impedance of the whole stack, thus leaving only the complex membrane impedance from which the dielectric constant and conductivity can be calculated.

III.F.3 Apparatus

The impedances were measured with an "RX Meter" Type 250 (Boonton Radio Corp., Boonton, New Jersey) the cell being mounted directly on top of the chassis. The cell is shown in Figure 22 and the principle of measurement at two different electrode distances in Figure 23. Note that the length of the transmission line is the same in both positions and the geometry of the line is similar. The two electrode distances are 1 inch and 0.5 inch respectively.

The cell material was "Plexiglas" in our first experiments, but when unduly high dissipation was found above 50 megacycle sec^{-1} , it was replaced by "Teflon" which indeed has lower dissipation in this range. The experiments were performed in a constant-temperature room (18°C). The liquids used were 0.001N and 0.01N aqueous NaCl solutions and distilled water, and the membranes Ionics III BZL 183 (anion-exchange) and CR-61 (cation-exchange). Only the measurements with Ionics III BZL 183 in distilled water have been evaluated so far and are reported in the following.

III.F.4 Evaluation and Results

a. Calculation of sample impedance. To calculate the impedance of the stack containing 10 membranes (total thickness 0.25 inch) and associated solution layers (total thickness 0.75 inch), it was first necessary to eliminate the transmission line impedance by calculation. The impedances were interpreted in terms of circuits of the type shown in Figure 24 (a) and (c). These networks consist simply of two impedances in series, shunted by a parallel capacitor, C_t (μf farad). One of the series impedances, Z_{tr} (ohm), represents the transmission line, the other, composed of a resistance and a capacitance in parallel [R_s , C_s and R_s/l , lC_s in Figure 24 (a) and (c), respectively] represents

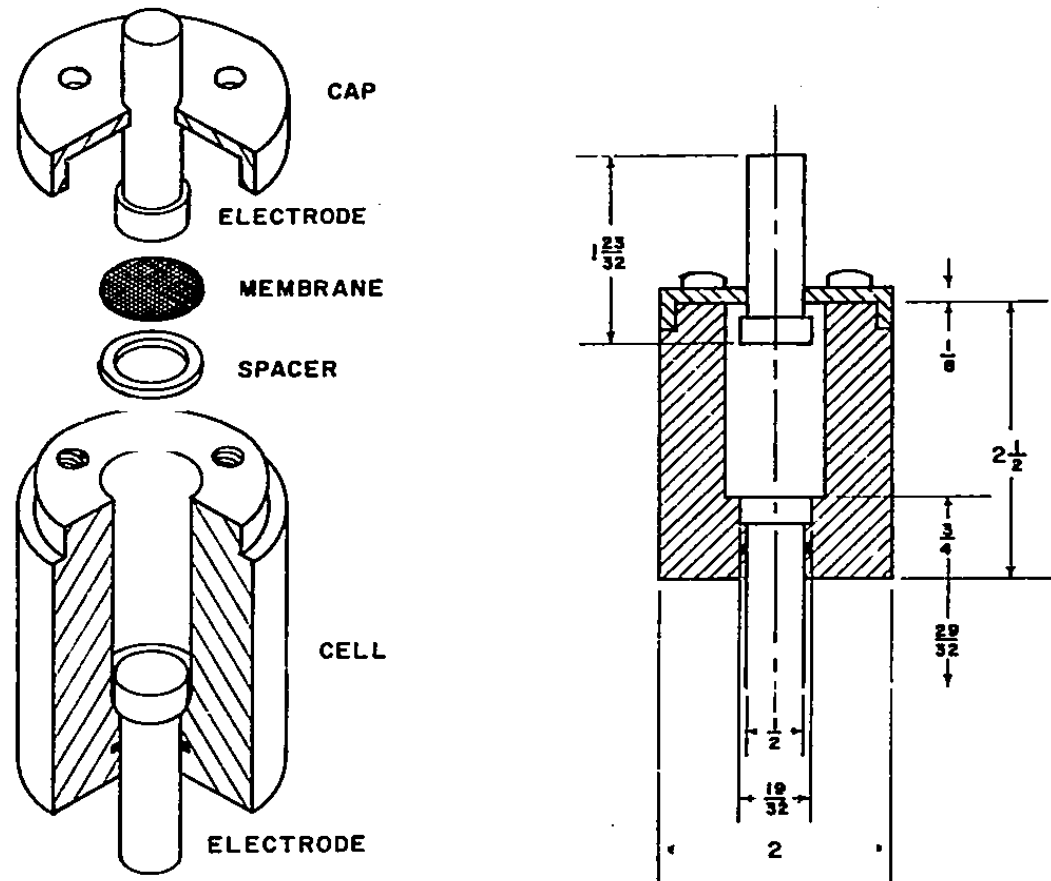


FIGURE 22. CELL FOR RADIO-FREQUENCY MEASUREMENTS AT DIFFERENT ELECTRODE DISTANCES

(Cell dimensions are in inches.)

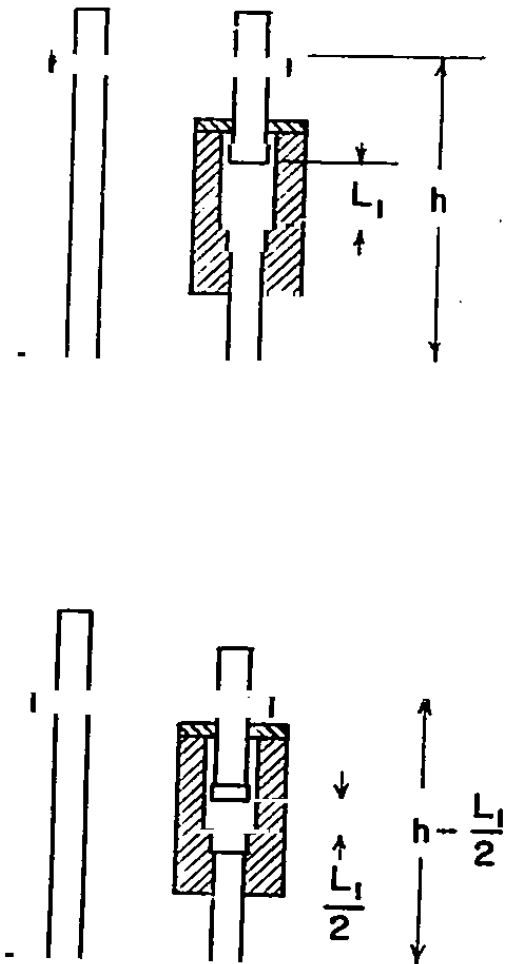
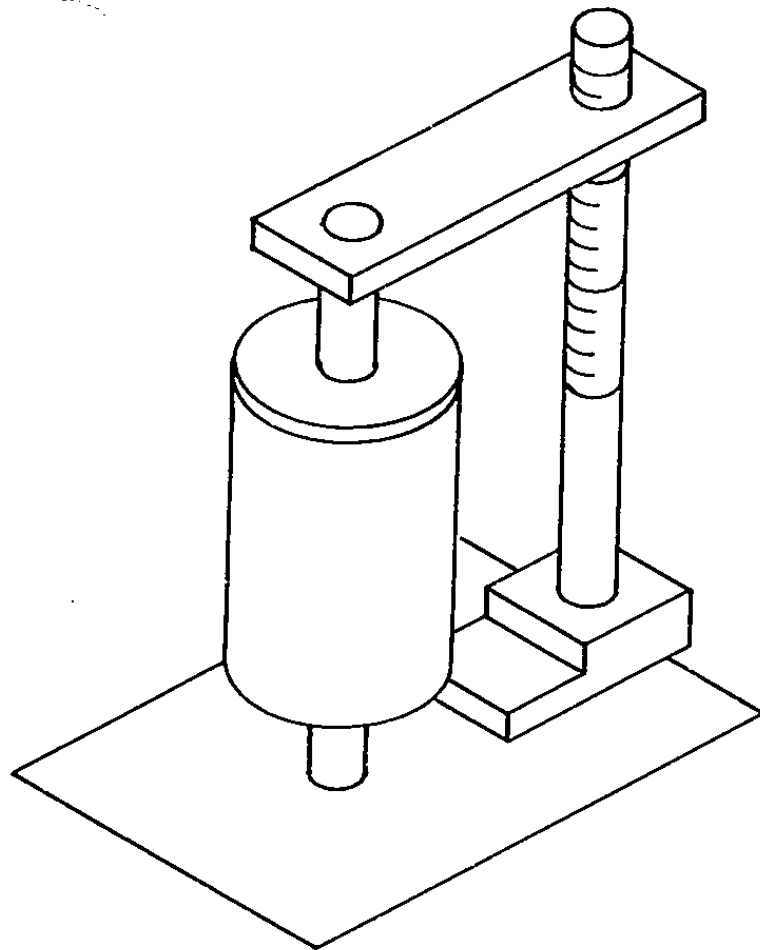
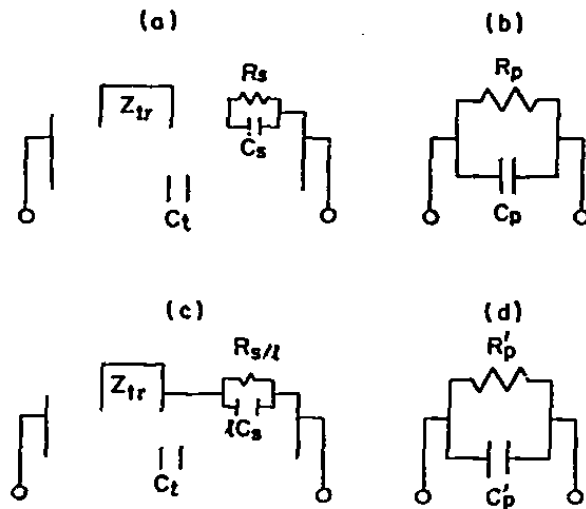


FIGURE 23. SCHEMATIC REPRESENTATION OF CELL AND TRANSMISSION LINE AT TWO DIFFERENT ELECTRODE DISTANCES



$$R_s = \frac{\left[\frac{R_p^2(C_p - C_t)}{1 + R_p^2\omega^2(C_p - C_t)^2} - \frac{R_p'^2(C_p' - C_t)}{1 + R_p'^2\omega^2(C_p' - C_t)^2} \right]^2 \left[(1 + R_p^2\omega^2(C_p - C_t)^2)(1 + R_p'^2\omega^2(C_p' - C_t)^2) \right] \omega^2}{[R_p(1 + R_p'^2\omega^2(C_p' - C_t)^2) - R_p'(1 + R_p^2\omega^2(C_p - C_t)^2)](l - 1)} + \frac{\{R_p(1 + R_p'^2\omega^2(C_p' - C_t)^2) - R_p'(1 + R_p^2\omega^2(C_p - C_t)^2)\}^2}{[(1 + R_p^2\omega^2(C_p - C_t)^2)(1 + R_p'^2\omega^2(C_p' - C_t)^2)](l - 1)} \quad (69)$$

$$C_s = \left[\frac{(1 + R_p^2\omega^2(C_p - C_t)^2)(1 + R_p'^2\omega^2(C_p' - C_t)^2)(l - 1)}{R_s\omega^2\{R_p(1 + R_p'^2\omega^2(C_p' - C_t)^2) - R_p'(1 + R_p^2\omega^2(C_p - C_t)^2)\}l} - \frac{1}{R_s^2\omega^2} \right]^{1/2} \quad (70)$$

FIGURE 24. EQUIVALENT CIRCUITS FOR CELL AND TRANSMISSION LINE^(4B)

Networks (a) and (c) describe line impedance, Z_{tr} , stray capacitance, C_t , and impedance of material in cell, represented by a resistor, R_s , and capacitor, C_s , in parallel. Electrode distances in measurements represented by networks (a) and (c), respectively, are in ratio l . "RX" meter presents results in terms of (b) and (d), respectively.

the sample. C_t represents the stray capacitance of the transmission line and the electrodes, i.e., the capacitance measured when there is no sample between the electrodes. It was found to be 3.00 and 2.75 μf for the "Plexiglass" and "Teflon" cells respectively, almost independent of the frequency. In our experiments $l=2$.

Equating the expressions for the impedances of circuits (a) and (c) obtained from elementary network analysis⁽⁵⁰⁾ to those of (b) and (d), respectively, one obtains two equations of complex variables from which the line impedance, Z_{tr} , can be eliminated. The real and imaginary parts of the resulting single equation then lead to Equations 69 and 70 for the true resistance (ohms) and capacitance (μf) of the sample of l inch length, respectively, at frequency f (sec^{-1}) (48,51).

Equations 69 and 70 contain R_p , C_p , R_p' , and C_p' which are read directly from the "RX Meter," the stray capacitance, C_t , determined previously when the sample is not in the circuit, and the angular frequency $\omega = 2\pi f$ at which the measurement is carried out.

A computer program was written and used for rapid evaluation of the stack resistance, R_s , and capacitance, C_s , by Equations (69) and (70) respectively. The same equations were used to determine resistance, R_w , and capacitance, C_w , respectively of a 1 inch deep layer of liquid alone. The resistance, R_m , and capacitance, C_m , of the membranes alone was then calculated by subtracting vectorially the impedance of the liquid column of height 0.75 inch from the total impedance of the stack.* This is an elementary operation⁽⁵⁰⁾ which yields the following result:

$$R_m = \left[\frac{R_s}{1 + \omega^2 R_s^2 C_s^2} - \frac{D' R_w}{1 + \omega^2 R_w^2 C_w^2} \right] \left\{ 1 + \left[\frac{\omega R_s^2 C_s}{1 + \omega^2 R_s^2 C_s^2} - \frac{D' \omega R_w^2 C_w}{1 + \omega^2 R_w^2 C_w^2} \right] / \left[\frac{R_s}{1 + \omega^2 R_s^2 C_s^2} - \frac{D' R_w}{1 + \omega^2 R_w^2 C_w^2} \right] \right\}^2 \quad (71)$$

$$C_m = \left[\frac{1}{\omega R_m} - \frac{\omega R_s^2 C_s}{1 + \omega^2 R_s^2 C_s^2} - \frac{D' \omega R_w^2 C_w}{1 + \omega^2 R_w^2 C_w^2} \right] / \left[\frac{R_s}{1 + \omega^2 R_s^2 C_s^2} - \frac{D' R_w}{1 + \omega^2 R_w^2 C_w^2} \right] \quad (72)$$

*The exact height was 0.752 inch. The factor 0.752 is designated D' in Equations (71) and (72).

The specific conductance, κ_m ($\text{ohm}^{-1} \text{cm}^{-1}$) and the dielectric constant, ϵ_m , of the membrane are then calculated from Equations (73) and (74):

$$\kappa_m = \frac{L^2}{AR} \quad (73)$$

$$\epsilon_m = 11.3 \frac{L^2 C}{A} \quad (74)$$

where L^2 is the combined thickness of 10 membranes, 0.635 cm, and A the cross-sectional area of the membranes (1.78 cm^2). R is in ohm and C in $\mu\mu$ farad. The results are shown in Figures 25 to 27. The apparent dielectric constants and conductivities were computed from equations 71-74 with further correction for edge effects, measured in blank experiments with spacers and membrane rings only. These corrections (which were not done in the first experiments) are sufficiently large to affect the results appreciably.

It is seen that the computed dielectric constants and conductivities show dispersions in the range 1 - 20 megacycle sec^{-1} . It should be noted, that at these relatively low radio-frequencies the series impedance of the water layers separating the membranes is still relatively large. Therefore the results represent relatively small differences between large numbers. This explains the scatter of the points. In spite of this scatter, these preliminary results focus attention on the range 1 - 20 megacycle sec^{-1} for dispersions characteristic of the membrane. This range is roughly the same as found for aqueous polyelectrolyte solutions (52); it would therefore be of considerable interest to examine the possible application to the membranes of some of the concepts developed for these solutions.

It is of interest that in all cases the conductivities of the membranes at low frequencies were found to be extremely low. It is hard to assess the reliability of these figures at this stage, because literature values of membrane conductivities usually refer to membranes equilibrated with solutions. It remains to be seen whether a steep decrease of conductivity in membranes with decreasing solution concentrations occurs in very dilute solutions, or if this feature of the

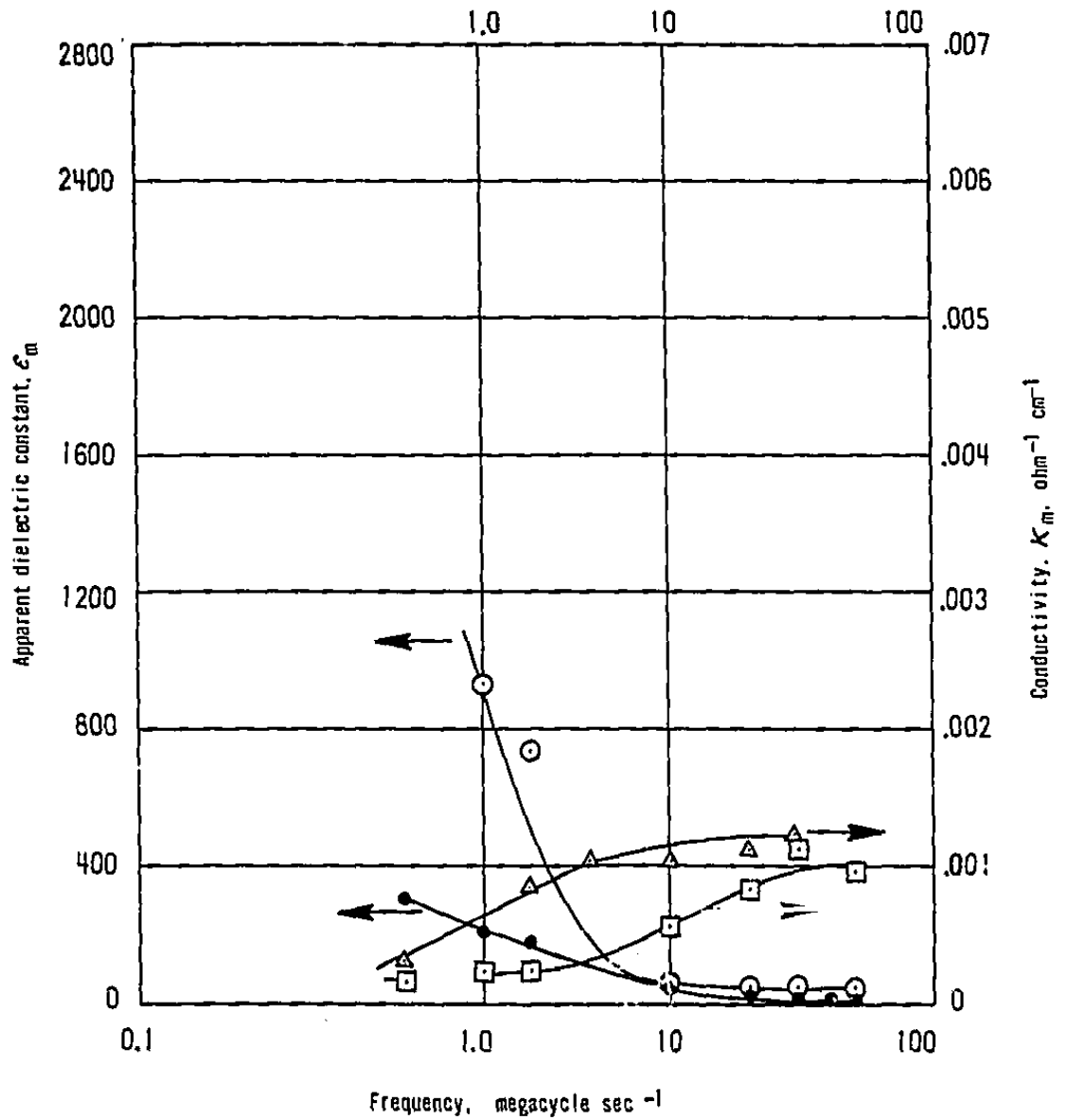


Figure 25. RADIO-FREQUENCY RESPONSE CHARACTERISTICS OF ION-EXCHANGE MEMBRANES (AMERICAN MACHINE & FOUNDRY CO.)

- Dielectric Constant } A 101B (A.E.)
- Conductivity } A 101B (A.E.)
- Dielectric Constant } C 103C (C.E.)
- △ Conductivity } C 103C (C.E.)

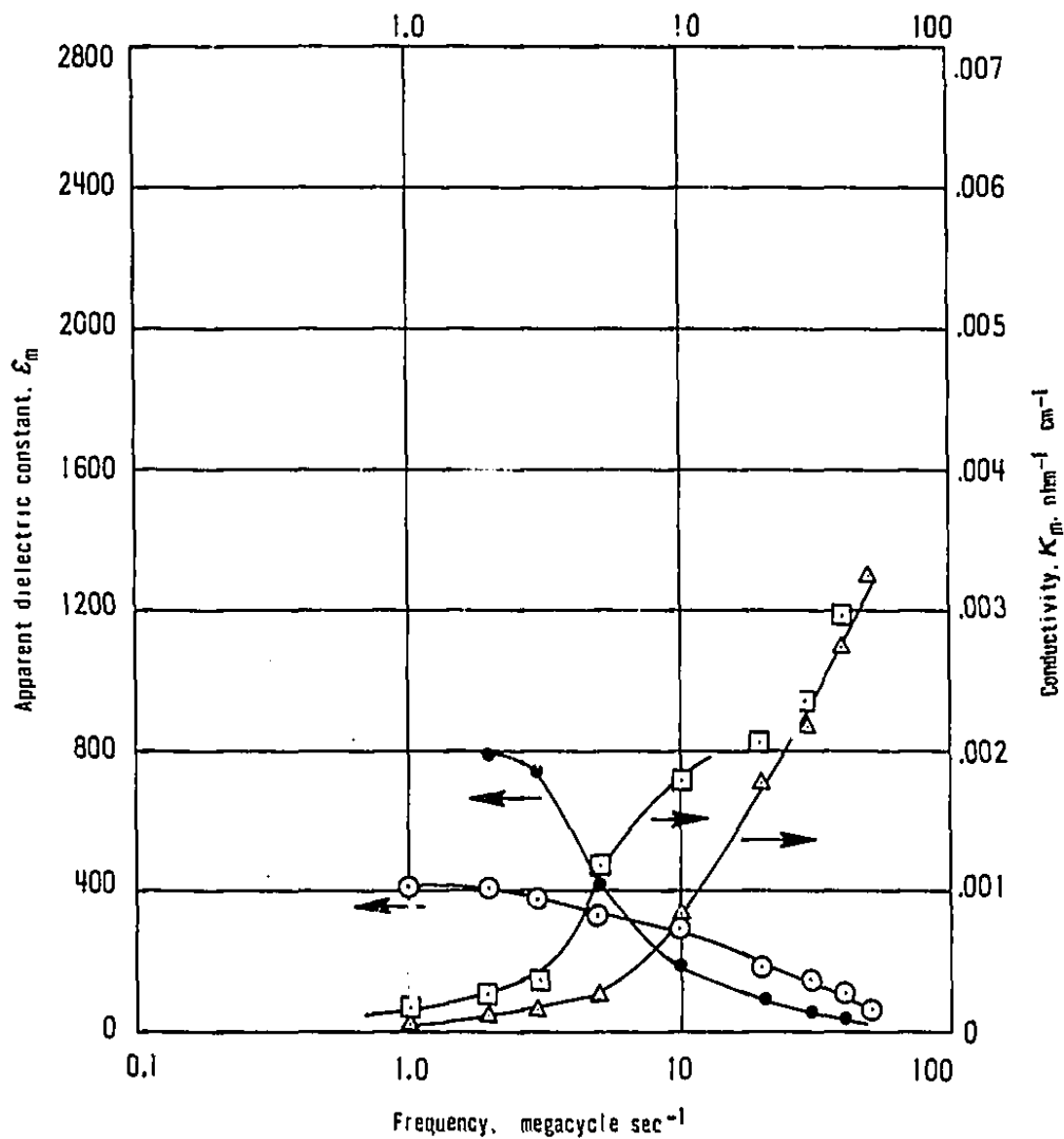


Figure 26. RADIO-FREQUENCY RESPONSE CHARACTERISTICS OF ION-EXCHANGE MEMBRANES (IONICS, INC.)

- | | |
|-----------------------|----------------------|
| ● Dielectric Constant | } 111 BZL 183 (A.E.) |
| □ Conductivity | |
| ○ Dielectric Constant | } 61 AZL 183 (C.E.) |
| △ Conductivity | |

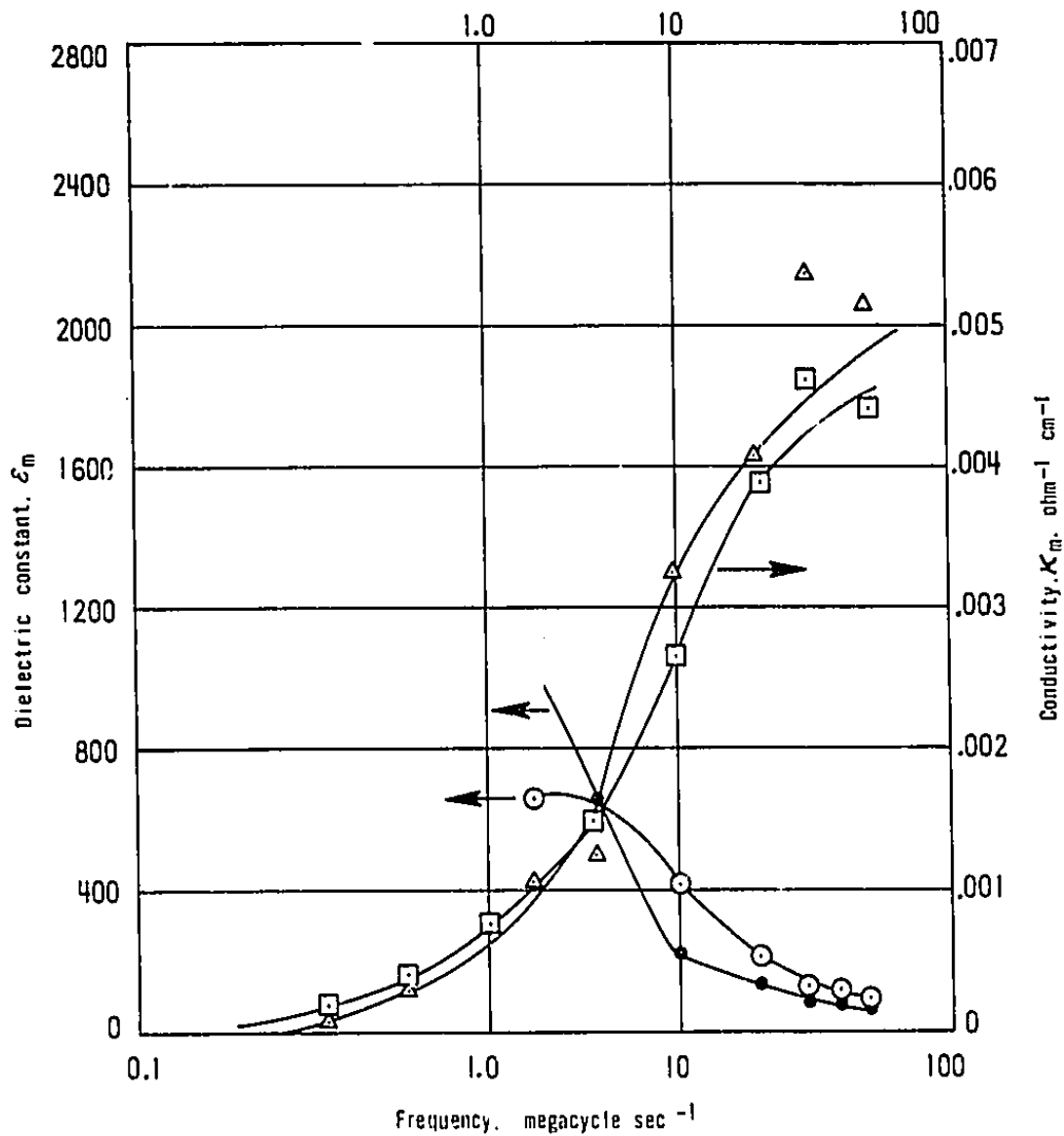


Figure 27. RADIO-FREQUENCY RESPONSE CHARACTERISTICS OF ION-EXCHANGE MEMBRANES (ASAHI CHEMICAL CO.)

- | | | |
|---|---------------------|---------------|
| ● | Dielectric Constant | } CA-1 (A.E.) |
| □ | Conductivity | |
| ○ | Dielectric Constant | } CK-1 (C.E.) |
| △ | Conductivity | |

curves is due to the relatively high impedance of the water layers separating the membranes and consequent inaccuracy of the results in the range as mentioned above. [A large decrease of the counterion self-diffusion coefficient in this concentration range has been reported⁽⁵³⁾.] At any rate the results point to the desirability of continuing these measurements with a redesigned cell incorporating considerably thinner water layers between the membranes.

IV. REVERSE OSMOSIS

IV.1 Introduction

The purpose of this study is the observation of electrical potential differences across membranes during the process of reverse osmosis, and in particular, their correlation with the mechanism of the reverse osmosis process, the operating variables, and, eventually, the nature of the membrane and the change of its performance with time.

Electrical potential differences had been observed previously in reverse osmosis experiments with ion-exchange membranes⁽⁵⁴⁾ where the mechanism can be readily explained by the fixed-charge nature of these materials. It was found, however, that potential differences develop even across seemingly neutral modified cellulose acetate membranes, and that these potential differences depend on the applied pressure and the brine circulation rate. The utilization of this phenomenon for quantitative monitoring of concentration polarization seems therefore reasonable.

Work during this grant period constitutes the beginning of this kind of investigation. In the first preliminary stage, we constructed a simple reverse osmosis test rig, utilizing a tubular modified cellulose acetate membrane, through which dilute sodium chloride solutions were recirculated from a tank at atmospheric pressure. The circulating solutions were pressurized up to 800 psi and the potential differences measured between a central, rod-shaped silver-silver chloride electrode (electrically insulated from the rest of the rig) and the membrane support tube on the low-pressure side whose inner surface was effectively converted into a silver-silver chloride electrode. After potential changes with pressure and circulation rate were measured, the second stage of this research was begun, namely the design and construction of a test rig for higher pressures (up to 1200 psi) and continuous circulation under high pressure (rather than from atmospheric to high pressure) at considerably higher rates (up to 195 gal/hr), enabling us to work beyond the laminar flow regime. All experiments during the grant period were performed with the first rig; the second rig was designed and built, and experiments with it are being carried out under a new grant (14-01-0001-1295).

IV.2 Layout of Apparatus

Cylindrical membranes, developed by Loeb and co-workers, similar to those used at the hyperfiltration pilot plant at Coalinga, California, were used⁽⁵⁵⁻⁵⁷⁾. This geometry was chosen not only for practical reasons, but also because in this case one can be reasonably sure what the high pressure saline water velocity profiles look like in both laminar and turbulent flow in the test cell. The difficulty with this geometry is the design of suitable electrodes. Membrane sealing presents no formidable problems.

As a first step, it was decided to use a concentric tubular assembly with a central rod electrode (Figures 28-29). The outer tube, which has the membrane mounted in it, served as the low-pressure electrode. The high-pressure saline water flowed longitudinally through the annulus, and the desalinated product water flowed through the membrane and then through porous nylon backing material between the membrane and tube. Water left the test section through a 1/16-inch diameter hole drilled through the tube wall. A copper nipple (1/4-inch OD) fitted around this hole conducted the hyperfiltrate into a graduate cylinder. Both electrodes were electrolytically coated with fine silver and then partially converted to silver chloride. The membrane was then mounted in the outer tube after completion of the chloridizing step. The result is a system in which two identical (silver-silver chloride) electrodes are placed on either side of the membrane. A short copper nipple soldered to the copper tube serves as electrical connection to the low-pressure electrode.

The electrodes were isolated from each other by replacing certain of the customary metal construction materials by plastic. A 316 stainless steel end manifold was built to support both electrodes. One end of the outer tube was connected to this manifold by a plastic copy of a Parker Triple Lok F5BX 37° flare tube adapter fitting (Parker-Hannifin Corp., Cleveland, Ohio), made from glass-filled "Delrin" (E. I. du Pont Company, Wilmington, Delaware). Saline feedwater entered the end manifold through this fitting. The high-pressure saline feedwater exited the manifold from the bottom while the inner electrode was mounted on the

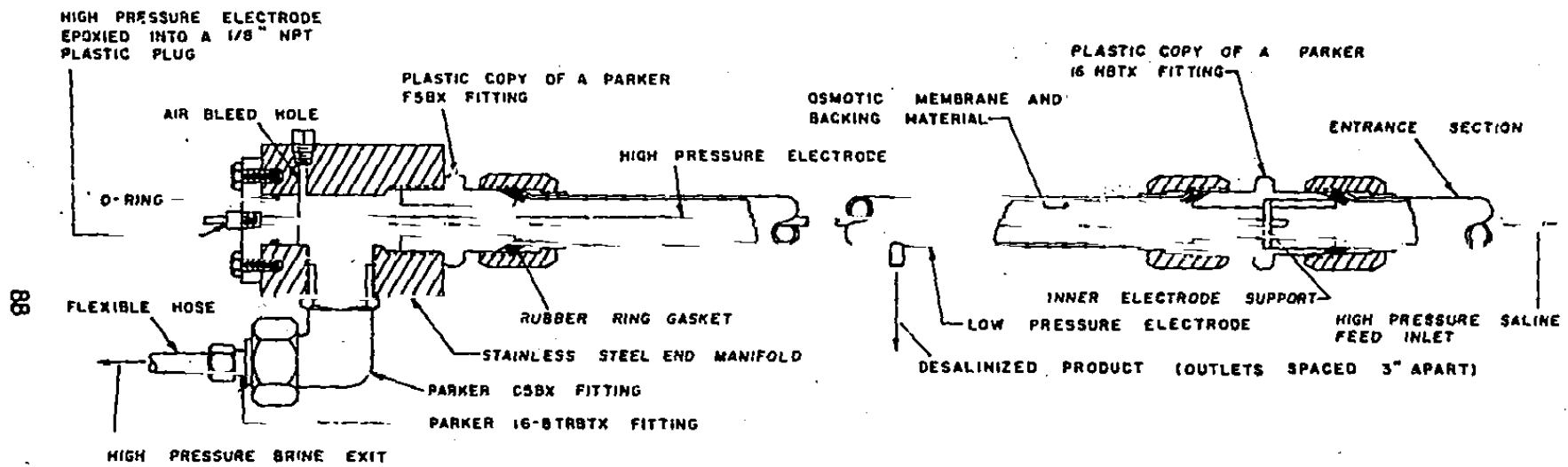


FIGURE 28. TEST SECTION FOR MEASURING ELECTRIC POTENTIALS DURING REVERSE OSMOSIS.

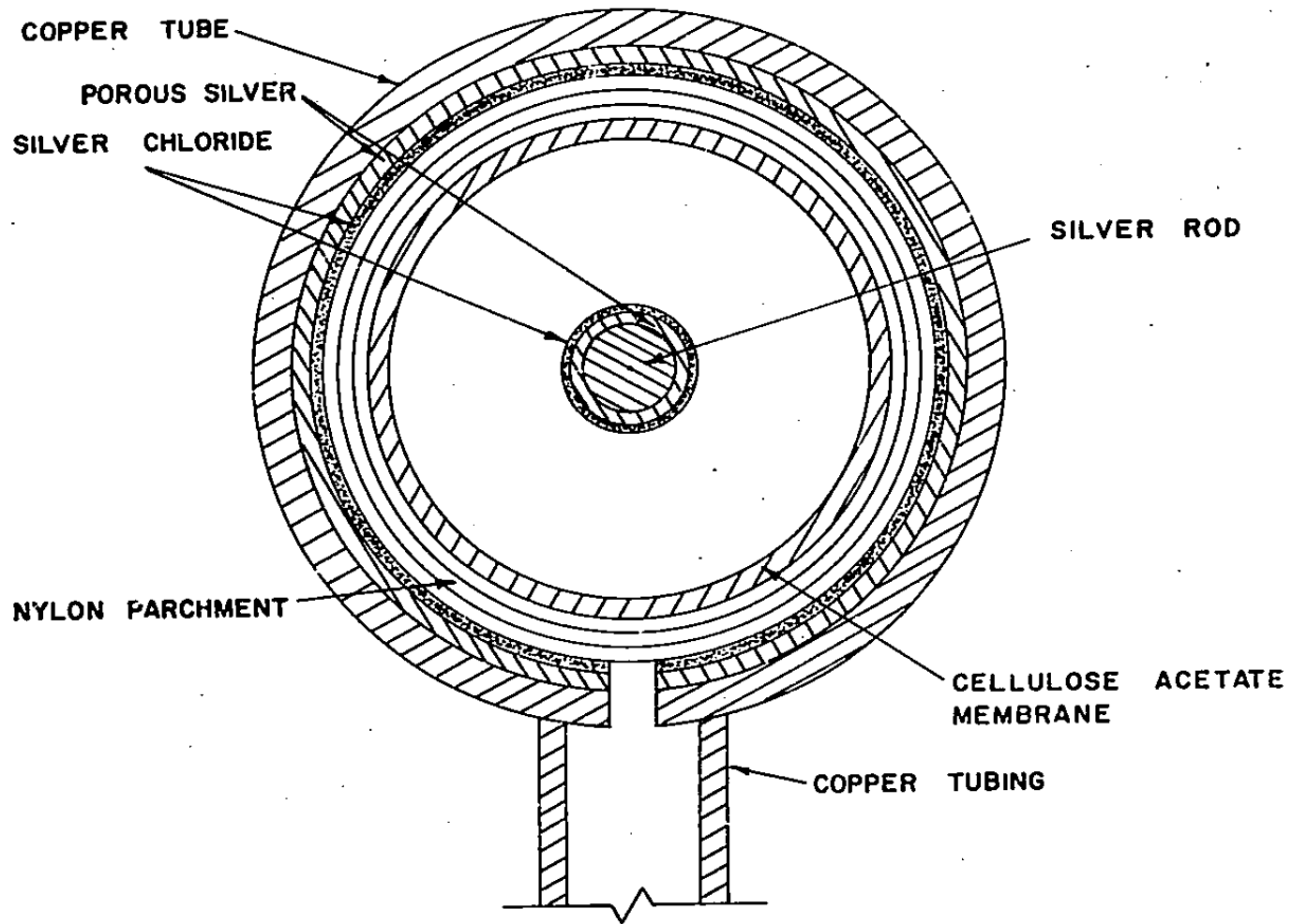


FIGURE 29. PROFILE OF REVERSE OSMOSIS TEST SECTION

manifold on the side opposite the tube entrance. This inner electrode was mounted in a plastic end cap which was then bolted to the manifold. For convenience, the inner electrode was epoxied into a 1/8-inch NPT plastic plug which fits into the plastic end cap that bolts onto the end manifold. The other end of the inner electrode was supported by a plastic retainer that fitted into a plastic copy of a Triple Lok HBTX 37° flare tube union (Parker-Hannifin Corp., Cleveland, Ohio) fitted to the other end of the tube. The electrodes were therefore isolated not only from each other but from the rest of the system as well, since they contact no other metallic parts.

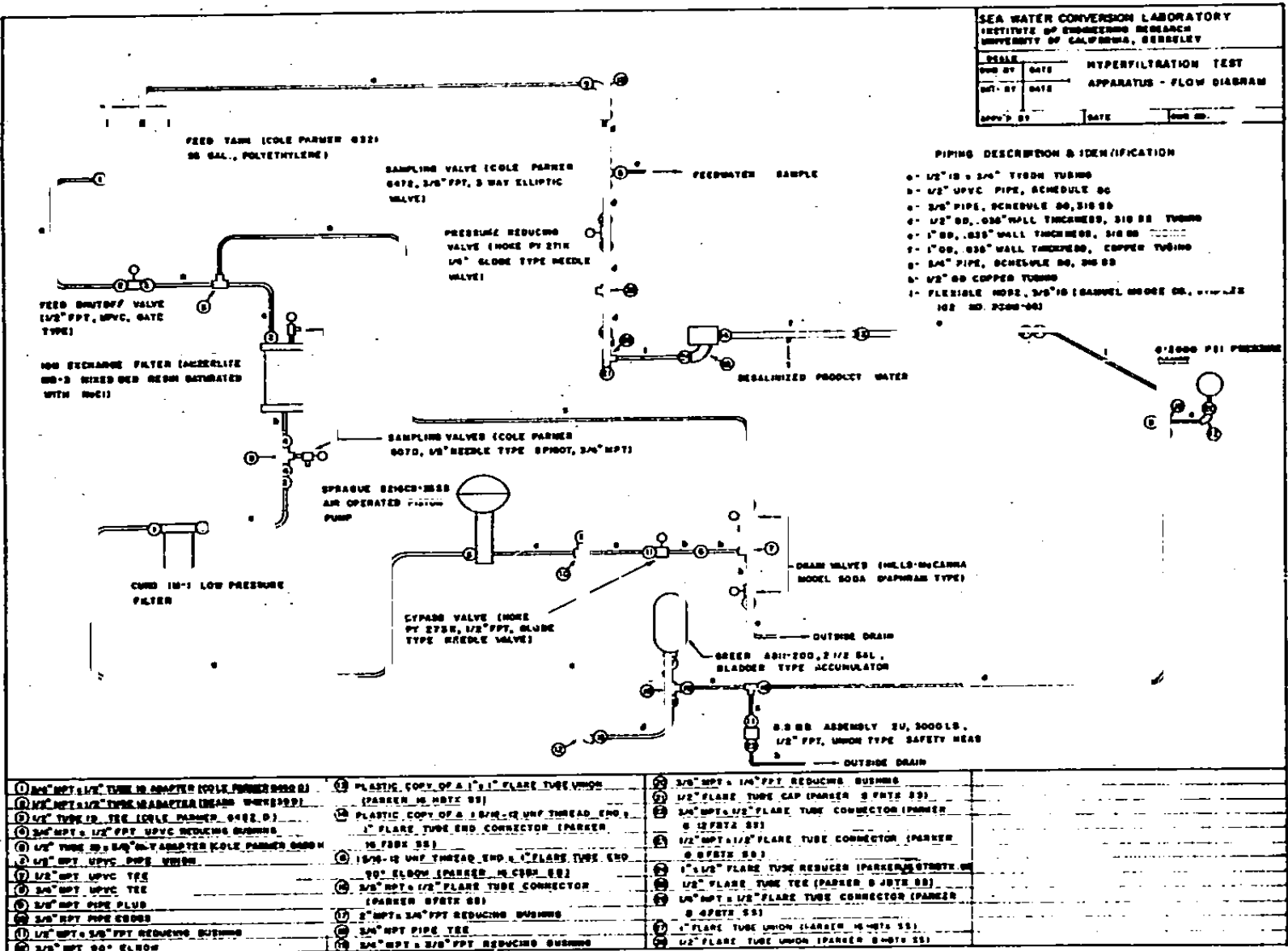
The voltage across the membrane was measured by connecting a high impedance voltmeter (Keithley 610B Electrometer, Keithley Instruments, Inc., Cleveland, Ohio) across the electrodes and observing how this voltage increases with pressure.

The flow scheme is shown in Figure 30. An entrance section preceded the test section. Made of 316 stainless steel tubing, this section served to reduce the effects of a sudden fluid flow transition from 3/8-inch ID to the 0.93-inch ID of the test section and to eliminate entrance effects for later mass transfer studies.

To minimize saline solution contact with metal, plastic fittings were used in the pressure section of the apparatus. A 55-gallon polyethylene tank was used to store saline feed solution, and most of the low-pressure flow lines were flexible "Tygon" tubing. Where threaded pipe and greater strength was required, 1/2-inch schedule 80 UPVC pipe (polyvinylchloride) was used. The "Tygon" tubing permitted observation of the condition of both saline feedwater flowing to the pump inlet and the saline effluent returning to the feed tank after going through the pressure-reducing valve.

The high-pressure lines, not including the entrance and test sections, were of either 3/8-inch schedule 80 pipe or 1/2-inch OD, 0.035-inch wall thickness tubing. The inner diameters were 0.423-inch and 0.430-inch respectively, and both can be used for pressures below 2000 psig. Lines and fittings were made of 316 stainless steel. The pipe was used where there are relatively few modifications expected for the future. The tubing was used where modifications, such as length changes in the test

FIGURE 30. REVERSE OSMOSIS FLOW SHEET, TEST SECTION



section, will be frequent, and also where maintenance operations might prove necessary (e.g. in the accumulator).

There were two lengths of flexible hose, one 3 feet long and the other 2 feet long. This hose (Synflex 102 No. 3000-08, Samuel Moore Co., Mantua, Ohio) has an inner diameter of 0.375 inch and is lined with teflon. With the exception of the metal end fittings, there was no other metal in the hose. The purpose of the flexible hose is to accommodate length changes in both the entrance and test sections.

The high-pressure fittings were all of 316 stainless steel, except for the plastic tube fittings. The pipe fittings were of the schedule 80 type or of the schedule 40 type specially tested to 3000 psig internal pressure. Parker Triple Lok 37° flare tube fittings were used in making various types of tubing connections. The flare tube fittings were readily available and can be used at high liquid pressures. As with the 3/8-inch pipe, the pipe fittings are used where there is relatively little possibility of future piping changes or where structural strength is needed.

Two methods of sealing pipe threads were tried. It was found that teflon tape gave better sealing results than the Baker Seal Product No. 899-21 Sealing and Lubricating Compound (Baker Oil Tools, Inc., Los Angeles, California). This is particularly so when large diameter pipe threads, as found in the accumulator, had to be sealed against high pressure liquid leaks. So far, tests up to 1000 psig have created no leakage problems.

All the valves are made of either plastic or 316 stainless steel. The high pressure valves are globe pattern needle-type valves [PY 271K (1/4-inch) and PY 273K (1/2-inch), Hoke, Inc., Cresskill, New Jersey]. They are used for pressure reducing, system filling, and flushing service. These valves use Kel-F stems to prevent galling of the valve seat. The low-pressure valves are of four types: (a) needle angle pattern [#6070, 1/2-inch needle-type spigot, Cole-Parmer Instrument & Equipment Company, Chicago, Illinois]; (b) diaphragm [Model 500A diaphragm-type valve, Hills-McCanna Company, Chicago, Illinois]; (c) gate [1/2-inch threaded UPVC gate valve, Tube Turns Plastics, Inc., Louisville, Kentucky]; and (d) three-way elliptic [Cole-Parmer #G472, three-way elliptic valve]. The gate valve served as a feed shutoff to the entire system, while the

diaphragm valves served as system and feed tank drain valves. The needle valves (one on either side of the ion-exchange column) and the three-way elliptic valve served as sampling valves for the feed and effluent streams of the test section respectively.

The ion-exchange column in the low-pressure feed line to the pump suction inlet served to remove traces of corrosion products and other ionic impurities. It was constructed from clear "Plexiglass" and used Amberlite MB-3 (Rohm & Haas Company, Philadelphia, Pennsylvania) mixed-bed resin equilibrated with sodium chloride and washed prior to the reverse osmosis experiments. The column used distributor plates which were sealed by 1/8-inch thick soft rubber gaskets to prevent liquid leakage. One of the plastic needle-type sampling valves was also used as an air purge valve when the ion-exchange column was being filled with liquid. The resin rested on a mat of glass wool, and the wool was supported on a 1-inch bed of 5 mm glass beads. An expanded plastic mesh screen prevented the glass beads from flowing out of the column and being sucked into the pump inlet.

As added protection against particulate matter flowing into the pump inlet, a small IM-1 filter unit (Cuno Engineering Corporation, Meriden, Connecticut) with a clear plastic housing was used. A cellulose cartridge filtered particles of greater than 5 microns in diameter.

To smooth out pressure surges due to the piston action of the pump, a heavy 2-1/2 gallon bladder-type accumulator (Greer Hydraulics, Inc., Los Angeles, California), specially modified for seawater, was used. The accumulator uses a cushion of nitrogen, supplied from an external source, to absorb the energy of the pressure fluctuations. High-pressure saline solution flowed directly into the accumulator, which was mounted vertically, and a tee, mounted directly below the accumulator, allowed the saline feedwater to flow to the test section.

To provide a measure of safety against the piping and tubing bursting under high internal pressure, a B.S.&B. (Black, Sivalls, & Bryson, Inc., Kansas City, Missouri) union-type safety head was employed as shown in Figure 30. In case the disc should rupture, the high pressure saline water is discharged, by means of a copper tube, to an area outside the laboratory and away from operating personnel and instruments.

An air-operated pump (Model S216CS-35SS Sprague Engineering Corp., Gardena, California) was used to pressurize the saline solution. The maximum pump pressure was 4600 psig at 100 psig operating air pressure. Operating air was supplied by a compressor in the laboratory. The Sprague pump is capable of providing liquid flowrates suitable for laminar-flow mass-transfer studies at high pressures. This pump is small and can be moved around if necessary. When the high pressure circulation pump was installed in the second stage of the investigation, the Sprague pump served as a make-up pump in order to maintain a constant saline feedwater concentration to the membrane test section.

The test and entrance sections were attached to a rack mounted on a 12-foot long table, constructed from slotted steel members (Acme Steel Company, Chicago, Illinois).

A tower assembly, which was not directly connected to the table which mounts the test and entrance sections, was built in order to elevate the feed tank and also to mount the pump, mixed-bed ion-exchange column, filter, and the accumulator. The feed tank had to be mounted about ten feet above the pump inlet in order to provide enough intake pressure for satisfactory performance of the pump piston packings. In addition to elevating the feed tank, the observation deck of the tower was built to accommodate two or three observers. The Sprague pump was bolted to the lower table in the tower, and a hole was cut in the upper table in the tower to accommodate mounting the accumulator. The observation deck was 8 feet and the feed tank deck 9 feet above the floor.

During the operation of the system, care was taken to purge air from the liquid flow lines. To accomplish this, a 1/8-inch NPT hole was drilled into the top section of the end manifold. The 1/8-inch NPT plug fitting into this hole was tightened only when water began to leak out when the system was being filled with saline solution. In addition, the pressure-reducing valve was brought to the wide open position, and the Sprague pump was operated to expel any air left in the lines. The expelled air was vented from the system effluent return line to the feed tank via the wide open pressure-reducing valve.

IV.3 Membranes

The membranes were cellulose acetate of the type developed by Dr. S. Loeb and co-workers at the University of California, Los Angeles. These membranes are cylindrical and are backed by a thin layer of porous nylon parchment inserted in a 1-inch OD support tube which has hyperfiltrate sampling outlet tubes soldered to it. [In our experiments, the inside of the tube was treated to be effectively a Ag/AgCl electrode. See section "Electrodes."] We wish to thank Dr. Loeb and his collaborators for the supply of the membranes and for the helpful advice and guidance he has given us on their preparation, use, and properties. The cellulose acetate membrane was used as a specific example of particular interest, but it is known that other types of reverse osmosis membranes also exhibit streaming potentials⁽⁵⁴⁾.

The method for membrane preparation is described in considerable detail in the literature⁽⁵⁵⁻⁵⁷⁾. Briefly, the membrane tube is cast from a mixture of cellulose acetate, formamide, and acetone in the proportions 25:30:45 weight percent respectively. The casting operation takes place at room temperature, and the membrane tube is subsequently immersed in ice water for approximately one hour. The membranes, in the "as cast" form have an average thickness of 0.0197 cm and an outer diameter of 2.29 cm, while the inner diameter of the 1-inch OD hard-drawn copper tube is 2.36 cm. The silver coating on the inside diameter of the copper tube is approximately 0.005 cm thick. The membrane is wrapped up to the flared ends of the tube with three layers of porous nylon parchment (French Fabrics No. 627T) to provide a low resistance path for the product water coming through the membrane. The wrapped membrane is then fitted into the treated copper tube. A rubber ring gasket is used to provide end seals between the flared tube ends and the flared tube fittings. The entire assembly is then heated to 91°C by passing 13 liters of hot water through the tube during 10 minutes at a gauge pressure of 0.40 to 0.55 atm. After the heating is completed, water at ambient temperature is passed through the tubular assembly at 0.6 to 0.8 atm until the assembly is cool. The tubular membrane assembly is then ready for use.

The tubes with the membranes were always kept filled with deionized water and closed to prevent membrane deterioration by drying.

IV.4 Electrodes

In the experiments reported here, the potential difference was measured between a cylindrical electrode placed at the axis of the hyperfiltration tube ("high-pressure electrode") and the outside pipe which held the membrane ("low-pressure electrode"). It was deemed important that both electrodes be reversible to chloride ion. Hence both were suitably treated, so as to convert their surfaces into large silver-silver chloride electrodes.

The potential measurements were carried out with a short reverse osmosis tube (length 6 inches) which had only one hyperfiltrate outlet tube. The plating methods described in this section are suitable for longer tubes also.

The silver-plating solution used in preparing the electrodes was potassium silver cyanide solution [100 grams of $KAg(CN)_2$ crystals dissolved in one liter of distilled water]. The anodes were of fine silver (99.9+ percent) in the form of 1/4-inch diameter rods for plating the inside of the copper tubes, and four 1/8-inch diameter rods spaced at the corners of a rectangle for plating the exterior of the inner electrode of the membrane test section which was also a 1/8-inch diameter silver rod. The current was kept constant by using a Model 4100 Research Potential Controller (Magma Corporation, Santa Fe Springs, California) operating as a galvanostat.

To plate the inside of the copper tube, its lower end was closed with a plastic plug that resembles one end of a 1-inch 36° flare tube union. This plug had a 1/2-inch diameter hole drilled about one-half inch deep in the flared end so that the rotating electrode would not wobble. A small electric motor with a Jacob chuck rotated the anode. Electric contact was made by a stiff copper wire, one end of which bore against the rotating metal shaft. In this operation, the copper tube was the cathode and a voltmeter was connected parallel with the plating cell. Cell voltages were kept below one volt. Plating solution completely filled the cell, including the flared ends. The current density was about 0.8 ma/cm^2 (based on tube ID) at about 0.1 to 0.4 volts across the plating cell, part of which was due to the contact resistance between the rotating anode and the copper wire contact. In this method, the flared tube ends did not receive as thick a silver coat as does the rest of the

tube wall; therefore, a second plating step was added: We immersed the inner electrode only 1/4-inch to 1/2-inch in the plating cell solution, making sure that the solution completely filled the cell and covered the flared ends, and continued silver plating at about 30 ma with the inner electrode rotating. The plating operation was periodically stopped and the plastic end fitting inserted into the opposite end of the tube so that the other flared end could be plated. For the 6-inch tubes, 5 to 6 grams of silver were plated on the inside diameter in order to insure a thick coating that would not permit the exposure of copper to the chloridizing solution. After the plating was completed, the inside diameter of the tube was soaked in concentrated ammonium hydroxide from 6 to 12 hours. If copper was exposed through the silver coating, this was detected by the blue color appearing in the ammonia solution. (In that case the electrode was cleaned and replated.) The silver-plated surface was then soaked for 6 to 12 hours in deionized water which was frequently changed.

Before silver plating, the surface was sanded with #120-J emery paper, followed by Croccus cloth. The surface was then rinsed with dilute nitric acid followed by distilled water. The anode was washed with concentrated nitric acid, rinsed in distilled water, sanded with #120-J emery paper, and then rinsed with distilled water again before being used for silver plating.

A portion of the deposited silver was then converted to chloride, by making the electrode the anode. IN hydrochloric acid solution was used and a different fine silver rod served as the rotating cathode. Currents of about 30 ma were used at from 0.6 to 0.9 volts across the cell. Hydrogen bubbles formed on the cathode and only a few, if any, bubbles formed on the surface being chloridized. About twenty to thirty percent of the silver layer was converted to silver chloride and the flared ends of the tubes were also included in the chloridizing operation. After the chloridizing operation was completed, the electrode was soaked in distilled water for about one hour. Both electrodes were stored in distilled water until they were ready to be used.

IV.5 Results and Discussion

Systematic measurements of the potential difference between the electrodes as a function of pressure and circulation rate were performed. Hyperfiltration rates and product concentration were determined at the same time.

The experiments were performed in two time-sequences; viz. (a) four series in which the circulation rate was kept constant and the pressure varied in steps after the observed voltage reached a constant value and (b) four series in which the pressure was kept constant and the circulation rate varied systematically after attainment of steady state. Comparison of the results showed fairly good reproducibility of the change of streaming potential with both parameters; the reproducibility of the absolute values of the potentials was only fair; this is due to asymmetry potentials which are not of major significance for the evaluation of the results.

Figure 31 shows the measured potentials in the constant-circulation series as a function of the pressure; these are raw data, as recorded. The low pressure side was always positive. Figures 32 and 33 show the data for both the constant-circulation and constant-pressure series respectively after correction for the influence of chloride concentration on the potentials of the silver-silver chloride electrodes:*

$$(E^I - E^II) = \left(\frac{RT}{zF} \right) \ln (c^I / c^{II})$$

This correction was done using the data for product concentration, c^{II} , shown in Figures 34 and 35. The feed concentration, c^I , was always 0.0081N. The hyperfiltration rates are shown in Figure 36. They were

* $(E^I - E^{II})$, volt, is the potential difference due to the difference of the concentrations c^I and c^{II} (mole cm^{-3}) on the high and low pressure side respectively. R is the gas constant [8.317 watt sec mole $^{-1}$ ($^{\circ}\text{K}$) $^{-1}$], T the temperature ($^{\circ}\text{K}$), F Faraday's constant (96,500 coul eq) and z the valency of the ion to which the electrode is responsive (-1 for the chloride-responsive Ag-AgCl electrodes).

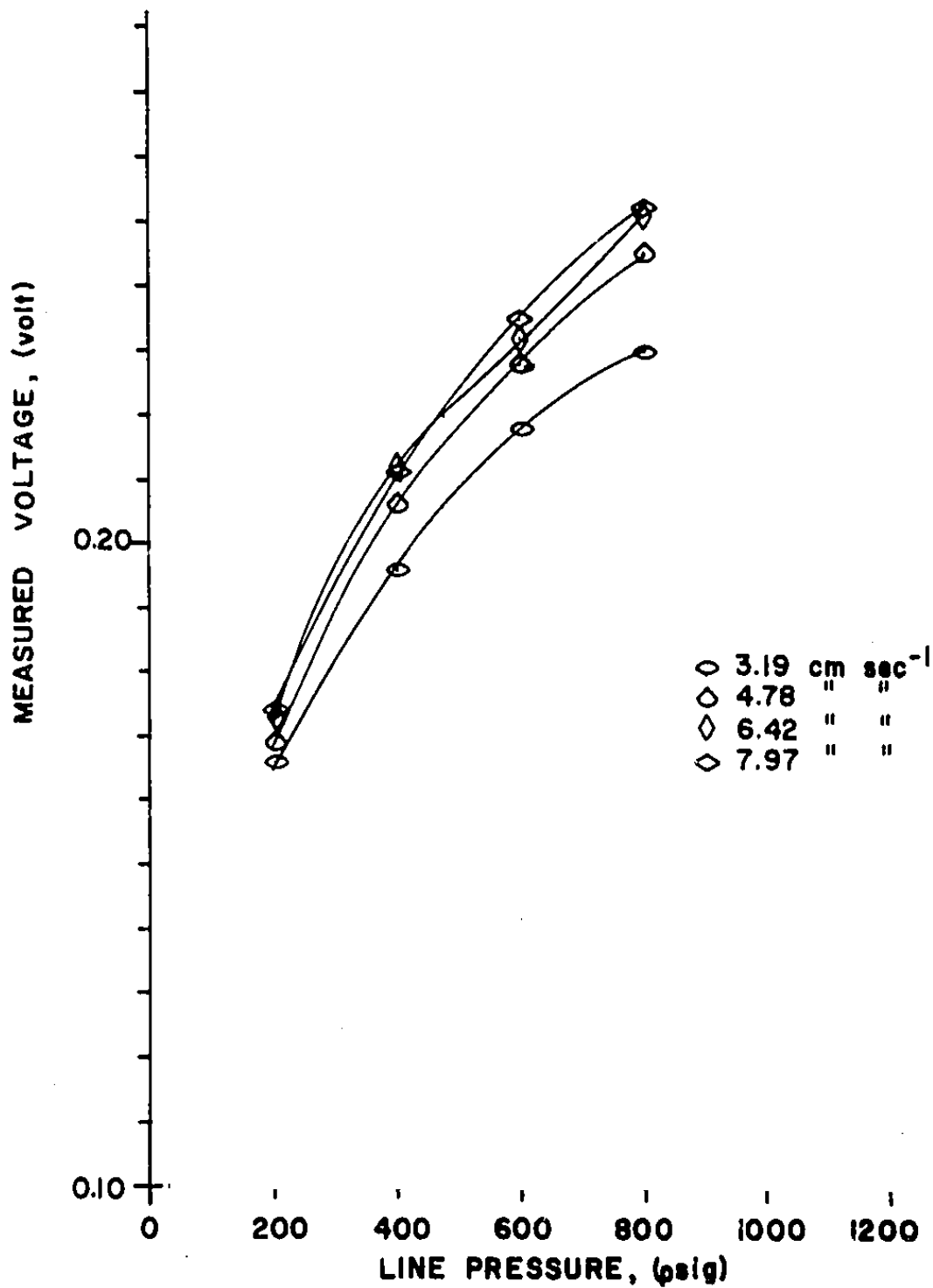


FIGURE 31. VOLTAGE ACROSS MEMBRANE VS. PRESSURE (70°F)

Feed: 0.0081N NaCl. Membrane: modified cellulose acetate. Different curves refer to series of experiments in which circulation rate was held constant and pressure varied.

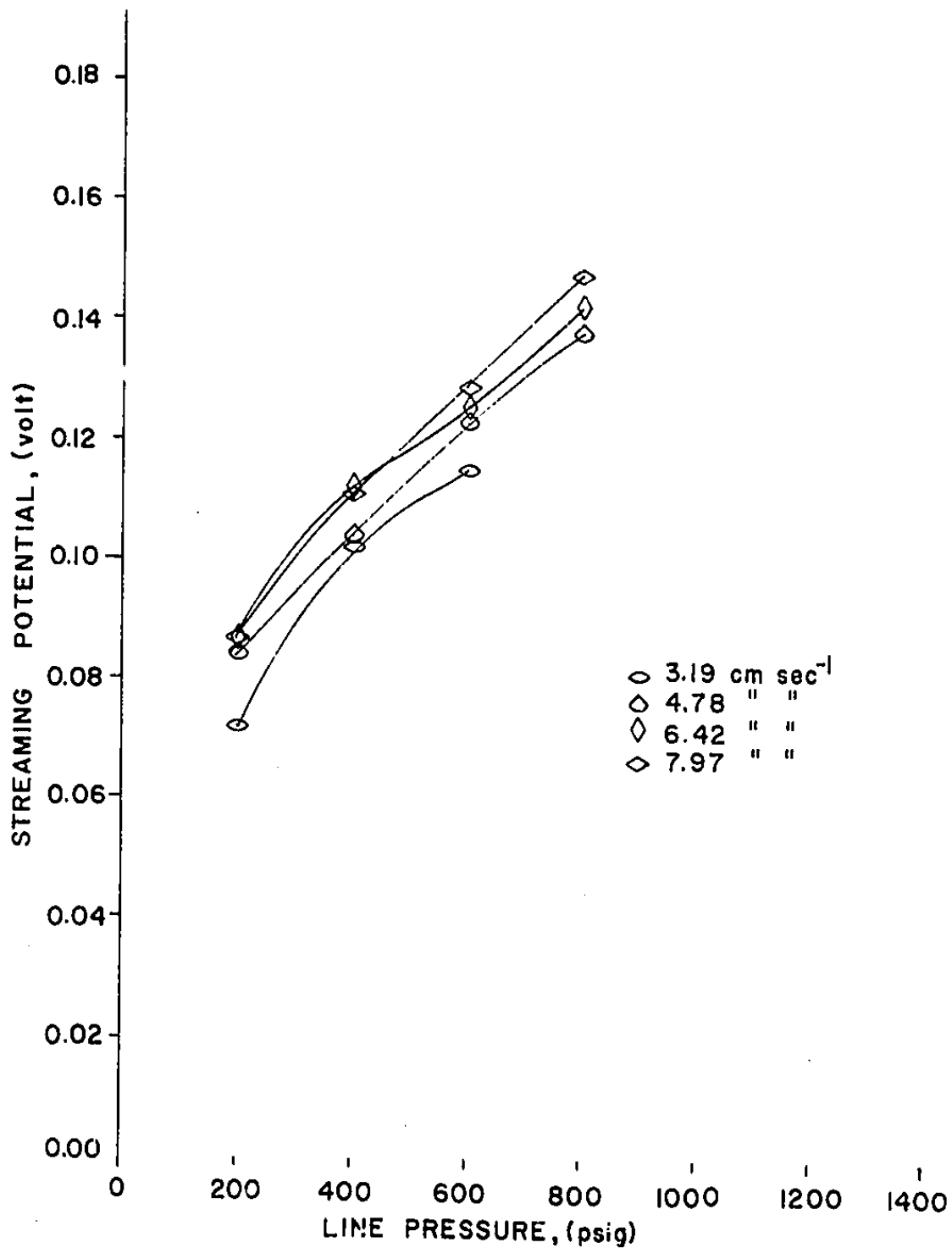


FIGURE 32. STREAMING POTENTIAL VS. PRESSURE (70°F)

Feed: 0.0081N NaCl. Membrane: modified cellulose acetate.
 Different curves refer to series of experiments in which
 circulation rate was held constant and pressure varied.

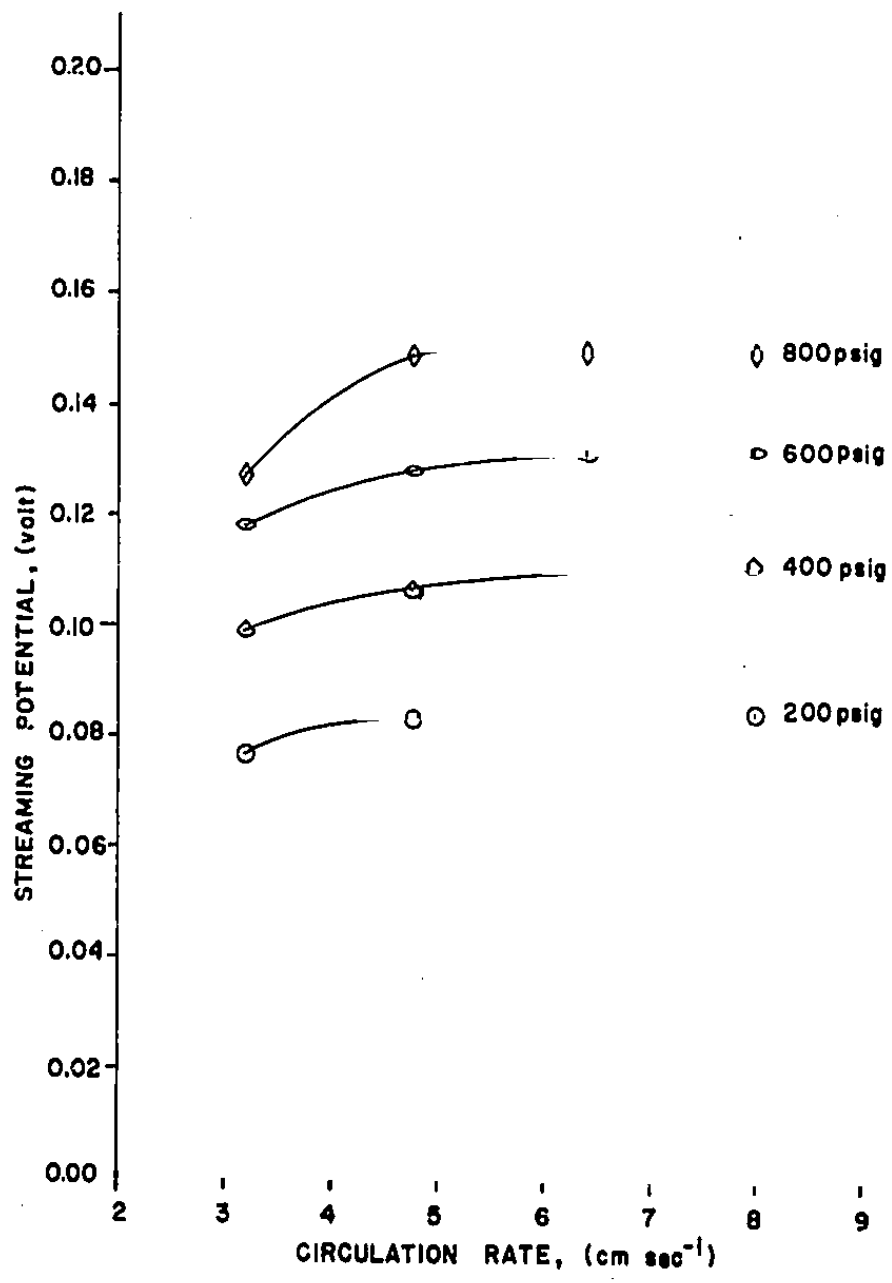


FIGURE 33. STREAMING POTENTIAL VS. CIRCULATION RATE (70°F)

Feed: 0.0081N NaCl. Membrane: modified cellulose acetate. Different curves refer to series of experiments in which pressure was held constant and circulation rate varied.

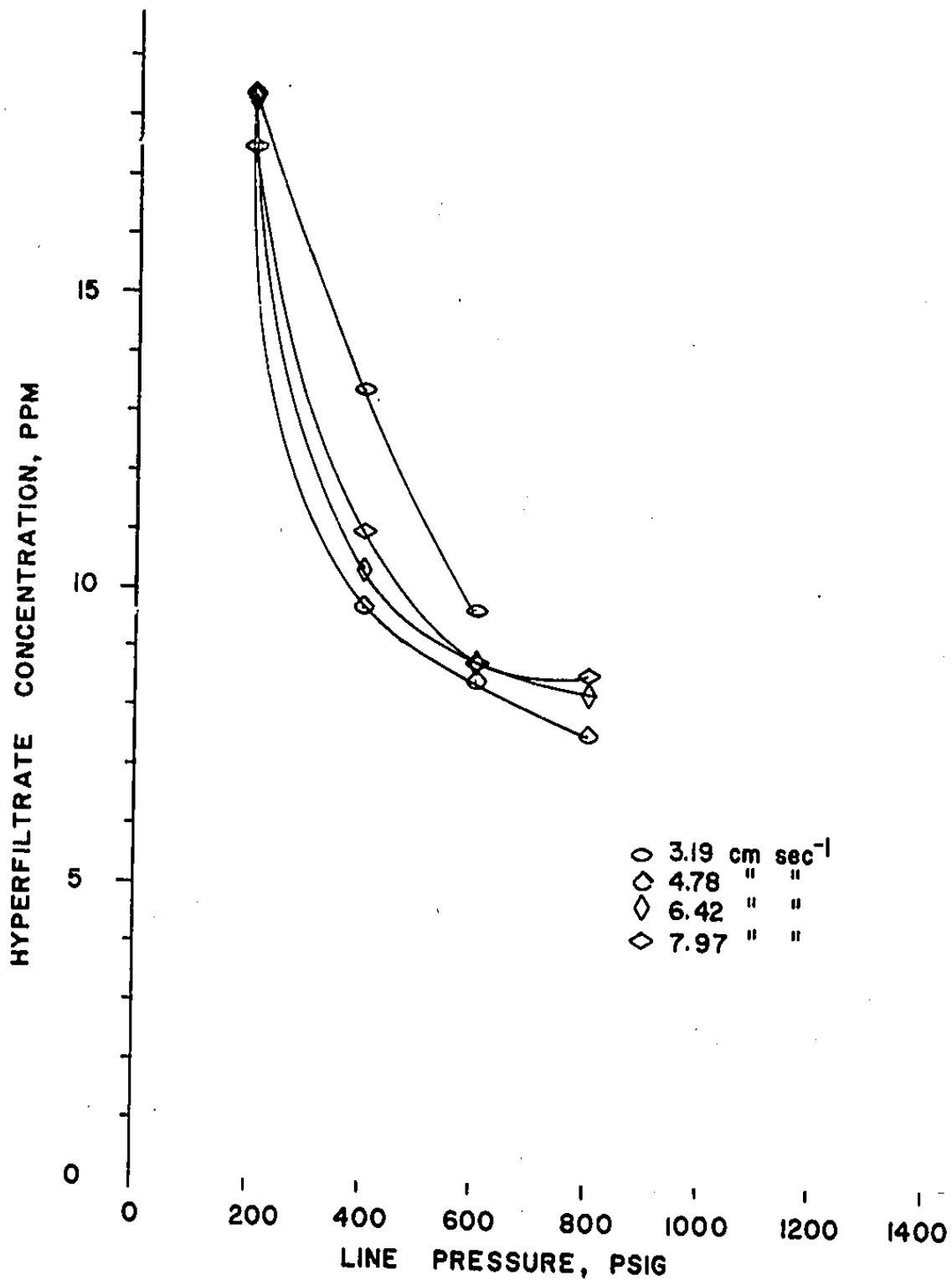


FIGURE 34. HYPERFILTRATE CONCENTRATION VS. PRESSURE (70°F)

Feed: 0.0081N NaCl. Membrane: modified cellulose acetate. Different curves refer to series of experiments in which circulation rate was held constant and pressure varied.

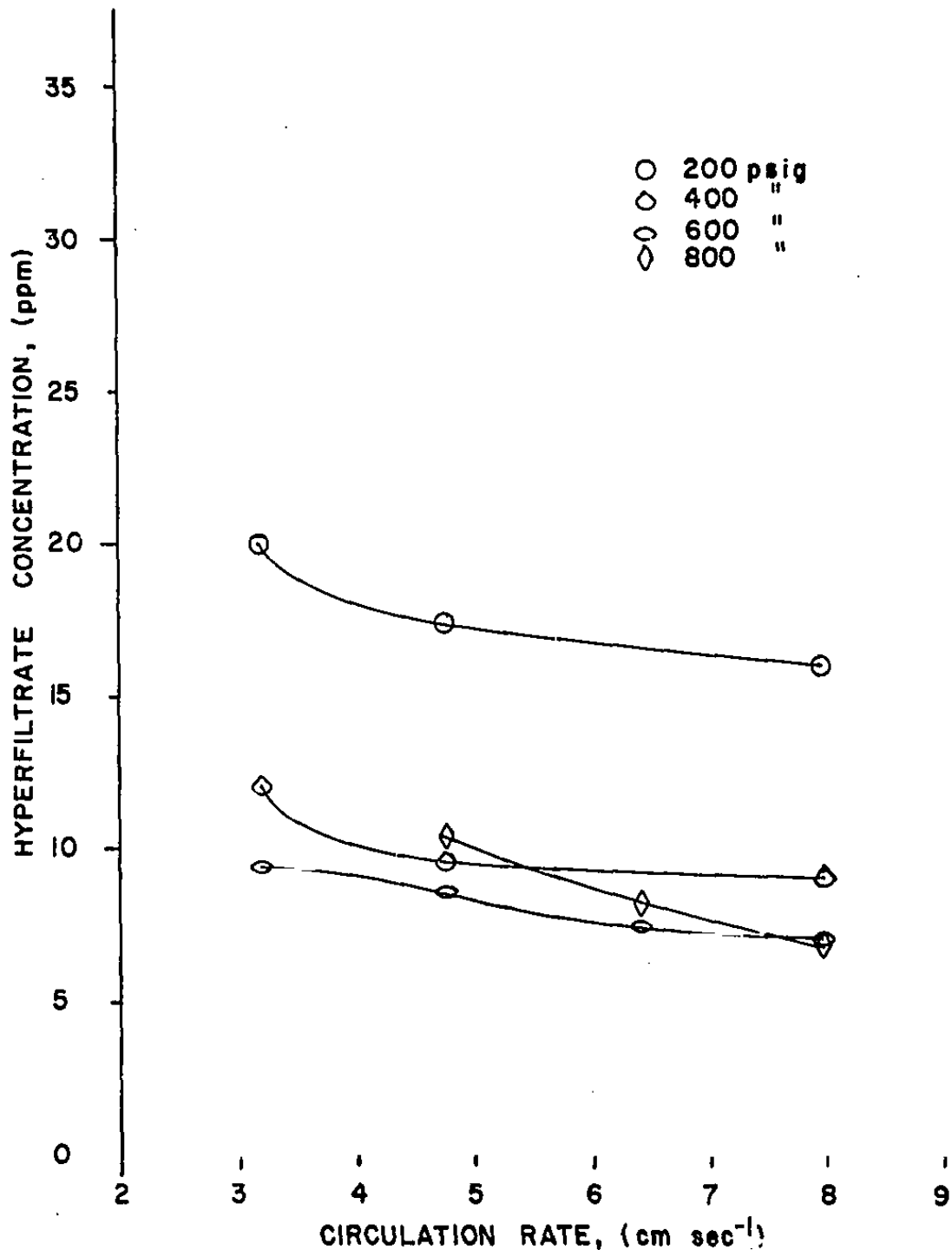


FIGURE 35. HYPERFILTRATE CONCENTRATION VS. CIRCULATION RATE

Feed: 0.0081N NaCl. Membrane: modified cellulose acetate.
 Different curves refer to series of experiments in which pressure was held constant and circulation rate varied.

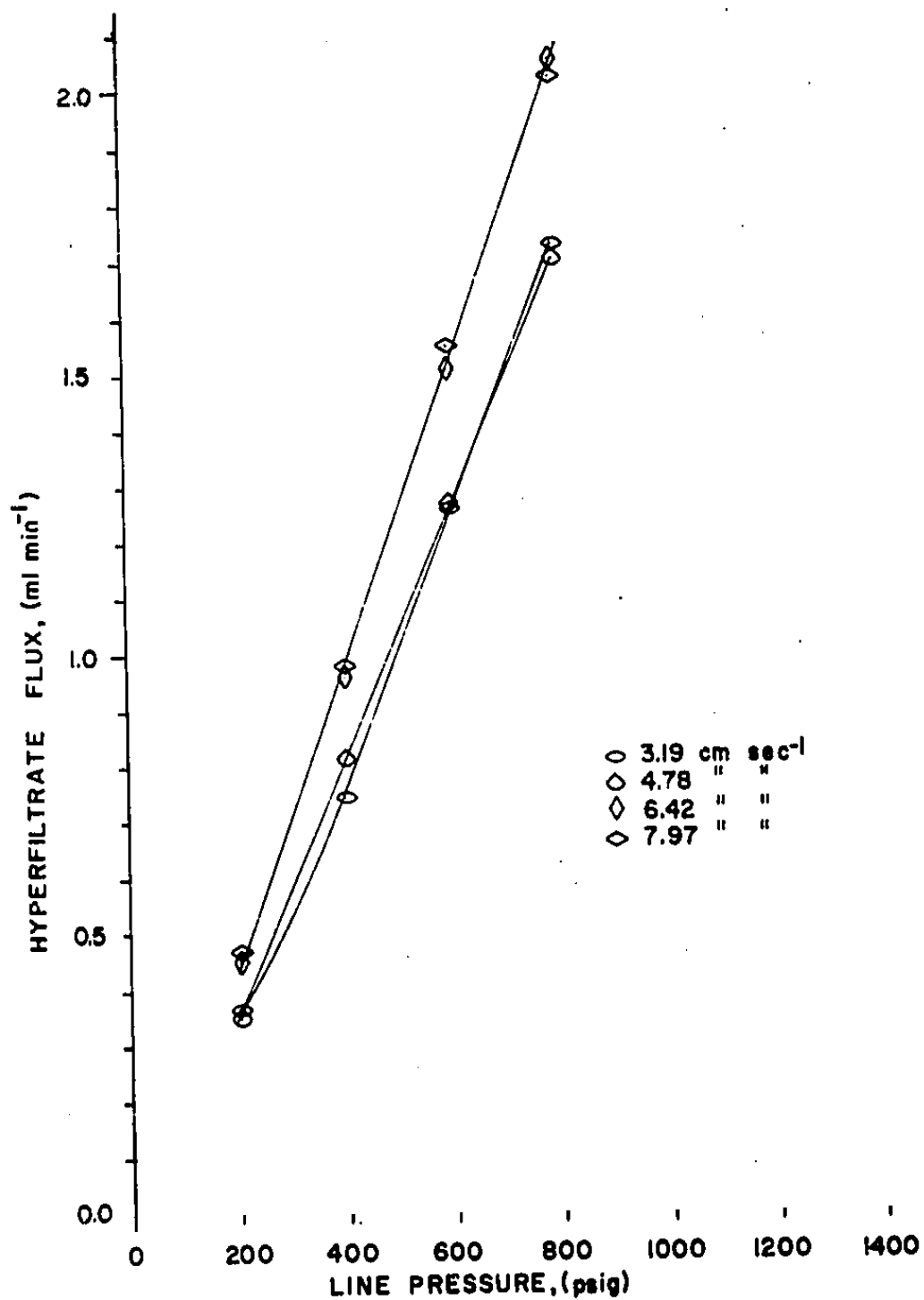


FIGURE 36. HYPERFILTRATION FLUX VS. PRESSURE (70°F)
 Feed: 0.0081N NaCl. Membrane: modified cellulose acetate.

practically identical in the constant-pressure and constant-flow rate series. The results are shown in terms of cm sec^{-1} .*

It is seen that the streaming potentials increase with the pressure, at a rate of 8-10 millivolt/100 psi. It will be of considerable interest to observe the variation of the streaming potentials in the extension of these experiments to gradually increasing salt concentrations. Such experiments might shed some light on the exclusion mechanism in the "pores": modified cellulose acetate is generally assumed to have but few, if any, fixed charges. For fixed-charge membranes, on the other hand, a large reduction of streaming potential (which also implies an equal reduction in electroosmotic water transfer) is indicative of media having a very low concentration of fixed charges^(58,59).

The streaming potentials also increase with the circulation rate, this variation being most pronounced at the lowest flow rates. It is planned to investigate the relation of this variation to concentration polarization.

Theory of Reverse Osmosis

During the period of this grant, there has been much activity in the United States and abroad in the field of thermodynamic theory of osmosis and reverse osmosis^(56,57,60,61) and the application of the theoretical concepts to the calculation of the intrinsic water/salt permeability requirements of any membrane capable of reverse osmosis⁽⁶²⁾. Theoretical work under this grant was performed jointly with Professor O. Kedem, Weizmann Institute of Science, Rehovoth, Israel. Since this work has already been published ["Thermodynamics of Hyperfiltration (Reverse Osmosis): Criteria for Efficient Membranes," Desalination 1, 311 (1966)], only the abstract is repeated in Section II of this report.

$$* 1 \text{ cm sec}^{-1} = \frac{1}{3780} \times 929 \times 86,400 = 2.12 \times 10^4 \text{ gal ft}^{-2} \text{ day}^{-1}$$

REFERENCES

1. Rosenberg, N. W. and Tirrell, C. E., *Ind. Eng. Chem.* 49, 780 (1957).
2. Cooke, B. A., *Electrochimica Acta* 3, 307 (1961); 4, 179 (1961).
3. Cooke, B. A. and S. J. Van Der Walt, *Electrochimica Acta* 5, 216 (1961).
4. Wilson, J. R., ed., *Deminerlization by Electrodialysis*, Academic Press, New York (1966).
5. Spiegler, K. S., *Advances in Chemistry Series*, Amer. Chem. Soc., Washington, D. C. 38, 179 (1963).
6. Cowan, D. A. and J. H. Brown, *Ind. Eng. Chem.* 51, 1445 (1959).
7. Forgacs, C., *Dechema Monograph* 47, 601 (1962), Verlag Chemie, Weinheim Bergstrasse, W. Germany.
8. Cooke, B. A., *Proc. First International Symposium on Water Desalination*, Washington, D. C. 2, 219 (1965).
9. Shaffer, L. H. and M. S. Mintz, Chap. 6, *Principles of Desalination*, Academic Press, New York (1966).
10. Fenech, E. J. and C. W. Tobias, *Electrochimica Acta* 2, 311 (1960).
11. Ibl, N., *Chemie-Ingenieur-Technik* 35, 353 (1963).
12. Vogtlaender, P. H. and C. A. P. Bakker, *Chem. Eng. Science* 18, 583, (1963).
13. Bates, R. G., *Determination of pH in Theory and Practice*, Wiley, New York (1964), pp. 282.
14. Cole, K. S. and U. Kishimoto, *Science* 136, 381 (1962).
15. Helfferich, F., *Ion Exchange*, McGraw Hill, New York (1962).
16. Spiegler, K. S. and M. R. J. Wyllie, "Electrical Potential Differences," in *Physical Techniques in Biological Research*, 2nd ed. II.A, D. H. Moore, ed., Academic Press, New York (1968).
17. Solt, G. S., *First International Symposium on Water Desalting*, Washington, D. C. (1965).
18. Wilke, C. R., M. Eisenberg, and C. W. Tobias, *J. Electrochem. Soc.* 100, 513 (1953).
19. Eisenberg, M., C. W. Tobias, and C. R. Wilke, *J. Electrochem. Soc.* 101, 306 (1954).

20. Kimura, S. and S. Sourirajan, A.I.Ch.E. J. 13, 497 (1967).
21. Wragg, A. A. and T. K. Ross, Electrochim. Acta 12, 1421 (1967).
22. Millar, J. R., D. G. Smith, and W. E. Marr, J. Chem. Soc. 340, 1789, (1962).
23. Moore, J. C., J. Polym. Sci. 2A, 835 (1964).
24. Soliner, K., J. Electrochem. Soc. 97, 139C (1950).
25. Spiegler, K. S., J. Electrochem. Soc. 100, 303C (1963).
26. Glueckauf, E. and R. E. Watts, Proc. Roy. Soc. 268, 339 (1962).
27. Block, M., Ph.D. thesis, Imperial College of Science and Technology, London (1964).
28. de Körösy, F. and J. Shorr, "Fresh Water from the Sea," Dechema Monograph 47, 477, Verlag Chemie, Weinheim/Bergstrasse, W. Germany (1962).
29. Small, H., U. S. Patent No. 2,961,417 (November 22, 1960).
30. Tolansky, S., An Introduction to Interferometry, Longmans (London), 1966.
31. O'Brien, R. N., Rev. Scient. Instrum. 35, 803 (1964).
32. O'Brien, R. N., C. A. Rosenfield, K. Kinoshita, W. F. Yakymyshyn, and J. Leja, Canad J. Chem. 43, 3304 (1965).
33. Frank, K. and Mary C. Becker in Physical Techniques in Biological Research, Vol. 5, W. L. Nastuk, ed., pp. 22-87, Academic Press, New York (1964).
34. Gibson, M. D. and W. H. Schwarz, J. Fluid Mech. 16, part 3, 357 (1963).
35. Williams, F. A., "Boundary Layer Flow Problems in Desalination by Reverse Osmosis," U. S. Department of the Interior, Office of Saline Water, Grant No. 14-01-0001-951 (1966).
36. Ives, D. J. G. and G. J. Janz, eds., Reference Electrodes, Academic Press, New York (1961).
37. Kohlrausch, F., Wied. Ann. 60, 315 (1897).
38. Leonard, J. E., Beckman Instruments, Fullerton, Calif. Private communication.
39. Bates, R. G., J. Electroanalyt. Chem. 2, 93 (1961).

40. Kleinberg, I., Brit. Dental J. 104, 197 (March 18, 1958).
41. Kollman, P., "Antipolarization Membrane Having Anionic and Cationic Areas," U. S. Patent No. 3,227,662 (1966).
42. Griessbach, R., Z. Elektrochem. (Ber. Bunsenges) 57, 147 (1953).
43. Grubhofer, N., Makromol. Chem. 30, 96 (1959).
44. Presland, A.E.B., A. D. Greenwood, and M. Block, Nature 212, 394 (1966).
45. Glueckauf, E., Proc. Roy. Soc. A 268, 350 (1962).
46. Crabtree, J. M. and E. Glueckauf, Trans. Farad. Soc. 59, 2639 (1963).
47. Schwan, H. P., in Adv. Biol. Med. Phys., p. 147, Lawrence, J. H. and C. A. Tobias, eds., Academic Press, New York (1957).
48. Sachs, S. B. and K. S. Spiegler, J. Phys. Chem. 68, 1214 (1964).
49. Bauman, W. C. and J. Eichhorn, J. Amer. Chem. Soc. 69, 2830 (1947).
50. LePage, W. R., Analysis of Alternating Current Circuits, McGraw Hill, New York (1952).
51. Sachs, S. B., M.S. thesis, Israel Institute of Technology, Haifa (1961).
52. Sachs, S. B., Ph.D. thesis, Weizmann Institute of Science (1966).
53. Richman, D. and H. G. Thomas, J. Phys. Chem. 60, 237 (1956).
54. McKelvey, J. S. Jr., K. S. Spiegler, and M.R.J. Wyllie, Chem. Engr. Progress Symposium Series 55, No. 24, 199 (1959).
55. Loeb, S., "A Composite Tubular Assembly for Reverse Osmosis Desalination," Desalination 1, 35 (1966).
56. Johnson, J. S. Jr., L. Dresner, and Kurt A. Kraus, Chapter 8 in Principles of Desalination, K. S. Spiegler, ed., Academic Press, New York (1966).
57. Merten, U., ed., Desalination by Reverse Osmosis, M.I.T. Press, Cambridge, Mass. (1966).
58. Spiegler, K. S., Trans. Farad Soc. 54, 1408 (1958).
59. Gray, D. H., "Coupled Flow Phenomena in Clay-Water Systems," Ph.D. thesis, Dept. of Civil Engin., University of California, Berkeley (1966).
60. Spiegler, K. S. and O. Kedem, Desalination 1, 311 (1966).

61. Podall, H. E., "Theoretical and Practical Aspects of the Evaluation of Candidate Reverse Osmosis Membranes for Desalination," U. S. Dept. Interior, Office of Saline Water, Research & Development Report No. 267, U. S. Government Printing Office, Washington, D. C., (1967).
62. Podall, H. E., "Permeability Requirements of Membranes for Use in Desalination by Reverse Osmosis," U. S. Dept. Interior, Office of Saline Water, Research & Development Report No. 255, U. S. Government Printing Office, Washington, D. C., (1967).

LIST OF PUBLICATIONS RESULTING FROM THIS RESEARCH

"Thermodynamics of Hyperfiltration (Reverse Osmosis): Criteria for Efficient Membranes," with O. Kedem, *Desalination* **1**, 311 (1966).

"Technologie des Membranes à Perméabilité Sélective," Colloque "Membranes à perméabilité sélective," Délégation générale à la recherche scientifique et technique, Paris, France, (in press).

"Fundamentals of Electrically Driven Processes," in "Membrane Processes for Industry," pp. 1-34, Southern Research Institute, Birmingham, Alabama, (1966).

"Polarization Phenomena on Membrane Solution Interfaces," with R. N. O'Brien, Abstract in Proceedings of CITCE (International Committee on Thermodynamics & Electrochemical Kinetics) Meeting, Tokyo, (1966).

"Concentration Polarization in Electrodialysis and in Reverse Osmosis Processes," Preprints of Papers Presented, Division of Water, Air, and Waste Chemistry, American Chemical Society Meeting, San Francisco, California (March 31-April 5, 1968).

"Laser Interferometry of the Electrodialysis of a KCl Solution," with R. N. O'Brien, joint meeting of American Institute of Chemical Engineers, Canadian Institute of Chemical Engineers, and Institute of Chemical Engineers (Great Britain), Montreal, Canada, (September, 1968).

LIST OF SYMBOLS

This list contains the symbols for Section III.A.3 only [Eq. (1)-(62)]. The few additional symbols in other sections are defined where used.

Subscripts $+$, $-$, and $=$ refer to K^+ , Cl^- and PSS^- respectively. All properties of PSS are calculated per equivalent. Note that the concentrations are in mole or equivalent per cm^3 , not per liter. Primes and double primes stand for left and right boundary respectively (Figure 2).

Units are identical or consistent with those suggested on page 1409 of Trans. Farad. Soc. 54 (1958).

$B, B_=_$	Expressions defined in equations (24) and (60) resp., amp cm^2 mole
c	Concentration, mole cm^{-3} or equivalent cm^{-3}
c_o, c_m	Concentration of KCl in bulk electrolyte (outside boundary layer), and at membrane surface, respectively, mole cm^{-3}
$s c_m^l$	Concentration of Cl^- at left membrane surface when supporting electrolyte is present, equiv cm^{-3}
C	Expression defined in equation (38), volt
\bar{C}	Expression defined in equation (34), volt
D	Diffusion coefficient of low-molecular weight electrolyte (KCl) in solution, $cm^2 sec^{-1}$
$D_+, D_-, D_=_$	Ionic diffusion coefficients of K^+ , Cl^- and PSS^- , respectively, $cm^2 sec^{-1}$
E	Electric potential, volt
\mathcal{F}	Faraday's constant, 0.96×10^5 coul mole $^{-1}$
J	Flux, mole $cm^{-2} sec^{-1}$
m	Ion mobility, $cm^2 volt^{-1} sec^{-1}$

c_+^0, c_-^0, c_m^0	Concentration of K^+ , Cl^- and PSS^- respectively in bulk solution, when supporting electrolyte is present, equiv cm^{-3}
R	Gas constant, 8.32 watt sec mole $^{-1}$ ($^{\circ}K$) $^{-1}$
R_m	Membrane resistance (calculated for unit cross section), ohm cm^2
R_s	Resistance of solution between probe electrode and boundary layer, in absence of supporting electrolyte, ohm cm^2
R_{SP}	Resistance of solution between probe electrode and membrane surface, in presence of supporting electrolyte, ohm cm^2
\mathcal{R}	Resistance of boundary layer (calculated for unit cross section, and in absence of supporting electrolyte), ohm cm^2
t_+, t_-	Transport number of K^+ and Cl^- respectively in solution
\bar{t}_+, \bar{t}_-	Transport number of K^+ and Cl^- respectively in membrane
T	Absolute temperature, $^{\circ}K$
z	Length coordinate, cm
z_+, z_-	Ionic valency; positive for cations, negative for anions
δ	Boundary layer thickness, cm
ΔE_b	Ohmic potential drop across boundary, volt
ΔE_j	Junction potential ("concentration potential") in boundary, volt
ΔE_m	Membrane potential, volt
λ	Equivalent conductance, ohm $^{-1}$ cm^{-2} equiv $^{-1}$
μ	Chemical potential, watt sec mole $^{-1}$
ρ	Specific resistance, ohm cm